UNIVERSITY OF HELSINKI REPORT SERIES IN ASTRONOMY

No. 1

Molecular line and continuum studies of the early stages of star formation

Oskari Miettinen

ACADEMIC DISSERTATION

Department of Physics
Faculty of Science
University of Helsinki
Helsinki, Finland

To be presented, with the permission of the Faculty of Science of the University of Helsinki, for public criticism in Auditorium XV of the University Main Building on 19 November 2010, at 12 o'clock noon.

Helsinki 2010

Cover picture: The IRAM 30-m telescope on Pico Veleta in the Spanish Sierra Nevada. Photo taken by O. Miettinen.

ISSN 1799-3024 (printed version)
ISBN 978-952-10-5981-0 (printed version)
Helsinki 2010
Helsinki University Printing House (Yliopistopaino)

ISSN 1799-3032 (pdf version)
ISBN 978-952-10-5982-7 (pdf version)
ISSN-L 1799-3024
http://ethesis.helsinki.fi/
Helsinki 2010
Electronic Publications @ University of Helsinki (Helsingin yliopiston verkkojulkaisut)

Oskari Miettinen: **Molecular line and continuum studies of the early stages of star formation**, University of Helsinki, 2010, 98 p.+appendices, University of Helsinki Report Series in Astronomy, No. 1, ISSN 1799-3024 (printed version), ISBN 978-952-10-5981-0 (printed version), ISSN 1799-3032 (pdf version), ISBN 978-952-10-5982-7 (pdf version), ISSN-L 1799-3024

Classification (INSPEC): A9580D, A9580E, A9580G, A9710B, A9720D, A9840B, A9840C, A9840J, A9840K, A9840L
Keywords: interstellar medium, molecular clouds, clumps, cores, star formation, molecular spectral lines, dust continuum, radio continuum

Abstract

New stars form in dense interstellar clouds of gas and dust called molecular clouds. The actual sites where the process of star formation takes place are the dense clumps and cores deeply embedded in molecular clouds. The details of the star formation process are complex and not completely understood. Thus, determining the physical and chemical properties of molecular cloud cores is necessary for a better understanding of how stars are formed. Some of the main features of the origin of low-mass stars, like the Sun, are already relatively well-known, though many details of the process are still under debate. The mechanism through which high-mass stars form, on the other hand, is poorly understood. Although it is likely that the formation of high-mass stars shares many properties similar to those of low-mass stars, the very first steps of the evolutionary sequence are unclear.

Observational studies of star formation are carried out particularly at infrared, submillimetre, millimetre, and radio wavelengths. Much of our knowledge about the early stages of star formation in our Milky Way galaxy is obtained through molecular spectral line and dust continuum observations. The continuum emission of cold dust is one of the best tracers of the column density of molecular hydrogen, the main constituent of molecular clouds. Consequently, dust continuum observations provide a powerful tool to map large portions across molecular clouds, and to identify the dense star-forming sites within them. Molecular line observations, on the other hand, provide information on the gas kinematics and temperature. Together, these two observational tools provide an efficient way to study the dense interstellar gas and the associated dust that form new stars. The properties of highly obscured young stars can be further examined through radio continuum observations at centimetre wavelengths. For example, radio continuum emission carries useful information on conditions in the protostar+disk interaction region where protostellar jets are launched.

In this PhD thesis, we study the physical and chemical properties of dense clumps and cores in both low- and high-mass star-forming regions. The sources are mainly studied in a statistical sense, but also in more detail. In this way, we are able to examine the general characteristics of the early stages of star formation, cloud properties on large scales (such as fragmentation), and some of the initial conditions of the collapse process that leads to the formation of a star. The studies presented in this thesis are mainly based on molecular line and dust continuum observations. These are combined with

archival observations at infrared wavelengths in order to study the protostellar content of the cloud cores. In addition, centimetre radio continuum emission from young stellar objects (YSOs; i.e., protostars and pre-main sequence stars) is studied in this thesis to determine their evolutionary stages.

The main results of this thesis are as follows: **i)** filamentary and sheet-like molecular cloud structures, such as infrared dark clouds (IRDCs), are likely to be caused by supersonic turbulence but their fragmentation at the scale of cores could be due to gravo-thermal instability; **ii)** the core evolution in the Orion B9 star-forming region appears to be dynamic and the role played by slow ambipolar diffusion in the formation and collapse of the cores may not be significant; **iii)** the study of the R CrA star-forming region suggests that the centimetre radio emission properties of a YSO are likely to change with its evolutionary stage; **iv)** the IRDC G304.74+01.32 contains candidate high-mass starless cores which may represent the very first steps of high-mass star and star cluster formation; **v)** SiO outflow signatures are seen in several high-mass star-forming regions which suggest that high-mass stars form in a similar way as their low-mass counterparts, i.e., via disk accretion.

The results presented in this thesis provide constraints on the initial conditions and early stages of both low- and high-mass star formation. In particular, this thesis presents several observational results on the early stages of clustered star formation, which is the dominant mode of star formation in our Galaxy.

Acknowledgements

Most of the work carried out for this PhD thesis has been done at the Observatory of the University of Helsinki. The historical observatory building offered a great environment to work on astronomy. The present thesis was completed at the Department of Physics to which the Department of Astronomy merged with at the beginning of 2010.

First of all, I am deeply grateful to my thesis supervisor, Docent Dr. Jorma Harju. His continuous help, advice, and encouragement (to mention just a few things) through all these years have been indispensable. I thank Docent Dr. Lauri Haikala for acting as a second supervisor, and in particular for his guidance in the dust continuum studies. I wish to express my sincere gratitude to Professor Dr. Kalevi Mattila for giving me the chance to work in the Interstellar Medium and Star Formation-research group at the observatory already during my second year of study. In addition to the above named persons, I have received help in one way or another from many other people, and they are all greatly acknowledged (forgive me not mentioning you all here). It has been my pleasure to have collaborated with all of you. Also, thank you to everybody who read and commented different parts of this thesis.

I am indebted to the pre-examiners Professor Dr. René Liseau (Onsala) and Dr. Friedrich Wyrowski (Max-Planck-Institut für Radioastronomie (MPIfR), Bonn), for taking some of their valuable time to review this thesis.

For the financial support during the thesis work, I am grateful to the Finnish Graduate School in Astronomy and Space Physics, the Research Foundation of the University of Helsinki, and the Academy of Finland. Moreover, the Magnus Ehrnrooth Foundation is acknowledged for providing travel support.

I would like to thank the staff at the IRAM 30-m telescope for their hospitality and help during the observations presented in Paper I of this thesis. Doctor Alex Kraus and the operators of the Effelsberg 100-m telescope are thanked for their help during the observations presented in Paper II. I also should sincerely thank the staff at the APEX telescope in Chile; many of the observations presented in this thesis are carried out with APEX in service mode. I would like to thank Dr. Martin Hennemann, who is currently at CEA Saclay (France), and Dr. Hendrik Linz at the Max-Planck-Institut für Astronomie (MPIA) for their collaboration with several proposals concerning the studies of infrared dark clouds, and for their kind hospitality during my visit to MPIA. Doctor Jouni Kainulainen, the former member of the ISM/SF-group, and who is currently at the MPIA, is thanked for several collaborations (e.g., Paper I and solving all sorts of never ending computer problems). Thank you, Laura, for your love, care and kind-heartedness. Finally, very special thanks go to my mother for her outstanding support.

Oskari Miettinen
Helsinki, September 2010

List of publications

This thesis consists of an introductory review part, followed by five research publications:

Paper I: Miettinen, O., Harju, J., Haikala, L. K., Kainulainen, J., and Johansson, L. E. B., "Prestellar and protostellar cores in Orion B9", 2009, A&A, 500, 845

Paper II: Miettinen, O., Harju, J., Haikala, L. K., and Juvela, M., "Physical properties of dense cores in Orion B9", 2010, A&A, in press

Paper III: Miettinen, O., Kontinen, S., Harju, J., and Higdon, J. L., "Radio continuum imaging of the R Coronae Austrinae star-forming region with the ATCA", 2008, A&A, 486, 799

Paper IV: Miettinen, O., and Harju, J., "LABOCA mapping of the infrared dark cloud MSXDC G304.74+01.32", 2010, A&A, in press

Paper V: Miettinen, O., Harju, J., Haikala, L. K., and Pomrén, C., "SiO and CH_3CCH abundances and dust emission in high-mass star-forming cores", 2006, A&A, 460, 721

These papers will be referred to in the text by their Roman numerals, and are summarised in Chapter 7, where also author's contribution are described. The articles are reprinted with kind permission of *Astronomy and Astrophysics*.

List of abbreviations

AD	Ambipolar diffusion
ALMA	Atacama Large Millimetre/submillimetre Array
APEX	Atacama Pathfinder Experiment
ATCA	Australia Telescope Compact Array
BE	Bonnor-Ebert (sphere)
CMF	Core mass function
CTTS	Classical T Tauri star
FIR	Far infrared
GMC	Giant molecular cloud
HC	Hypercompact (HII region)
HH	Herbig-Haro (object)
HMC	Hot molecular core
HPBW	Half-power beam width
HMPO	High-mass protostellar object
HMSC	High-mass starless core
IMF	Initial mass function
IR	Infrared
IRAM	Institut de Radioastronomie Millimétrique
IRAS	Infrared Astronomical Satellite
IRDC	Infrared dark cloud
ISM	Interstellar medium
ISRF	Interstellar radiation field
KL	Kleinmann-Low (nebula)
K-S	Kolmogorov-Smirnov (test)
LABOCA	Large APEX Bolometer Camera
LTE	Local thermodynamic equilibrium
MHD	Magnetohydrodynamic
MIR	Mid-infrared
MSX	Midcourse Space Experiment
NIR	Near infrared
PI	Principal investigator
PMS	Pre-main sequence (star)
SED	Spectral energy distribution
SEST	Swedish-ESO Submillimetre Telescope
SFE	Star formation efficiency
SFR	Star formation rate
SIMBA	SEST Imaging Bolometer Array
SN	Supernova (plural SNe)
UC	Ultra-compact (HII region)
UV	Ultraviolet
WTTS	Weak-line T Tauri star
YSO	Young stellar object
ZAMS	Zero-age main sequence

Contents

Chapter 1

Introduction

1.1 Background

Star formation has an essential role in the universe as it plays a key role in determining the structure and evolution of galaxies. It is thus not surprising that star formation studies have become an integral part of modern astrophysics.

Stars form in interstellar molecular clouds that consist of gas (mostly molecular hydrogen, H_2) with a small fraction of dust. The entire molecular gas mass of the Galaxy is $\sim 10^9$ $M_\odot$. Most of the molecular material is in the form of giant molecular clouds (GMCs), which are the largest structures within our Galaxy and the primary sites of star formation. They have masses of $\sim 10^4 - 10^6$ $M_\odot$, sizes from ~ 20 to ~ 100 pc, gas kinetic temperatures of 10–30 K, and average H_2 densities of $\langle n(H_2) \rangle \sim 10^2 - 10^3$ cm^{-3} (e.g., Blitz 1993). More precisely, it is the dense *clumps* and *cores* within molecular clouds where the gravitational collapse and the actual star formation take place; the terms "clump" and "core" are often used to refer to objects with masses, sizes, and mean densities of $\sim 10-1000$ $M_\odot$, $\sim 0.5-1$ pc, 10^3-10^4 cm^{-3}, and $\sim 1-10$ $M_\odot$, ~ 0.1 pc, $10^4 - 10^5$ cm^{-3}, respectively (e.g., Bergin & Tafalla 2007). It is thus important to study the properties and dynamical evolution of these objects. On the other hand, the origin of dense cores is not yet fully understood. Shock compression by turbulent flows within molecular clouds is considered to be a likely mechanism of core formation.

The salient feature of star formation in our Galaxy is that most stars form in groups and clusters which contain tens to hundreds of objects, whereas isolated star formation is rare (e.g., Lada & Lada 2003). The most detailed observational studies and theoretical models deal with low-mass star formation in isolated dense cores (e.g., Shu et al. 1987, 2004). It is useful to extend the investigations to the regions where stars form in clustered mode. The star formation process is governed by the interplay between gravity, gas dynamics, turbulence, magnetic fields, and both electromagnetic and cosmic-ray radiation. The details of the physical processes, however, remain an open question. For example, it is still a matter of debate what is the relative importance of turbulence and magnetic fields (McKee & Ostriker 2007). In addition to the processes mentioned above it has also become clear that interstellar chemistry is of utmost importance to star formation studies. Chemistry plays a role in the ionisation degree of the gas, and controls, e.g., the cooling of the gas. Thus, chemistry affects the dynamics of the star-forming core.

The main features of the process of low-mass star formation are already relatively well

understood. For example, low-mass dense cores can be distinguished into several stages which are likely to represent an evolutionary sequence, i.e., starless cores, prestellar cores, Class 0–I protostellar cores and, furtheron, Class II and III pre-main sequence (PMS) stars. In contrast, the formation of high-mass stars, which are more important for the evolution of galaxies, is still poorly understood. There are several reasons for this. Especially, high-mass stars and their formation sites are rare, and high-mass stars form in highly clustered regions making it diffucult to determine which processes are at play. Nevertheless, in recent years the knowledge of high-mass star formation has increased considerably. This is, in part, due to the discovery of the so-called infrared dark clouds (IRDCs) and the clumps and cores within them, some of which are likely to represent the earliest stages of high-mass star and star cluster formation. Particularly, IRDCs may contain high-mass analogues of cold low-mass prestellar cores.

Among the most useful observational tools to study the earliest stages of star formation are molecular spectral lines and dust continuum emission. Molecular lines provide information on the gas temperature, kinematics (e.g., turbulence and infall), and molecular abundances. Continuum emission of dust can be used to determine the basic properties of star-forming structures, such as mass, size, and column density of H_2. Moreover, when studying objects that are already in the protostellar or PMS stage, radio continuum emission, such as thermal free-free emission from ionised gas, can be used to study e.g, the properties of the circumstellar environment and associated protostellar winds and jets.

1.2 Purpose and scope of this thesis

In this thesis, both low- and high-mass star-forming regions are investigated by means of molecular lines, dust continuum, and radio continuum observations. Studies of the physical and chemical properties of star-forming cores presented in this thesis provide information on *the initial conditions and early stages of star formation*. This is the main purpose of the thesis.

Because the studied regions represent clustered regions of star formation, the results of our studies provide useful information on the dominant star formation mode in the Galaxy. Most of the studies presented in this thesis are survey-like and address statistical properties. For some individual objects also more detailed studies of the physical and chemical properties are presented. The latter studies are needed to shed light on, e.g., the protostellar collapse. In particular, because the thesis include studies on both the low- and high-mass star formation, the results obtained can help to answer the question whether the formation of low- and high-mass stars can proceed in a similar manner.

1.3 Structure of the thesis

The thesis consists of an introductory review part and five original publications. Three of the papers are published in the international peer-review journal Astronomy and Astrophysics (A&A), and two of them will appear in the same journal (in press).

The introductory part of the thesis is organised as follows. In Chapter 2, the observational techniques and tools are briefly described, including descriptions of the telescopes and instruments used in the studies. In Chapter 3, the most relevant equations for this thesis are derived. In Chapter 4, an overview of low-mass star formation is given, emphasising the topics which are relevant for the thesis (e.g., prestellar cores). Chapter 5 is dedicated to high-mass star formation. Large-scale properties (or "macrophysics") of star formation in Galactic molecular clouds are discussed in Chapter 6, the emphasis being in the interstellar turbulence and how it is related to the origin of dense cores and their mass distribution. Summaries of Papers I–V are given in Chapter 7, including a description of the authors contribution to the papers. Finally, concluding remarks are presented in Chapter 8. The original publications are included at the end of the thesis.

Chapter 2

Observational techniques and tools

The star formation process is obscured by large amounts of gas and dust in the dense interiors of molecular clouds. The bulk of the associated matter is very cold during the earliest stages. For these reasons, the proper way to probe this process is through observations at infrared (IR), (sub)millimetre, and radio wavelengths. At these wavelengths, the interstellar dust becomes increasingly transparent, i.e., extinction is greatly diminished compared to the optical wavelengths.

The main constituent of molecular clouds and dense star-forming cores, H_2, is a homonuclear molecule, so its permanent electric dipole moment vanishes. H_2 has only electric quadrupole transitions which are very weak. Moreover, the moment of inertia of the H_2 molecule is low so the rotational levels have large energy spacing with no excited levels populated in cold clouds. Thus, star formation studies rely on spectral lines of trace molecules and continuum observations of the thermal emission from dust (Papers I, II, IV, and V). These two observational tools have their own advances and disadvantages:

- Molecular line studies have the advantage of tracing kinematics, temperature, and internal dynamics of dense cores. For example, the width of a spectral line provides information on the gas turbulent motions. Velocity information provided by molecular lines can also be used, due to Galactic rotation, to estimate the distance to the source (e.g., Fich et al. 1989).

- Different molecular species and their different transitions trace different gas layers because of density and temperature gradients within the source.

- Dust emission is generally optically thin ($\tau \ll 1$) at (sub)mm wavelengths. This is due to the fact that, at long wavelengths, the dust opacity, κ_λ, decreases with increasing wavelength, λ, as $\kappa_\lambda \propto \lambda^{-\beta}$, with $\beta \sim 1-2$ (e.g., Dunne & Eales 2001). If gas-to-dust mass ratio is known, dust continuum emission can thus be used as a direct tracer of the mass content of molecular cloud cores. Moreover, dust emission is able to trace large density contrasts and can be used to identify dense clumps and cores within molecular clouds.

- Dust continuum studies suffer from uncertainties related to dust emissivity and temperature, both of which are likely to change within dense cores.

Radio continuum observations at cm-wavelengths can be used to further constrain the properties of dense cores associated with already formed protostars (Paper III). Centimetric continuum observations are a powerful tool to study, for example, both ionised jets and winds, and magnetic fields around young stellar objects (YSOs), through the associated thermal free-free emission (bremsstrahlung) and non-thermal emission, respectively.

Several telescopes and instruments were used to gather the data presented in this thesis. These include both single-dish radio telescopes and a radio interferometer. We have also used archival data from IR satellites. Single-dish telescopes are suitable, e.g., for searching the star-forming cores, whereas high-resolution interferometric techniques are needed to study their properties and structure in more detail. Below is a list of the telescopes/instruments used for the studies of this thesis (in alphabetical order).

APEX The Atacama Pathfinder Experiment (APEX) is a 12-m radio telescope located at an altitude of 5105 m, at Llano de Chajnantor in the Chilean Atacama desert at the site of the upcoming ALMA (Atacama Large Millimetre/submillimetre Array) observatory. The submm dust continuum observations presented in Papers I and IV were acquired with the Large APEX Bolometer Camera (LABOCA), which is a 295-channel bolometer array operating at 870 μm. The N_2H^+ molecular line observations presented in Paper II were obtained with the APEX heterodyne receivers.

ATCA The Australia Telescope Compact Array (ATCA) is an array of six antennas, each 22 m in diameter. The array is located near the town of Narrabri in New South Wales. Radio continuum observations at 3, 6, and 20 cm wavelengths presented in Paper III were obtained using the ATCA.

Effelsberg 100-m telescope The Effelsberg 100-m radio telescope located in a valley near the village of Effelsberg, next to Bad Münstereifel, and operated by the Max Planck Institute for Radio Astronomy (MPIfR), is the second largest fully steerable radio telescopes in the world (see Fig. 2.1, right panel). Paper II presents ammonia (NH_3) spectral line observations made with the Effelsberg telescope.

IRAM 30-m telescope The IRAM (Institut de Radioastronomie Millimétrique) 30-m telescope is located on Pico Veleta in the Spanish Sierra Nevada, at an altitude of 2920 m (see Fig. 2.1, left panel). The 30-m telescope was used to carry out the spectral line observations presented in Paper I.

IRAS The Infrared Astronomical Satellite (IRAS) was the very first space-based observatory to perform a survey of the entire sky at IR wavelengths. Archival IRAS data were used in Papers I and IV.

MSX The Midcourse Space Experiment (MSX) was a Ballistic Missile Defense Organization satellite experiment, designed to map bright IR sources in the sky. We used MSX

Figure 2.1: **Left:** The IRAM 30-m telescope. **Right:** The Effelsberg 100-m telescope. Photos taken by the author.

archival images and data in Paper IV.

SEST The Swedish-ESO Submillimetre Telescope (SEST) was a 15-m radio telescope, which was built in 1987 on the ESO (European Southern Observatory) site of La Silla, in the Chilean Andes, at an altitude of 2400 m. The telescope was decommissioned in 2003. Molecular line observations presented in Paper V were the last line observations carried out with the SEST. Dust continuum observations at 1.2 mm presented in Paper V were performed with the SEST IMaging Bolometer Array (SIMBA).

Spitzer The Spitzer Space Telescope is a space-borne, cryogenically-cooled IR observatory, which was launched into space on August 25, 2003 (Werner et al. 2004). In Paper I, we used Spitzer/MIPS archival data at 24 and 70 μm.

2MASS The Two Micron All Sky Survey (2MASS) was a ground-based survey which uniformly scanned the whole sky in three near-infrared (NIR) bands [J (1.25 μm), H (1.65 μm), $K_{\rm s}$ (2.16 μm)] between 1997 and 2001. The 2MASS data were used in Papers I and IV.

Chapter 3

Basic equations

In this chapter, the most important equations for this thesis are derived. These include the molecular column density determined from spectral line emission, H_2 column density and total mass determined from dust continuum emission, and the spectral index of thermal cm-wave radio continuum emission. Most of the theory presented in this chapter can be found in books by Scheffler & Elsässer (1987) and Rohlfs & Wilson (2004).

3.1 Molecular column density calculation

We start the derivation of the column density of molecules, i.e., the number of molecules per unit area, by considering the propagation of radiation through a cloud, as illustrated in Fig. 3.1.

The radiative transfer equation in differential form is given by

$$\frac{\mathrm{d}I_\nu}{\mathrm{d}s} = -\kappa_\nu I_\nu + \epsilon_\nu \,, \tag{3.1}$$

where I_ν is the intensity of the radiation, $\mathrm{d}s$ is the infinitesimal length of a medium, κ_ν is the absorption coefficient, and ϵ_ν is the emission coefficient. The latter two are defined by

$$\kappa_\nu = \frac{h\nu_{ul}}{4\pi} \left(n_l B_{lu} - n_u B_{ul}\right) \phi(\nu) \,, \tag{3.2}$$

$$\epsilon_\nu = \frac{h\nu_{ul}}{4\pi} n_u A_{ul} \phi(\nu) \,. \tag{3.3}$$

In the above equations, h is the Planck constant, ν_{ul} is the transition frequency (from the upper energy state to the lower state, $u \rightarrow l$), n_u and n_l are the number densities of molecules in the upper and lower states, the Einstein coefficients A_{ul}, B_{lu}, and B_{ul} are the propabilities of radiation transfer for spontaneous emission, absorption, and stimulated emission, respectively, and $\phi(\nu)$ is the normalised line profile function (i.e., $\int_0^\infty \phi(\nu)\mathrm{d}\nu = 1$).

The Einstein A-coefficient (in SI units) is given by

$$A_{ul} = \frac{16\pi^3 \nu_{ul}^3}{3h\epsilon_0 c^3} \left|\mu_{ul}\right|^2 \,, \tag{3.4}$$

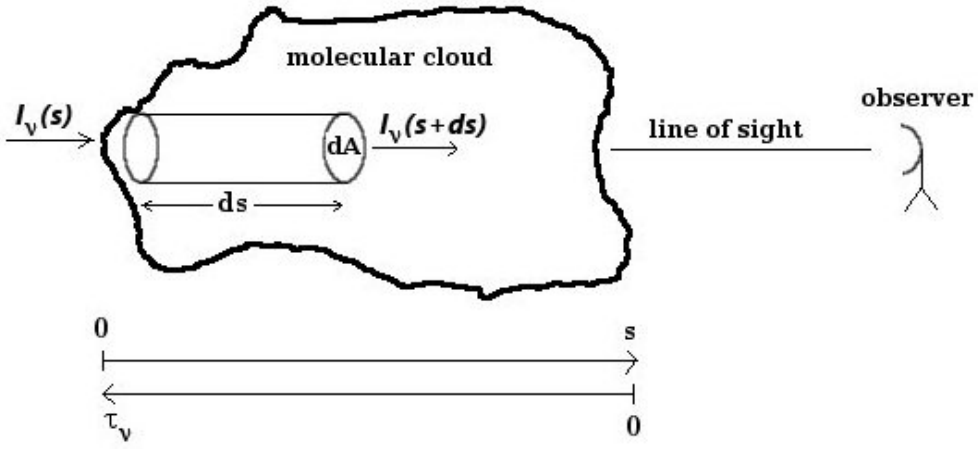

Figure 3.1: Illustrating radiative transfer through a molecular cloud.

where ϵ_0 is the vacuum permittivity, c is the speed of light, and $|\mu_{ul}|^2$ is the electric dipole moment matrix element. Following the definiton given by Condon & Shortley (1935), $|\mu_{ul}|^2 = \mu^2 S$, where μ is the permanent electric dipole moment of the molecule, and S is the line strength. Here, S is defined so that for a linear molecule transition $J \rightarrow J-1$, it is $S = J/(2J+1)$, and for a symmetric top molecule transition $(J,\ K) \rightarrow (J,\ K)$, it is $S = K^2/[J(J+1)]$, where J is the rotational quantum number of the upper state, and K is the projection of J on the molecule's symmetry axis. The Einstein coefficients are related to each other in the following way:

$$A_{ul} = \frac{2h\nu_{ul}^3}{c^2} B_{ul}\,, \tag{3.5}$$

$$g_l B_{lu} = g_u B_{ul}\,, \tag{3.6}$$

where g_u and g_l are the statistical weights (or level degeneracies) of the states u and l. From Eqs. (3.3) and (3.2), and using the relations (3.5) and (3.6), we get

$$\frac{\epsilon_\nu}{\kappa_\nu} = \frac{2h\nu_{ul}^3}{c^2} \frac{1}{\frac{n_l g_u}{n_u g_l} - 1}\,. \tag{3.7}$$

The excitation temperature, $T_{\rm ex}$, of the spectral line is defined according to the Boltzmann distribution:

$$\frac{n_u}{n_l} = \frac{g_u}{g_l} e^{-\frac{h\nu_{ul}}{k_{\rm B} T_{\rm ex}}}\,, \tag{3.8}$$

where $k_{\rm B}$ is the Boltzmann constant. With the aid of Eq. (3.8), we can write Eq. (3.7) as

$$\frac{\epsilon_\nu}{\kappa_\nu} = \frac{2h\nu_{ul}^3}{c^2}\frac{1}{e^{h\nu_{ul}/k_{\rm B}T_{\rm ex}}-1} = B_\nu(T_{\rm ex})\,, \tag{3.9}$$

where $B_\nu(T_{\rm ex})$ is the Planck function at the temperature $T_{\rm ex}$. Equation (3.9) is the so-called Kirchhoff's law. By using the Eqs. (3.6) and (3.8), we can write Eq. (3.2) as follows:

$$\kappa_\nu = \frac{h\nu_{ul}}{4\pi}\frac{B_{ul}}{F(T_{\rm ex})}n_u\phi(\nu)\,, \tag{3.10}$$

where the function $F(T)$ is defined by $F(T) \equiv \left(e^{h\nu_{ul}/k_{\rm B}T}-1\right)^{-1}$.

Integration of Eq. (3.3), and substitution of Eq. (3.4), yields

$$\int \epsilon_\nu {\rm d}\nu = \frac{4\pi^2\nu_{ul}^4}{3\epsilon_0 c^3}\mu^2 S n_u\,. \tag{3.11}$$

On the other hand, the optical thickness of a spectral line, τ_ν, is an integral of the absorption coefficient along the line of sight through the cloud (see Fig. 3.1):

$$\tau_\nu = \int \kappa_\nu {\rm d}s\,. \tag{3.12}$$

Next, we integrate Eq. (3.9) over the observed spectral line profile and along the line of sight:

$$\int\int \epsilon_\nu {\rm d}\nu {\rm d}s = B_\nu(T_{\rm ex})\int\int \kappa_\nu {\rm d}\nu {\rm d}s\,. \tag{3.13}$$

Here, we have assumed that $B_\nu(T_{\rm ex})$ is constant along the line of sight. Substitution of Eqs. (3.11) and (3.12) into Eq. (3.13) yields

$$\int \frac{4\pi^2\nu_{ul}^4}{3\epsilon_0 c^3}\mu^2 S n_u {\rm d}s = B_\nu(T_{\rm ex})\int \tau_\nu {\rm d}\nu\,. \tag{3.14}$$

The column density of the molecules in the upper state is defined by $N_u \equiv \int n_u {\rm d}s$. Using the latter definition and Eq. (3.9), and integrating τ_ν with respect to velocity (${\rm d}v = \frac{c}{\nu}{\rm d}\nu$), we get the following expression for N_u:

$$N_u = \frac{3h\epsilon_0}{2\pi^2}\frac{1}{\mu^2 S}F(T_{\rm ex})\int \tau(v){\rm d}v\,. \tag{3.15}$$

In order to calculate the total column density of a molecule from the column density in a single energy level, we need to use the partition function. N_u is related to the total molecular column density, $N_{\rm tot}$, as follows:

$$\frac{N_{\rm tot}}{N_u} = \frac{Z_{\rm rot}(T_{\rm ex})}{g_u g_K g_I}e^{E_u/k_{\rm B}T_{\rm ex}}\,, \tag{3.16}$$

where $Z_{\rm rot}(T_{\rm ex})$ is the rotational partition function, $g_u = 2J_u + 1$ is the rotational degeneracy of the upper state, g_K is the K-level degeneracy, g_I is the reduced nuclear

spin degeneracy (see, e.g., Turner 1991), and E_u is the upper state energy. Note that for linear molecules, $g_K = g_I = 1$ for all levels. By substituting Eq. (3.15) into (3.16), we get

$$N_{\rm tot} = \frac{3h\epsilon_0}{2\pi^2}\frac{1}{S\mu^2}\frac{Z_{\rm rot}(T_{\rm ex})}{g_u g_K g_I} e^{E_u/k_{\rm B}T_{\rm ex}} F(T_{\rm ex}) \int \tau(v){\rm d}v\,. \tag{3.17}$$

If the gas emitting the spectral line has a Gaussian distribution of line-of-sight velocities, i.e, the line profile, $\tau(v)$, can be represented by a Gaussian shape, we can write $\int \tau(v){\rm d}v = \frac{\sqrt{\pi}}{2\sqrt{\ln 2}}\Delta v \tau_0$, where Δv is the linewidth (full width at half maximum, FWHM), and τ_0 is the peak optical thickness of the line. In this case, column density can be calculated by using the formula

$$N_{\rm tot} = \frac{3h\epsilon_0}{4\pi^2}\sqrt{\frac{\pi}{\ln 2}}\frac{1}{S\mu^2}\frac{Z_{\rm rot}(T_{\rm ex})}{g_u g_K g_I} e^{E_u/k_{\rm B}T_{\rm ex}} F(T_{\rm ex}) \Delta v \tau_0\,. \tag{3.18}$$

In Papers I and V, spectral line intensities are presented in units of the antenna temperature corrected for atmospheric attenuation, $T_{\rm A}^*(v)$. In Paper II, the line intensity scales are given in units of the main-beam brightness temperature, $T_{\rm MB}$. The value of $T_{\rm MB}$ is given by $T_{\rm MB} = T_{\rm A}^*/\eta_{\rm MB}$, where the main beam efficiency of the telescope is $\eta_{\rm MB} = \frac{B_{\rm eff}}{F_{\rm eff}}$, and $B_{\rm eff}$ and $F_{\rm eff}$ are the telescope beam and forward efficiencies, respectively. The so-called antenna equation is given by

$$T_{\rm A}^*(v) = \eta\frac{h\nu}{k_{\rm B}}\left[F(T_{\rm ex}) - F(T_{\rm bg})\right]\left(1 - e^{-\tau(v)}\right)\,, \tag{3.19}$$

where $\eta \equiv \eta_{\rm MB} f_{\rm beam}$ is the beam-source coupling efficiency, $f_{\rm beam}$ is the beam filling factor, and $T_{\rm bg}$ is the background brightness temperature (in many directions it can be assumed to be equal to the cosmic microwave background temperature of 2.73 K). In the optically thin case, $\tau \ll 1$ ($e^{-\tau} \approx 1-\tau$), Eq. (3.19) can be used to express Eq. (3.17) as follows:

$$N_{\rm tot} = \frac{3k_{\rm B}\epsilon_0}{2\pi^2}\frac{1}{\nu S\mu^2}\frac{Z_{\rm rot}(T_{\rm ex})}{g_u g_K g_I}\frac{1}{1-\frac{F(T_{\rm bg})}{F(T_{\rm ex})}} e^{E_u/k_{\rm B}T_{\rm ex}}\frac{1}{\eta}\int T_{\rm A}^*(v){\rm d}v\,. \tag{3.20}$$

Equations (3.18) and (3.20) were used to calculate the column densities of the different molecules in Papers I, II, and V. By combining Eqs. (3.15) and (3.16) with the assumption that the lines are optically thin and $T_{\rm ex} \gg T_{\rm bg}$, and taking natural logarithms, one obtains the rotational diagram equation used in Paper V (Eq. (3) therein).

3.2 H_2 column density from (sub)millimetre dust continuum emission

The intensity emitted by a column of dust of temperature $T_{\rm d}$ and optical thickness τ_ν can be solved from Eq. (3.1), which, assuming an isothermal object without a background source, reads

$$I_\nu = B_\nu(T_\mathrm{d})\left(1 - e^{-\tau_\nu}\right) . \tag{3.21}$$

The optical thickness defined in Eq. (3.12) can be written as

$$\tau_\nu = \int \kappa_\nu \rho \mathrm{d}s \,, \tag{3.22}$$

where κ_ν [m^2 kg^{-1}] is now the specific absorption coefficient per unit mass of dust, i.e., the dust opacity, and ρ is the mass density.

In molecular clouds most hydrogen is in H_2 molecules. Thus, the H_2 column density can be related to τ_ν as

$$N(\mathrm{H_2}) = \int n(\mathrm{H_2})\mathrm{d}s = \int \frac{\rho}{\mu_{\mathrm{H_2}} m_\mathrm{H}} \mathrm{d}s = \frac{1}{\mu_{\mathrm{H_2}} m_\mathrm{H} \kappa_\nu} \int \kappa_\nu \rho \mathrm{d}s = \frac{\tau_\nu}{\mu_{\mathrm{H_2}} m_\mathrm{H} \kappa_\nu R_\mathrm{d}} \,, \tag{3.23}$$

where $n(H_2)$ is the H_2 number density, μ_{H_2} is the mean molecular weight per H_2 molecule (2.8 for gas consisting of H_2 and 10% He)[1], and m_H is the mass of the hydrogen atom. In the above equation, we have also introduced the dust-to-gas mass ratio, R_d. The round value 1/100 for R_d is used in the papers of this thesis although the true value in the Galaxy appears to be clearly smaller, i.e., $R_\mathrm{d} \approx 1/180 - 1/160$ (Zubko et al. 2004; Draine et al. 2007). In dense star-forming regions the value of R_d can be somewhat larger than 1/100, about $1/95 - 1/80$ (Vuong et al. 2003).

Thermal dust emission in the (sub)mm wavelengths is optically thin ($\tau_\nu \ll 1$; see Chapter 2). Consequently, Eq. (3.21) can be written as

$$I_\nu \approx B_\nu(T_\mathrm{d})\tau_\nu \,. \tag{3.24}$$

With the aid of Eq. (3.24), Eq. (3.23) can be expressed as

$$N(\mathrm{H_2}) = \frac{I_\nu}{B_\nu(T_\mathrm{d})\mu_{\mathrm{H_2}} m_\mathrm{H} \kappa_\nu R_\mathrm{d}} \,. \tag{3.25}$$

The H_2 column density calculations in Papers I, II, IV, and V are done by using Eq. (3.25).

3.3 Mass determination from dust continuum emission

The mass of the source can be calculated by integrating the mass surface density, $\Sigma = \mu_{\mathrm{H_2}} m_\mathrm{H} N(\mathrm{H_2})$, across the source:

$$M = \int \Sigma \mathrm{d}A = \mu_{\mathrm{H_2}} m_\mathrm{H} \int N(\mathrm{H_2})\mathrm{d}A \,. \tag{3.26}$$

[1] Here, instead of $\mu_{\mathrm{H_2}}$, the mean molecular weight per free particle, μ_p, is sometimes used (e.g., Paper V). $\mu_\mathrm{p} = 2.33$ for an abundance ratio H/He = 10, and a negligible amount of metals (heavier elements).

The surface element, $\mathrm{d}A$, is related to the solid angle element, $\mathrm{d}\Omega$, by $\mathrm{d}A = d^2\mathrm{d}\Omega$, where d is the source distance. Substitution of Eq. (3.25) into Eq. (3.26) yields

$$M = \frac{d^2}{B_\nu(T_\mathrm{d})\kappa_\nu R_\mathrm{d}} \int I_\nu \mathrm{d}\Omega \,. \tag{3.27}$$

Because the integrated flux density is $S_\nu = \int I_\nu \mathrm{d}\Omega$, Eq. (3.27) can be written as

$$M = \frac{S_\nu d^2}{B_\nu(T_\mathrm{d})\kappa_\nu R_\mathrm{d}} \,. \tag{3.28}$$

Equation (3.28) is used in Papers I, II, IV, and V to derive the clump and core masses.

3.4 Spectral index of thermal radio continuum emission

In an ionised gas, i.e., plasma, the electrons have a Maxwellian velocity distribution with electron temperature, T_e. Free-free emission, or bremsstrahlung, is produced when individual electrons are deflected in the electrostatic Coulomb fields of ions owing to their accelerated motions.

It can be shown, that the optical thickness in the case of thermal free-free radio continuum emission depends on the frequency as $\tau_\nu \propto \nu^{-2.1}$ (see Scheffler & Elsässer 1987, Sect. 5.1.3 therein). This frequency dependence results from the fact that for low radio frequencies the free-free Gaunt factor, g_ff, varies as $\nu^{-0.1}$. In the Rayleigh-Jeans approximation, $\frac{h\nu}{k_\mathrm{B}T} \ll 1$, the brightness temperature, $T_\mathrm{B} = \frac{T_\mathrm{A}^*}{\eta}$ (assuming the source is extended with respect to the beam, and that T_B is constant across the source), is given by (cf. Eq. (3.19))

$$T_\mathrm{B} = (T_\mathrm{e} - T_\mathrm{bg})\left(1 - e^{-\tau_\nu}\right) \approx T_\mathrm{e}\left(1 - e^{-\tau_\nu}\right) \,, \tag{3.29}$$

where it is assumed that $T_\mathrm{e} \gg T_\mathrm{bg}$.

At low frequencies, it can be assumed that the medium is optically thick, $\tau_\nu \propto \frac{1}{\nu^{2.1}} \gg 1$. Equation (3.29) then reduces to $T_\mathrm{B} \approx T_\mathrm{e}$. Furthermore, by using the definition of T_B

$$T_\mathrm{B} = \frac{\lambda^2}{2k_\mathrm{B}} I_\nu \,, \tag{3.30}$$

the source flux density can be written as

$$S_\nu = I_\nu \Omega_\mathrm{source} = \frac{2k_\mathrm{B}T_\mathrm{B}\nu^2}{c^2}\Omega_\mathrm{source} \propto \nu^2 \,, \tag{3.31}$$

where Ω_source is the solid angle subtended by the source. Thus, the medium behaves like a blackbody.

At high frequencies, the medium becomes optically thin ($\tau_\nu \ll 1$). From Eq. (3.29), it then follows that $T_\mathrm{B} \approx T_\mathrm{e}\tau_\nu \propto \nu^{-2.1}$. In this case, the flux density depends on frequency as

$$S_\nu = \frac{2k_\mathrm{B}T_\mathrm{B}\nu^2}{c^2}\Omega_\mathrm{source} \propto \nu^{-2.1}\nu^2 \propto \nu^{-0.1}\,. \tag{3.32}$$

Thus, the flux density is almost independent of frequency.

According to the above analysis, the spectral index, α, of thermal radio continuum emission is defined as

$$S_\nu \propto \nu^\alpha\,, \quad \alpha \in [-0.1,\, 2]\,. \tag{3.33}$$

This is illustrated in Fig. 3.2. When the source flux density is determined at two different frequencies, ν_1 and ν_2, the spectral index can be calculated as

$$\alpha = \frac{\ln(S_{\nu_1}/S_{\nu_2})}{\ln(\nu_1/\nu_2)}\,. \tag{3.34}$$

In Paper III, we examine the radio spectral indices of YSOs in the R CrA star-forming region.

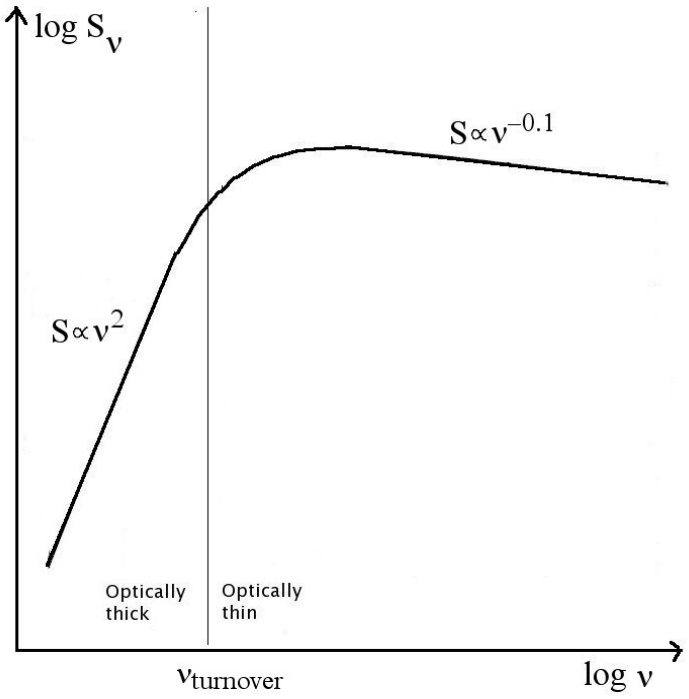

Figure 3.2: A schematic representation of the radio spectrum of thermal free-free emission. The vertical line indicates the turnover frequency, where $\tau_\nu = 1$.

Chapter 4

Low-mass star formation

Most papers of this thesis (Papers I–III) deal with the formation of low-mass ($\sim 0.1 - 2$ $M_\odot$) stars. Thus, this topic deserves a rather detailed introductory overview.

4.1 Low-mass starless/prestellar cores

The earliest observable precursors of forming stars are the dense starless cores within molecular clouds. In the beginning, these objects are just density enhancements with respect to their parent cloud[1]. Starless cores are compact (size ~ 0.1 pc, i.e., $\sim 2 \times 10^4$ AU), cold ($T_{\rm kin} \lesssim 10$ K), and dense ($n(H_2) \gtrsim 10^4$ cm^{-3}) condensations with typical masses of $\sim 1 - 10$ $M_\odot$ (di Francesco et al. 2007). Consequently, these cores are most easily identified as compact (sub)mm dust emission peaks (see, e.g., Fig. 1 in Paper I). Starless cores have no embedded IR point sources, neither do they show any other signs of star formation activity[2].

Only a subset of starless cores collapse into stars. Some of the cores have "too much" internal energy compared to their self-gravity, and they will eventually redisperse and merge with the surrounding cloud material (McKee & Ostriker 2007). Observations have suggested such a transient nature of some cores (e.g., Morata et al. 2005), and transient cores are also seen in numerical simulations of turbulence (Padoan & Nordlund 2002; Vázquez-Semadeni et al. 2005; Nakamura & Li 2005). In the simulations by Vázquez-Semadeni et al. (2005), the transient cores rarely exceeded peak densities of $\sim 5 \times 10^4$ cm^{-3}. Thus, they are expected to be rare in dust continuum surveys which are only sensitive to the high column density cores within the clouds (Motte & André 2001; Galván-Madrid et al. 2007; Hatchell & Fuller 2008).

By definition, those starless cores that are gravitationally bound, and will form stars at some point in the future, are called *prestellar* cores (see di Francesco et al. 2007; Ward-Thompson et al. 2007; André et al. 2009 for reviews). Prestellar cores are especially useful for the studies of the initial stages of the process because they best represent the physical and chemical conditions of gas and dust before star formation and are relatively simple objects (Bergin & Tafalla 2007). In what follows is an introduction to the main physical and chemical characteristics of these objects.

[1] The origin of starless cores is not well understood. This topic will be further discussed in Sect. 6.1.

[2] Some of the low-mass starless core candidates may contain very low-luminosity IR sources undetected so far (e.g., Dunham et al. 2008).

4.2 Physical properties of prestellar cores

4.2.1 Gas dynamics, kinematics, and thermodynamics

Prestellar cores are, by definition, gravitationally bound objects. To examine whether this is the case for a particular core, the relative importance of the gravitational and kinetic energies, U and T, needs to be estimated. This is often done by calculating the virial parameter, i.e., the ratio of the virial mass to core mass (Bertoldi & McKee 1992)

$$\alpha_{\rm vir} \equiv \frac{M_{\rm vir}}{M_{\rm core}} = \frac{5R\sigma_{\rm ave}^2}{aGM_{\rm core}} \,. \tag{4.1}$$

Here, G is the gravitational constant, R is the core radius, and $\sigma_{\rm ave}$ is the velocity dispersion of the "average" gas particles with a mean molecular mass $\mu = 2.33$. The quantity $\sigma_{\rm ave}$ can be derived from the observed velocity dispersion, $\sigma_{\rm obs}$, of emitting molecule as

$$\sigma_{\rm ave}^2 = \sigma_{\rm T}^2 + \sigma_{\rm NT}^2 = \sigma_{\rm obs}^2 + \frac{k_{\rm B}T_{\rm kin}}{m_{\rm H}} \left(\frac{1}{\mu} - \frac{1}{\mu_{\rm obs}} \right) , \tag{4.2}$$

where $\sigma_{\rm T}$ and $\sigma_{\rm NT}$ are the one-dimensional thermal and non-thermal velocity dispersions, respectively, $T_{\rm kin}$ is the gas kinetic temperature, and $\mu_{\rm obs}$ is the mass of the emitting molecule in units of atomic mass number (Myers et al. 1991b). The parameter $a = (1 - p/3)/(1 - 2p/5)$, where p is the power-law index of the density profile ($n(r) \propto r^{-p}$), is a correction for deviations from constant density (e.g., Enoch et al. 2008). $M_{\rm core}$ can be derived from the dust continuum emission as described in Sect. 3.3. Note that the inverse of Eq. (4.1) is also often used to study the core dynamical state (e.g., Papers I, IV, and V). The value $\alpha_{\rm vir} = 1$ corresponds to the virial equilibrium, $2\langle T \rangle = -\langle U \rangle$, where angle brackets represent the average over time. The self-gravitating limit, defined by $\langle T \rangle = -\langle U \rangle$, corresponds to $\alpha_{\rm vir} = 2$. As self-gravitating condensations, prestellar cores are expected to have virial parameters $\alpha_{\rm vir} < 2$.

Prestellar cores evolve towards higher degree of central concentration, and they are on the verge of collapse or already collapsing (see below), but there is no central hydrostatic protostar yet within the core (Ward-Thompson et al. 1994, 1999, 2002). Thus, high density starless cores are likely to be prestellar (e.g., Enoch et al. 2008; Papers I and II). Prestellar core morphologies vary from filamentary to roundish, but typically, they are *not* spherical in shape (i.e., circular in projection; e.g., Myers et al. 1991a). Instead, their shapes are more often elongated (prolate), which suggest that the cores are not in exact equilibrium or the presence of a non-symmetric force component (Jones et al. 2001; Goodwin et al. 2002; Bergin & Tafalla 2007).

The mean H_2 number densities of observed prestellar cores are $\gtrsim 5 - 10$ times higher than those of their parent molecular clouds (for H_2 column densities the factor is $\gtrsim 2$; e.g., André et al. 2009). The (column) density structures of prestellar cores typically show a uniform-density centre (flat radial profile) surrounded by a power-law envelope extending to an outer radius ~ 0.1 pc (e.g., Shirley et al. 2000; Bacmann et al. 2000; Evans et al. 2001; Alves et al. 2001; Kirk et al. 2005; Kandori et al. 2005; Schnee &

Goodman 2005). The explanation for this is that in the core centre, density fluctuations are smoothed out by pressure waves, and the gas is confined by the overlying gas pressure (and not by the weak self-gravity; e.g., Keto & Caselli 2010). The profiles can be successfully approximated by Bonnor-Ebert (BE) spheres that describe a self-gravitating, non-rotating, non-magnetised, pressure confined isothermal sphere in hydrostatic equilibrium (Ebert 1955; Bonnor 1956). The observed core centre-to-edge density contrasts often exceed the maximum value of ≈ 14 allowed for a stable BE sphere (e.g., Evans et al. 2001). It has also been found in numerical simulations that dense cores formed within turbulent flows (Sect. 6.1) can have density profiles resembling BE spheres (Ballesteros-Paredes et al. 2003).

Some prestellar cores show kinematic evidence of central infall, i.e., spectral line profiles show a double peaked-feature with the blueshifted peak being stronger than the redshifted peak (e.g., Lee et al. 1999; Sohn et al. 2007). For example, the best-studied prestellar core, L1544 in Taurus, shows infall asymmetry on scales from 0.01 to 0.1 pc (Ohashi et al. 1999). Such detections are among the key indicators of the process leading to star formation. Indeed, prestellar cores offer a unique opportunity to study infall motions because they are not contaminated by e.g., protostellar outflows (Myers et al. 2000).

The main supporting agent against gravity in prestellar cores is thermal pressure, $p_{\rm T} = nk_{\rm B}T_{\rm kin}$, where n is the gas number density. Internal pressure has also a non-thermal component, which is widely accepted to be mainly due to turbulence and is thus given by $p_{\rm NT} = \mu m_{\rm H} n \sigma_{\rm NT}^2$. Observations have shown that low-mass prestellar cores are quiescent, i.e., they have subsonic ($\sigma_{\rm NT} < c_{\rm s}$) levels of internal turbulence, or at best transonic ($\sigma_{\rm NT} < 2c_{\rm s}$) (e.g., Myers & Benson 1983; Myers 1983; Jijina et al. 1999; Kirk et al. 2007; André et al. 2007; Lada et al. 2008; Paper II). The one-dimensional isothermal sound speed is $c_{\rm s} = \sqrt{\frac{k_{\rm B}T_{\rm kin}}{\mu m_{\rm H}}} = 0.19$ km s^{-1} for a 10 K gas assuming $\mu = 2.33$. Quiescent cores are also seen in turbulent simulations of core formation (Klessen et al. 2005; Offner et al. 2008, see Sect. 6.1). Transition from a turbulent molecular cloud to the quiescent core regime is a critical step in star formation process (e.g., Pineda et al. 2010; see Chapter 6). We note that the amount of turbulence within a core may increase due to the influence of a nearby/associated young stellar cluster (e.g., Caselli & Myers 1995; Ikeda et al. 2007; Foster et al. 2009). Dense cores are also observed to be rotating. However, it is well-known that rotation is not energetically important for the core support against self-gravity (e.g., Goodman et al. 1993; Jijina et al. 1999; Caselli et al. 2002a).

High densities of prestellar cores lead to very low gas temperatures in the core centres. Gas and dust temperatures in the central few thousand AU can be as low as $6 - 7$ K (Evans et al. 2001; Pagani et al. 2003, 2004; Young et al. 2004; Schnee & Goodman 2005; Pagani et al. 2007; Crapsi et al. 2007; Harju et al. 2008). Kinetic temperature of the gas is very close to dust temperature at densities $n({\rm H_2}) \geq 10^5$ cm^{-3}, because at these densities the gas and dust are thermally coupled via collisions (e.g., Goldsmith & Langer 1978). The gas cools through molecular line emission (mainly through rotational transitions of carbon species, such as CO and CS; e.g., Goldsmith 2001) and collisional

coupling with dust, where the impacting molecule imparts its energy to the grain lattice. These two mechanisms are equally efficient when the density is a few times 10^5 cm^{-3}; this density defines the boundary between thermally subcritical (line cooling dominates) and supercritical (coupling with dust cools the gas) cores (Keto & Caselli 2008). Because of the high extinction in prestellar cores, the primary heating mechanism of gas is the cosmic-ray heating due to ionising collisions (cf. Sect. 4.3.1). Photoelectric heating, where electrons removed from the dust grains heat the gas, is negligible at $A_{\rm V} \gtrsim 1$ (e.g., Keto & Caselli 2008). The dust component is cooled by optically thin thermal emission at far infrared (FIR) wavelengths, and it is predominantly heated externally by the interstellar radiation field (ISRF; e.g., Evans et al. 2001; Zucconi et al. 2001; Stamatellos et al. 2004; di Francesco et al. 2007). The core temperature decreases towards the centre because the molecular cooling rates depend strongly on density (which increases towards the centre), and because the central parts of the core are well-shielded from the ISRF. The above mentioned heating and cooling processes lead to an equilibrium temperature of ~ 10 K (e.g., Galli et al. 2002; Tafalla et al. 2004). The core temperature may also depend on the environment where the core resides: recently, Schnee et al. (2009) found that cores in clusters appeared to be warmer than cores unassociated with a cluster (see also Paper II). Because prestellar cores are cold, they emit almost all of their radiation at FIR and submm wavelengths (see Fig. 4.1). Low temperature also causes the dust grains in the deep interiors of prestellar cores to become coated with ice mantles and coagulate to form fluffy aggregates. These processes change the emissivity of dust grains (e.g., Ossenkopf & Henning 1994; Keto & Caselli 2008).

It is not clear yet how many stars an individual prestellar core typically forms. High-resolution observations have suggested that individual cores produce $2-3$ stars at most (e.g., Kirk et al. 2009; see also Goodwin & Kroupa 2005 and references therein). In the case the core forms a multiple stellar system, it is believed to take place *after* the prestellar stage by subsequent dynamical fragmentation during the collapse phase, i.e., close to the time of protostar formation (e.g., André et al. 2007; see Goodwin et al. 2007 for a review).

4.2.2 The role of magnetic field in the core dynamics

The role of magnetic fields in the star formation process is believed to be important, but is still a matter of debate (see Sect. 4.8 and references therein). For example, the coupling between the core and its surrounding envelope by magnetic field lines can provide a mechanism for transporting angular momentum outward from collapsing cores, and thus make it possible for stars to form (so-called "magnetic braking"; e.g., Mellon & Li 2008 and references therein). Magnetic fields are also likely to play a significant role in the physics of disk accretion and protostellar outflows. The role of magnetic field is difficult to determine because the magnetic field strength in a molecular cloud or cloud core is probably its most difficult property to measure. The primary method of measuring the magnetic fields in the dense interstellar medium (ISM) is based on the Zeeman effect. This method measures the line-of-sight component of the magnetic field, $B_{\rm los}$ (see the reviews by Crutcher (2005) and Heiles & Crutcher (2005)). Especially in

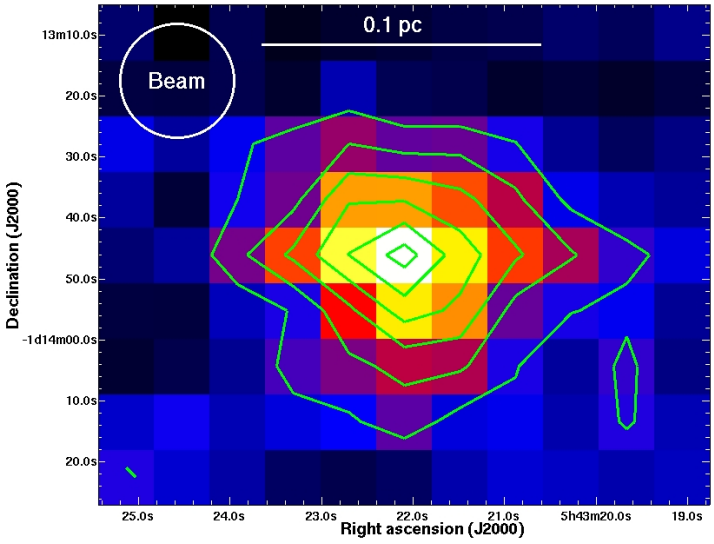

Figure 4.1: LABOCA 870 μm dust continuum image of the prestellar core SMM 7 seen towards the Orion B9 star-forming region. The core mass, effective radius, average H_2 number density, kinetic temperature, and non-thermal velocity dispersion are $M = 3.6 \pm 1.0$ $M_\odot$, $R_{\rm eff} = 0.07$ pc, $\langle n(H_2) \rangle = 4.8 \pm 1.3 \times 10^4$ cm^{-3}, $T_{\rm kin} = 9.4 \pm 1.1$ K, and $\sigma_{\rm NT} = 0.25$ km s^{-1}, respectively (Papers I and II). The contour levels go from 0.05 to 0.30 Jy beam^{-1} in steps of 0.05 Jy beam^{-1}. The beam HPBW (half-power beam width) of 18.6$''$ is shown in the top left corner. Enlargement of Fig. 1 of Paper I.

the case of low-mass star-forming regions, there is only a small number of observational constraints for magnetic fields (Turner & Heiles 2006). For instance, Troland & Crutcher (2008) examined altogether 34 cores in the well-known regions of low-mass star formation (e.g., Taurus and Perseus) in their Arecibo OH Zeeman survey. The Zeeman effect was seen in only 9 cores with $B_{\rm los}$ values in the range $\sim 9-26$ μG. Observational results by Troland & Crutcher (2008) suggest that the magnetic field energy in the cores is slightly subdominant to those contributed by gravity and turbulence. Their results conform with the earlier studies suggesting that both turbulence and magnetic field appear to play a roughly equal role in the support against gravitational collapse (e.g., also Kirk et al. 2006; Ward-Thompson et al. 2007).

The key parameter that defines the importance of a static magnetic field for the support against gravitational collapse is the mass-to-magnetic flux ratio, $M/\Phi_{\rm B}$ (e.g., Crutcher 1999; Crutcher et al. 2009). There is a critical mass-to-flux ratio, $(M/\Phi)_{\rm crit}$, above which the core cannot be supported by the magnetic field alone. For a spherical cloud $(M/\Phi)_{\rm crit} \simeq 0.13/\sqrt{G}$ (e.g., Mouschovias & Spitzer 1976). Thus, $M/\Phi_{\rm B}$ is often normalised to this critical value as

$$\lambda \equiv \frac{(M/\Phi)_{\rm observed}}{(M/\Phi)_{\rm crit}} \,. \tag{4.3}$$

If $\lambda > 1$, the core is said to be magnetically supercritical and the magnetic field is too weak for support against gravitational collapse by magnetic pressure alone. If the magnetic field is not strong enough to stop the initial collapse, its compression during the collapse cannot bring the core into equilibrium and halt the collapse. If $\lambda < 1$, the core is called magnetically subcritical and its self-gravity is counter-balanced by the magnetic field. In a magnetically critical core, the energy density of the magnetic field exactly balances the gravitational potential energy. Troland & Crutcher (2008) found that the mean value of λ in their sample of dense cores is $\bar{\lambda} \approx 2$, i.e., approximately critical or slightly supercritical (note that this value cannot rule out either extreme-case theory of low-mass star formation, see Sects. 4.8 and 6.5). Other observational results also suggest that, on average, cores are close to magnetically critical state (e.g., Falgarone et al. 2008; see André et al. 2009 for a review).

Another approach to examine the importance of a magnetic field is through the core morphology. This is based on the fact that magnetic forces act only perpendicular to the field lines. Due to the magnetic field, an initially spherical cloud core flattens along the field lines, while it remains supported perpendicular to the field lines. Thus, if the magnetic field is strong, the core should have an oblate spheroid or disk-like morphology, with minor axis parallel to the magnetic field direction (e.g., Crutcher et al. 2004). Such morphologies are predicted by the models of the evolution of self-gravitating cores supported by magnetic fields (e.g., Ciolek & Mouschovias 1994; Li & Shu 1996), but are in contradiction with observations.

The magnetic field only acts directly on charged particles, i.e., electrons, ions, and charged dust grains. However, the neutral particles can feel the presence of a magnetic field through collisions with charged particles. This "ion-neutral coupling" is weak in

dense cores because of the low level of ionisation, and thus the magnetic field is expected to be frozen only into the ions. In the presence of a magnetic field, the plasma may contain magnetohydrodynamic (MHD) waves. Non-thermal motions within the core can, in part, be caused by MHD fluctuations (Arons & Max 1975; see Paper I). Thus, MHD waves could provide support against gravity.

4.3 Chemistry of prestellar cores

The chemistry of dense cores is very sensitive to physical parameters discussed above (temperature, density, radiation field). In cold prestellar cores prior to star formation, the chemistry is triggered by cosmic-ray ionisation, and afterwards, it is dominated by low-temperature gas-phase ion-molecule reactions (see van Dishoeck & Blake 1998 for a review). The cold prestellar phase of star formation is characterised by such a high density that most molecules accrete onto the dust grains and form an icy mantle around them. This molecular freeze-out (depletion) together with ion-molecule chemistry are closely related to deuterium fractionation, which is another important factor in the chemistry of dense cores. In what follows, is an overview of these three topics.

4.3.1 Cosmic-ray ionisation and the ionisation degree

The ionisation degree (i.e., the electron abundance) is a very important parameter for the core dynamics. It determines the coupling between the gas and the magnetic field, and hence the timescale for ambipolar diffusion (see Sect. 4.8). Also, for instance, the damping of MHD waves which can also support the core depends on the ionisation degree (Kulsrud & Pearce 1969; Zweibel & Josafatsson 1983). The abundance of electrons has also a crucial role in the chemistry of molecular clouds and cores.

At the low temperature ($T \sim 10$ K) and high density ($n(\mathrm{H_2}) \gtrsim 10^4$ cm^{-3}) of prestellar cores, the main type of chemical reactions in the gas phase are ion-molecule reactions (Herbst & Klemperer 1973; Oppenheimer & Dalgarno 1974). These reactions usually do not have any activation barrier due to the strong long-range attraction force, and they usually proceed at about Langevin rate of $\sim 10^{-9}$ cm^3 s^{-1}.

The ion chemistry is initiated when $\mathrm{H_2}$ is ionised by low-energy cosmic rays (protons, electrons, and heavy nuclei)[3]. Cosmic ray particles are the primary source of ionisation when visual extinction is $A_\mathrm{V} > 4$ mag; at $A_\mathrm{V} < 4$ mag, the ionisation is dominated by ultraviolet (UV) photoionisation (McKee 1989). Thus, photoionisation is not believed to be important for dense prestellar cores.

In dense molecular clouds $\sim 97\%$ of the impacts between cosmic ray particles and $\mathrm{H_2}$ molecules lead to the formation of $\mathrm{H_2^+}$:

[3]In the case of protons and heavy nuclei, most of the ionisation is provided by particles with energies between 1 MeV–1 GeV (also protons with energies in the range 1–100 keV play a role). In the case of electrons, the energy range 10 keV–10 MeV is the most important one in the ionisation process (see Padovani et al. 2009)

$$\mathrm{H_2 + crp} \overset{\zeta_{\mathrm{H_2}}}{\rightarrow} \mathrm{H_2^+ + e^- + crp}\,, \tag{4.4}$$

where $\zeta_{\mathrm{H_2}}$ [$\mathrm{s^{-1}}$] is the cosmic-ray ionisation rate of $\mathrm{H_2}$. Reaction (4.4) is followed by the very rapid reaction

$$\mathrm{H_2^+ + H_2} \overset{k_1}{\rightarrow} \mathrm{H_3^+ + H}\,, \tag{4.5}$$

where k_1 [$\mathrm{cm^3\ s^{-1}}$] is the associated rate coefficient. The resulting trihydrogen ion, $\mathrm{H_3^+}$, is destroyed through dissociative electron recombination with the rate $k_{\mathrm{dr},1}$:

$$\mathrm{H_3^+ + e^-} \overset{k_{\mathrm{dr},1}}{\rightarrow} \mathrm{H_2 + H}\,. \tag{4.6}$$

$\mathrm{H_3^+}$ has a pivotal role in interstellar chemistry (see, e.g., reaction (4.17)). Due to its low proton affinity (proton can be easily removed), $\mathrm{H_3^+}$ reacts with several atomic and molecular species, leading to a rich ion-molecule chemistry. $\mathrm{H_3^+}$ has no permanent dipole moment, and thus its rotational transitions are not allowed (but see, e.g., McCall et al. 1999 for NIR absorption observations). Besides the deuteration reaction (4.17), $\mathrm{H_3^+}$ reacts with e.g., CO and $\mathrm{N_2}$, producing $\mathrm{HCO^+}$ and $\mathrm{N_2H^+}$ in the protonation reactions (with the rates k_2 and k_3, respectively):

$$\mathrm{H_3^+ + CO} \overset{k_2}{\rightarrow} \mathrm{HCO^+ + H_2}\,, \tag{4.7}$$

$$\mathrm{H_3^+ + N_2} \overset{k_3}{\rightarrow} \mathrm{N_2H^+ + H_2}\,. \tag{4.8}$$

$\mathrm{HCO^+}$ produced in the above reaction is destroyed, for example, by dissociative recombination

$$\mathrm{HCO^+ + e^-} \overset{k_{\mathrm{dr},2}}{\rightarrow} \mathrm{CO + H}\,. \tag{4.9}$$

At steady state ($\mathrm{d}n/\mathrm{d}t = 0$), reactions (4.7) and (4.9) lead to the $\mathrm{HCO^+}$ abundance, $x(\mathrm{HCO^+}) \equiv n(\mathrm{HCO^+})/n(\mathrm{H_2})$, given by

$$x(\mathrm{HCO^+}) = \frac{k_2 x(\mathrm{H_3^+}) x(\mathrm{CO})}{k_{\mathrm{dr},2} x(\mathrm{e})}\,. \tag{4.10}$$

Similarly, ignoring reaction (4.7) (taking to be negligible depletion channel), the $\mathrm{H_3^+}$ abundance can be written as

$$x(\mathrm{H_3^+}) = \frac{k_1 x(\mathrm{H_2^+})}{k_{\mathrm{dr},1} x(\mathrm{e})}\,. \tag{4.11}$$

From the reactions (4.4) and (4.5), it follows that

$$x(\mathrm{H_2^+}) = \frac{\zeta_{\mathrm{H_2}}}{k_1 n(\mathrm{H_2})}\,. \tag{4.12}$$

By combining Eqs. (4.10)-(4.12), we get the following expression for the ionisation fraction:

$$x(\mathrm{e}) = C \left(\frac{\zeta_{\mathrm{H_2}}}{n(\mathrm{H_2})} \right)^{1/2} , \tag{4.13}$$

where the factor C includes the rate coefficients and the fractional abundances of CO and HCO^+ (typically, $x(\mathrm{CO})/x(\mathrm{HCO^+}) \sim 10^4$). The above analysis demonstrates how the ionisation degree in dense cores is determined by cosmic-ray ionisation and dissociative recombination. The value of $\zeta_{\mathrm{H_2}}$ is commonly adopted to be $\approx 10^{-17}$ s^{-1}, the so-called "standard" cosmic-ray ionisation rate in molecular clouds (e.g., McKee 1989). By using this value of $\zeta_{\mathrm{H_2}}$, one ends up with the relation $x(\mathrm{e}) \sim 10^{-5}/\sqrt{n(\mathrm{H_2})}$ (cf. (4.13)).

From the observational point of view, the values of $\zeta_{\mathrm{H_2}}$ and $x(\mathrm{e})$ in dense cores can be constrained by determining the abundances of several ionic species, in particular HCO^+, DCO^+, N_2H^+, and N_2D^+ (e.g., Wootten et al. 1982; Guélin et al. 1982; Caselli et al. 1998; Williams et al. 1998; van der Tak & van Dishoeck 2000; Doty et al. 2002; Maret & Bergin 2007; Goicoechea et al. 2009; Paper I). However, N_2H^+ and N_2D^+ are better tracers of the ionisation degree in the nuclei of dense cores where HCO^+ and DCO^+ are (presumably) depleted (Caselli et al. 2002b; see Sect. 4.3.2). Studies of low-mass dense cores have revealed significant variations in both $\zeta_{\mathrm{H_2}}$ and $x(\mathrm{e})$ from core to core within a range $\sim 10^{-18} - 10^{-16}$ s^{-1} and $10^{-8} - 10^{-6}$, respectively (Caselli et al. 1998; Williams et al. 1998). Maret & Bergin (2007) concluded that $\zeta_{\mathrm{H_2}} = 1 - 6 \times 10^{-17}$ s^{-1} in the B68 prestellar core, and Flower et al. (2007) reported a value of $\zeta_{\mathrm{H_2}} = 2 \times 10^{-18}$ s^{-1} in TMC-1. In Paper I, we determined about an order of magnitude higher values of $\zeta_{\mathrm{H_2}}$ compared to the "standard" value, and the values of $x(\mathrm{e}) \sim 10^{-7}$ towards the selected positions in Orion B9. In general, large variations in the value of $\zeta_{\mathrm{H_2}}$ are known to exist in the Galaxy (Oka et al. 2005; van der Tak et al. 2006; Dalgarno 2006). The rate $\zeta_{\mathrm{H_2}}$ may also vary with position in dense molecular clouds (e.g., Flower et al. 2007). Umebayashi & Nakano (1981) studied the propagation of cosmic rays in interstellar clouds and concluded that the exponential attenuation of $\zeta_{\mathrm{H_2}}$ sets in for H_2 column densities larger than $\sim 10^{25}$ cm^{-2}. For the lower column densities of $\sim 10^{19} - 10^{25}$ cm^{-2}, Padovani et al. (2009) found that $\zeta_{\mathrm{H_2}}$ decreases with increasing column density as $\zeta_{\mathrm{H_2}} \propto N(\mathrm{H_2})^{-a}$ with $a \approx 0.4 - 0.8$. The physical origin of the large variations in $x(\mathrm{e})$ is not well understood. It is related, at least partly, to variations in the core density (Eq. (4.13)), the amount of metal depletion (see below), and the evolutionary stage (Padoan et al. 2004). Caselli et al. (1998) and Williams et al. (1998) found that there is no significant difference in the ionisation fraction between cores with embedded stars and those without, i.e., prestellar cores.

In the case of complete depletion of heavy elements, H^+ and H_3^+ together with its deuterated forms H_2D^+, D_2H^+ and D_3^+ are supposed to become the dominant ionic species in the centres of cold, dense cores (Walmsley et al. 2004; Flower et al. 2005, 2006b; see Fig. 4.3). In the outer layers of prestellar cores (where C-bearing species are still mainly in the gas phase), the main molecular ion is thought to be HCO^+ (e.g., di Francesco et al. 2007). Thus, it is very important to estimate the amount of molecular

depletion in order to reliably determine the ionisation degree (Caselli 2002). In Paper I, we concluded that the dominant ionic species in selected positions in Orion B9 is probably H^+ or HCO^+. The information on the the dominant ionic species is important when estimating the ambipolar diffusion timescale (see Sect. 4.8). Moreover, Walmsley et al. (2004) and Flower et al. (2005) have shown that ion abundances depend on the charge and size distributions of dust grains; the recombination timescale on dust grain surfaces depends on the grain size and, consequently, $x(\mathrm{e})$ depends on the grain size. However, the grain size distribution in prestellar cores is not known; it depends on the timescales for grain coagulation and mantle accretion (relative to the dynamical and chemical timescales; Walmsley et al. 2004). We note that the fraction of positively charged grains in dense clouds is always negligible (Walmsley et al. 2004; Flower et al. 2005; see also Weingartner & Draine 2001)[4].

Besides ionisation, cosmic rays are also the dominant source of heating of the gas shielded from ISRF. Moreover, cosmic rays can return weakly bound ice mantle species, such as N_2, back into the gas phase (the so-called cosmic ray driven desorption; Léger et al. 1985).

4.3.2 Molecular freeze-out

The low temperature and high density of prestellar cores lead to the freeze out of many of the molecules from the gas phase onto the dust grain surfaces. Freeze-out is one of the mechanisms of molecular depletion others being destructive gas phase reactions, and it was predicted theoretically before observational results (e.g., Léger 1983). Molecular freeze-out is particularly important for C-bearing species. This means that the usual spectroscopic tools, such as CO, CS, and their isotopologues, are not good probes of dense interiors of prestellar cores.

In particular, the amount of CO depletion is often described by the CO depletion factor, f_D. It is defined as the ratio between the "canonical" (undepleted) fractional abundance of CO, $x(\mathrm{CO})_\mathrm{can} \sim 10^{-4}$ (Frerking et al. 1982), and the observed CO abundance:

$$f_\mathrm{D} = \frac{x(\mathrm{CO})_\mathrm{can}}{x(\mathrm{CO})_\mathrm{obs}} \,. \tag{4.14}$$

In other words, $1/f_\mathrm{D}$ is the fraction of CO molecules left in the gas phase. The timescale for freeze out (or adsorption timescale) of molecules onto dust grains is (e.g., Rawlings et al. 1992)

$$\tau_\mathrm{freeze} = \left(n_\mathrm{g} \pi a_\mathrm{g}^2 v_\mathrm{th} S\right)^{-1} \,, \tag{4.15}$$

where n_g is the grain number density, a_g is a mean grain radius (πa_g^2 is the mean cross section of the dust grains, and $n_\mathrm{g} \pi a_\mathrm{g}^2$ is the grain opacity), v_th is the thermal speed of the species which sticks to the dust grain, and S is the sticking coefficient (or sticking

[4] In molecular clouds, dust grains are primarily charged by the collisional attachment of free electrons and ions.

probability). In the low temperature medium, the molecular sticking coefficients are expected to be unity, i.e., a molecule sticks to the dust grain in each collision (Draine & Sutin 1987; Bisschop et al. 2006). At low temperature (≈ 10 K) and high density ($n(\mathrm{H_2}) \approx 10^5$ cm^{-3}) of prestellar cores, the freeze-out timescale of CO is only $\sim 5.8 \times 10^4$ yr (assuming the dust-to-gas abundance ratio $n_\mathrm{g} = 3.2 \times 10^{-12} n(\mathrm{H_2})$, a "standard" mean grain radius of $a_\mathrm{g} = 0.1$ μm, and $S \simeq 1$). However, if dust grains coagulate in the dense interiors of prestellar cores, the freeze-out rate decreases because the total grain surface area decreases (see, e.g., Flower et al. 2006b; Vastel et al. 2006).

Strong depletion of CO and its isotopologues has been observed in a variety of dense cores (e.g., Willacy et al. 1998; Caselli et al. 1999; Kramer et al. 1999; Bergin et al. 2001; Bacmann et al. 2002; Redman et al. 2002; Tafalla et al. 2002; Bergin et al. 2002; Lee et al. 2003; Tafalla et al. 2004, 2006; Chen et al. 2009; Pagani et al. 2010). For their sample of 7 prestellar cores, Bacmann et al. (2002) found that the amount of CO depletion appears to increase with density as $f_\mathrm{D} \propto n(\mathrm{H_2})^{0.4-0.8}$. One of the most heavily CO-depleted prestellar cores is L1544, for which $f_\mathrm{D} \sim 10$ (Caselli et al. 2003). We note that there are also high-density ($\sim 10^5$ cm^{-3}) cores where CO depletion is not prominent, like L1495B, L1521B, and L1521E (Hirota et al. 2004; Tafalla & Santiago 2004). These cores are considered to be both chemically and dynamically young.

It has been found that N-bearing species, especially chemically closely related $\mathrm{N_2H^+}$ and $\mathrm{NH_3}$, remain in the gas phase at densities for which CO and other C-containing species have already frozen onto grains, i.e., at $n(\mathrm{H_2}) > 10^5$ cm^{-3} (for theoretical models, see Bergin & Langer 1997; Aikawa et al. 2001, 2003; for observations, see Caselli et al. 2002a; Papers I and II). The $\mathrm{N_2H^+}$ distribution is often found to closely follow the dust distribution traced by the continuum observations (e.g., Bacmann et al. 2002; Caselli et al. 2002b; Tafalla et al. 2002; Crapsi et al. 2004, 2005), and $\mathrm{NH_3}$ abundance seems to even increase towards the core centres (Tafalla et al. 2002). Thus, $\mathrm{N_2H^+}$ and $\mathrm{NH_3}$ are some of the best tracers of the prestellar phase of core evolution.

The reason for different freeze-out behaviour of N- and C-containing species is not well understood. It has been found by laboratory experiments that $\mathrm{N_2}$, the parent species of both $\mathrm{N_2H^+}$ and $\mathrm{NH_3}$, should freeze out at the same rate as CO (their binding energies are similar, e.g., $E_\mathrm{b}/k_\mathrm{B} = 1100$ K for CO, and 982.3 K for $\mathrm{N_2}$ on mixed CO-$\mathrm{H_2O}$ ice, and their sticking coefficients are also similar ($S = 1$); Öberg et al. 2005; Bisschop et al. 2006). On the other hand, $\mathrm{N_2H^+}$ is mainly destroyed by CO in the gas phase through the proton transfer reaction (e.g., Aikawa et al. 2005)

$$\mathrm{N_2H^+ + CO \rightarrow HCO^+ + N_2}\,, \tag{4.16}$$

and hence the rate of $\mathrm{N_2H^+}$ destruction decreases with increasing CO depletion (e.g., Bergin et al. 2002; Jørgensen et al. 2004b). In addition, $\mathrm{N_2}$, from which $\mathrm{N_2H^+}$ is formed (reaction (4.8)), forms slowly (much slower than CO) in the gas phase via neutral-neutral reactions such as $\mathrm{NO + N \rightarrow N_2 + O}$. Atomic nitrogen has a lower binding energy than $\mathrm{N_2}$ and CO, and a sticking coefficient lower than unity (Flower et al. 2006a; Akyilmaz et al. 2007). Slow formation of $\mathrm{N_2}$ further helps to maintain the N-bearing species in the gas phase (see also Maret et al. 2006).

Theoretical models have suggested that N_2H^+ starts to freeze-out at densities $\sim 10^6$ to 3×10^7 cm^{-3} (Bergin & Langer 1997; Aikawa et al. 2003). Indeed, observational works have found evidence of N_2H^+ depletion in dense cores (Bergin et al. 2002; Caselli et al. 2002a; Lee et al. 2003; Belloche & André 2004; Crapsi et al. 2004; Jørgensen 2004; di Francesco et al. 2004; Pagani et al. 2005, 2007; Schnee et al. 2007; Chen et al. 2008; Friesen et al. 2010). In Papers I and II, we found evidence for N_2H^+ depletion in the dense core SMM 4 in Orion B9: the core's submm dust peak does not correspond to any of the maxima in the $N_2H^+(1-0)$ map of the region, and the $N_2H^+(3-2)$ line was not detected towards this source. The regions where N_2H^+ is depleted are often called N_2H^+ "holes".

Because N_2H^+ is quickly destroyed when CO is released from dust grains back into the gas phase (see above), it is beside other N-bearing species considered a "late time" molecule (its abundance does not increase until CO is significantly depleted; e.g., Suzuki et al. 1992; Bergin & Langer 1997; Lee et al. 2003; Aikawa et al. 2005)[5]. Detailed chemical models indicate that the N_2H^+ abundance increases after $\sim 10^5$ yr (e.g., Aikawa et al. 2003). Although it has been found that the NH_3 abundance increases towards the core centres in some cases (see above), there are also indications that NH_3 freezes out at very high core densities (see Paper II and references therein). In Paper II, we found that the fractional abundance of NH_3 appears to decrease with increasing H_2 column and number densities, suggesting that NH_3 freezes out when the density becomes high enough (see Fig. 4.2).

As a result of different freeze-out behaviour of different molecules dense cores have a differentiated chemical composition, i.e. "onion-like" chemical structure as illustrated in Fig. 4.3. Central parts of the core are rich in N_2H^+ and NH_3, whereas outer layers contain C-bearing species. In the densest regions of the core nucleus, most species containing C, N, and O atoms freeze out onto the dust grains, and only light ions (such as H^+ and H_3^+) remain in the gas phase. Depletion of molecules hampers the observational studies of prestellar cores because the number of available tracers is limited. Moreover, chemical stratification complicates the interpretation of spectral line observations. Because gas and dust are efficiently coupled at densities where CO depletion is significant the effect of CO depletion and the freeze out of other molecular coolants on the gas temperature, and thus the density structure, is quite small; the gas temperatures in the cores where CO is depleted, and in the cores where CO is not depleted, are approximately the same (see Pavlyuchenkov et al. 2007; Keto & Caselli 2008). The depletion of CO has an important role in the process of deuterium fractionation, which will be discussed next.

4.3.3 Deuterium fractionation

In Paper I, we study the degree of deuteration in N_2H^+, i.e., the N_2D^+/N_2H^+ abundance ratio in dense cores in Orion B9. This section gives an overview of the process of deuterium fractionation.

[5]Carbon-chain molecules, on the other hand, are considered "early time" molecules, i.e., they are abundant in chemically young cores and depleted in more evolved cores.

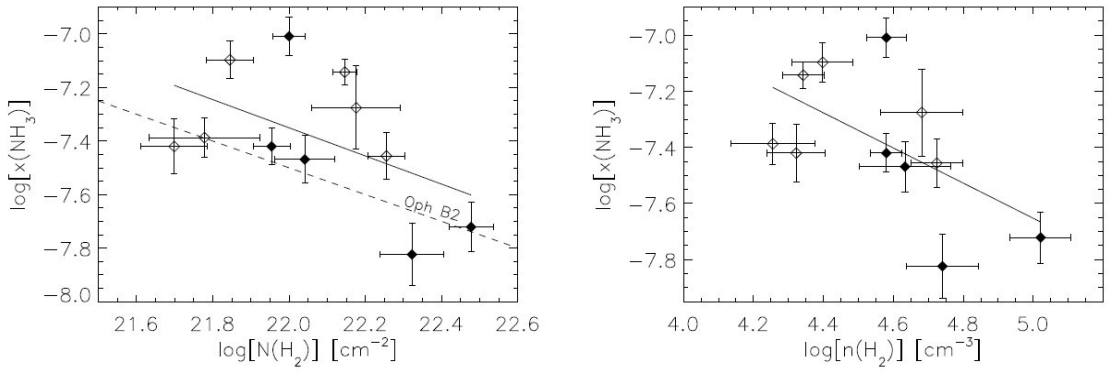

Figure 4.2: The fractional abundance of NH_3 versus the peak H_2 column density (left) and number density (right) in the Orion B9 cores. The solid lines represent the least-squares fits to the data, and the dashed line in the left panel indicates the relation derived by Friesen et al. (2010) for Oph B2. Both relations in the left panel are of the form $x(\mathrm{NH_3}) \propto 1/\sqrt{N(\mathrm{H_2})}$. In the right panel, the best-fit relation is $x(\mathrm{NH_3}) \propto n(\mathrm{H_2})^{-0.6\pm0.3}$. These results suggest that NH_3 freeze out at high densities. The filled and open circles indicate the protostellar and starless cores, respectively. Adapted from Paper II.

Deuterium fractionation means the enhancement of deuterated isotopologues above the elemental D/H ratio of $\sim 1.5 - 2.0 \times 10^{-5}$ (Oliveira et al. 2003; Linsky et al. 2006; Prodanović et al. 2010). Because the mass of the deuteron atom is higher than that of hydrogen, deuterated molecules have a smaller zero-point vibrational energy than their pure hydrogen analogues. Thus, in the gas phase the deuterium fractionation mainly arises because of the difference between the zero-point energies of H_2 and HD ($\Delta E/k_\mathrm{B} \sim 410$ K); because of this energy difference the chemical fractionation will favour the production of HD compared to H_2. The sequence of deuteration is initiated by the rapid proton-deuteron exchange reaction (e.g., Dalgarno & Lepp 1984; Millar et al. 1989)

$$\mathrm{H_3^+ + HD} \underset{k_-}{\overset{k_+}{\rightleftharpoons}} \mathrm{H_2D^+ + H_2}\,. \tag{4.17}$$

The forward reaction is exothermic by $\Delta E/k_\mathrm{B} \sim 230$ K, i.e., the reverse reaction with the rate coefficient $k_- = k_+ \mathrm{e}^{-230\,\mathrm{K}/T}$, has an activation barrier of 230 K, which is much higher than the temperature of cold ISM. Therefore, despite the high abundance of H_2, reaction (4.17) is essentially irreversible at low temperature (< 30 K; e.g., Vastel et al. 2006). For this reason, the degree of deuterium fractionation in H_2D^+ can become large. When the temperature increases, H_2D^+ is more and more destroyed by H_2 molecules. When the temperature becomes > 30 K, fractionation via H_2D^+ becomes negligible (Millar et al. 1989).

Besides the reverse reaction (4.17), H_2D^+ can be destroyed by dissociative recombina-

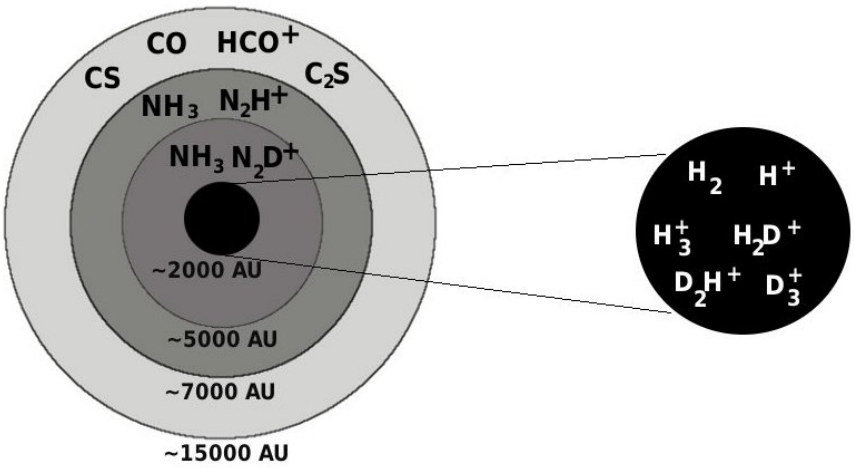

Figure 4.3: A sketch showing the chemical structure of a low-mass starless core. In the core envelope ($R \sim 7000 - 15\,000$ AU, $n(\mathrm{H_2}) \simeq 10^4$ cm^{-3}), C-bearing species are mostly in the gas phase, and HCO^+ is the main ionic species. When going towards the core centre ($R \sim 5000 - 7000$ AU), the gas density rises by an order of magnitude, and molecules such as CO freeze out on to dust grains. Consequently, the core layers where gas density is $n(\mathrm{H_2}) \simeq 10^5$ cm^{-3}, are best probed by N-bearing species, particularly by N_2H^+ and NH_3. At radii < 5000 AU, deuterium fractionation becomes important (see Sect. 4.3.3). In the high density nucleus of the core ($R \lesssim 2500$ AU, $n(\mathrm{H_2}) \gtrsim 10^6$ cm^{-3}), neutral species are expected to be depleted, and the chemistry is mainly driven by H_3^+ and its deuterated isotopologues. Figure is modified from di Francesco et al. (2007).

tion with electrons (e.g., $H_2D^+ + e^- \stackrel{k_e}{\rightarrow} H + H + D$), and by reactions (4.20) and (4.22) (see below). At steady-state, the above reactions lead to the equation

$$\frac{x(H_2D^+)}{x(H_3^+)} = \frac{k_+}{k_- + k_e x(e) + k_{CO} x(CO) + k_{HD,1} x(HD)} \frac{n(HD)}{n(H_2)} . \quad (4.18)$$

By assuming that (i) the reverse reaction (4.17) and the above dissociative recombination are negligible; (ii) the rate coefficients k_+, k_{CO}, and $k_{HD,1}$ are about the same; and (iii) $x(CO) \sim 10^{-4} \sim 10x(HD) \gg x(HD)$ (i.e., no CO depletion), we can write Eq. (4.18) as

$$\frac{x(H_2D^+)}{x(H_3^+)} \sim 10^4 \times \frac{n(HD)}{n(H_2)} . \quad (4.19)$$

Because $n(HD)/n(H_2) = 2\times[D/H]_{cosmic} \sim 3\times10^{-5}$, we see that the ratio $x(H_2D^+)/x(H_3^+)$ is of the order of ten percent. Note that in this simple approximation, the multiply deuterated species (see below) have been neglected, and it has also been assumed that dissociative recombination is faster than recombination onto dust grains.

Since H_2D^+ has a very low deuteron affinity, it reacts with almost all other interstellar species by donating a deuteron (e.g., Roberts et al. 2002). Consequently, deuterium enrichements are also passed forward to heavier species; important examples are the deuteron transfer reactions

$$\begin{array}{rcll} H_2D^+ + CO & \stackrel{k_{CO}}{\rightarrow} & HCO^+ + HD & (\text{for } 2/3) \\ & & DCO^+ + H_2 & (\text{for } 1/3) . \end{array} \quad (4.20)$$

$$\begin{array}{rcll} H_2D^+ + N_2 & \stackrel{k_{N_2}}{\rightarrow} & N_2H^+ + HD & (\text{for } 2/3) \\ & & N_2D^+ + H_2 & (\text{for } 1/3) . \end{array} \quad (4.21)$$

The numbers in parentheses indicate the statistical reaction branching ratios. Comparing with the above analysis we see that reaction (4.21) produces N_2D^+/N_2H^+ deuteration ratios of a few percent ($[N_2D^+/N_2H^+] \sim 1/3 \times [H_2D^+/H_3^+]$).

From an observational point of view, the degree of deuteration can be determined through observations of a hydrogen-bearing molecule and one of its deuterated isotopologues by calculating their column density ratio. In Paper I, we found that $N(N_2D^+)/N(N_2H^+) = 0.03 - 0.04$ in dense cores in Orion B9, which is comparable to the above theoretical estimate. These values are $\sim$ 3 orders of magnitude higher than the average ISM D/H ratio. This is at the low end of the values found by Crapsi et al. (2005); $N(N_2D^+)/N(N_2H^+) = 0.05 - 0.4$ for their sample of starless/prestellar cores. Recently, Pagani et al. (2009) found N_2D^+/N_2H^+ ratio of $\sim 0.7 \pm 0.15$ in the centre of L183, the highest ratio found to date.

Reaction (4.20) is the main destruction path of H_2D^+ when there is enough CO in the gas phase. Thus, the depletion of CO reduces the destruction rate of H_2D^+ and

consequently, the H_2D^+/H_3^+ ratio increases (e.g., Roberts & Millar 2000). For this reason, the molecular D/H ratio increases with increasing CO depletion (e.g., Bacmann et al. 2003; Crapsi et al. 2005; see also Aikawa et al. 2005). When CO is depleted, H_2D^+ is mainly destroyed via the reaction with HD producing D_2H^+ and D_3^+ (e.g., Phillips & Vastel 2003):

$$H_2D^+ + HD \overset{k_{HD,1}}{\rightleftharpoons} D_2H^+ + H_2 + 180\,K\,, \tag{4.22}$$

$$D_2H^+ + HD \overset{k_{HD,2}}{\rightleftharpoons} D_3^+ + H_2 + 230\,K\,. \tag{4.23}$$

D_2H^+ has been detected in the dense core IRAS 16293-2422E with an abundance similar to that of H_2D^+ (Vastel et al. 2004)[6]. Theoretical models have, indeed, predicted that the fractional abundances of D_2H^+ and D_3^+ are similar to that of H_2D^+ (Roberts et al. 2003; see also Flower et al. 2004). H_2D^+ itself is predicted to be the most abundant deuterated isotopologue of H_3^+, when $f_D \leq 30$ (see Ceccarelli et al. 2007). In the case of complete depletion of heavy species (C, N, O, ...), it was shown by Walmsley et al. (2004) that D_3^+ becomes the dominant deuterated isotopologue of H_3^+. On the verge of this condition, when there is still N_2 available, N_2D^+ is expected to become more abundant than N_2H^+ due to the reaction $D_3^+ + N_2 \rightarrow N_2D^+ + D_2$. Deuterium fractionation can also proceed via reactions on the grain surfaces, particularly in the case of methanol (e.g., Tielens 1983; Parise et al. 2004; Nagaoka et al. 2005).

The process of deuterium fractionation can be so efficient, that even doubly and triply deuterated molecules have been observed. These include, for example, doubly-deuterated ammonia (ND_2H), formaldehyde (D_2CO), and methanol (CHD_2OH) (Loinard et al. 2001; Parise et al. 2002), and triply-deuterated methanol (CD_3OH) (Parise et al. 2004). In fact, Parise et al. (2002) found that in the low-mass protostar IRAS 16293-2422, the total abundance of deuterated methanol exceeds that of the main isotopologue.

H_2D^+ produced by reaction (4.17) is probably the best molecular probe of the innermost regions of prestellar cores, where most of the heavy element species are depleted. Harju et al. (2006) detected H_2D^+ towards the dense cores within the clump associated with IRAS 05405-0117 in Orion B9. Although the physical characteristics of these cores resemble those of isolated starless cores, they are exceptional among sources detected in H_2D^+ so far, since the associated clump seems to be capable of forming a small stellar group (Paper I).

The sensitivity of the molecular D/H ratio to prevailing physical conditions and molecular depletion makes it a powerful probe of the chemical and dynamical evolution of dense molecular cloud cores. In particular the $N(N_2D^+)/N(N_2H^+)$ ratio shows an increasing trend with the core evolution towards the onset of star formation (Caselli 2002; Crapsi et al. 2005).

[6]The evolutionary stage of 16293E is somewhat uncertain. Castets et al. (2001) found it to be a low-luminosity protostar with an outflow activity. Stark et al. (2004) did not detect the outflow associated with 16293E, and they suggested it to be prestellar.

4.4 Protostellar cores, protostars and young stellar objects

The prestellar phase of core evolution ends when the formation of a central protostar takes place. However, the details of this process are still a matter of some debate (e.g., Ward-Thompson 2002). In short, this process includes the following steps (e.g., Masunaga & Inutsuka 2000; Chen et al. 2010b):

1. The isothermal gravitational contraction leads to a rapid increase of density in the core centre.
2. The gas and dust become optically thick ($\tau \gg 1$), and consequently, the heat generated by the gravitational collapse can no longer escape. The change of the isothermal collapse into adiabatic one occurs when the innermost parts of the core reach densities of $n(\mathrm{H_2}) \sim 10^{10} - 10^{11}$ cm^{-3}. The first hydrostatic core forms.
3. The contraction pauses because of the heat-up of the central region.
4. When the temperature has increased to $T \approx 2000$ K, $\mathrm{H_2}$ molecules start to dissociate.
5. Because the $\mathrm{H_2}$ dissociation absorbs energy (endothermic process), the hydrostatic core becomes unstable and starts to collapse again. At this stage, most of the released gravitational energy goes into the further dissociation of $\mathrm{H_2}$. Thus, the temperature increment is slow.
6. Finally, when all the $\mathrm{H_2}$ molecules in the core centre are dissociated, the temperature rises rapidly, and the collapse is halted. The resulting second hydrostatic core is the newly formed *protostar*.

André et al. (2000) list three properties that characterise the presence of a protostar in the core: (i) NIR or MIR emission; (ii) a bipolar molecular outflow; (iii) compact centimetric radio emission. (ii) and (iii) will be further discussed in Sects. 4.5 and 4.6, respectively.

The newly formed protostar will affect its surrounding medium. Radiation from the embedded protostar heats up the nearby gas and dust. In the case of low-mass protostars, however, the mean temperature of the parent core does not raise by more than a few kelvins (Jørgensen et al. 2006; Stamatellos et al. 2007). For example in Paper II, we determined the average kinetic temperature of the protostellar cores in Orion B9 to be ~ 12.7 K, whereas for the prestellar cores it is ~ 11.5 K. When heating is sufficiently strong, molecules start to evaporate from the grain mantles back into the gas phase. For instance, CO evaporates off the grains at ~ 20 K (e.g., Aikawa et al. 2008), which means that there are more molecular probes available in protostellar cores (particularly CO). In addition, neutral-neutral reaction pathways become important close to the central protostar. Consequently, species like $\mathrm{H_2D^+}$ and $\mathrm{N_2H^+}$ are destroyed by evaporated CO molecules in the vicinity of a protostar. For example, the protostar IRAS 05405-0117 studied in Papers I and II was not detected in $\mathrm{H_2D^+}$ by Harju et al. (2006). Deuterium

fractionation can still take place in the cold, extended envelope of the protostellar core (Emprechtinger et al. 2009; Paper I)[7]. Emprechtinger et al. (2009) showed that the N_2D^+/N_2H^+ column density ratio can also be used to trace the evolution of the youngest protostellar cores, see Sect. 4.4.2; later on, N_2D^+/N_2H^+ ratio is expected to drop when the central YSO starts to heat up its surroundings. Finally, powerful outflows driven by protostars create high-temperature shocks when propagating through the surrounding medium.

Protostellar cores can be studied by means of (sub)mm observations just like prestellar cores but observations at IR wavelengths are needed to study the protostars deeply embedded within their parent cores. In particular, Spitzer observations have been ideal in distinguishing between starless and protostellar cores (Enoch et al. 2008; Evans et al. 2009; Paper I). Unlike prestellar cores, however, protostellar cores are no longer representative of core initial conditions because some fraction of the core mass has been accreted onto the central protostar and ejected by outflows.

During the collapse, a protostellar core can fragment into smaller subunits. This process is believed to lead to the formation of binary and higher-order multiple stellar systems (e.g., Duchêne et al. 2007; Goodwin et al. 2007; McKee & Ostriker 2007). The typical number of stars forming from a single core is uncertain (e.g., Myers 2009), but as mentioned in Sect. 4.2.1, observations suggest that most cores produce 2–3 stars.

The observational classification of YSOs is traditionally based on the NIR to MIR spectral slope, $\alpha_{\rm IR}$ (Lada & Wilking 1984; Adams et al. 1987; Greene et al. 1994), or on the bolometric temperature, $T_{\rm bol}$ (Myers 1983; Chen et al. 1995). In this thesis, only the latter one is considered. Actually, $\alpha_{\rm IR}$ is not even well-defined for the earliest protostellar stage (Class 0 sources, see Sect. 4.4.2), because deeply embedded protostars were generally not visible in the MIR prior to Spitzer observations (see Enoch et al. 2009). Indeed, Enoch et al. (2009) concluded that $T_{\rm bol}$ is a more reliable evolutionary indicator of deeply embedded protostars than $\alpha_{\rm IR}$. In what follows, an overview is given of the spectral energy distributions (SEDs) of YSOs and the source classification based on the value of $T_{\rm bol}$.

4.4.1 Spectral energy distribution of YSOs

The physical conditions of protostellar and young stellar objects can be efficiently examined by determining their SEDs, S_ν or S_λ. In particular, classification of low-mass YSOs into the so-called Classes 0, I, II, and III objects, which form an evolutionary sequence, is based on their characteristic SEDs. The classification was developed by Lada (1987), André et al. (1993), and Myers & Ladd (1993), and the evolutionary sequence was supported by theoretical SEDs modelled by Adams et al. (1987).

The most important parameters describing the source SED are the bolometric temperature, $T_{\rm bol}$, and the bolometric luminosity, $L_{\rm bol}$. $T_{\rm bol}$ is defined as the effective temperature of a blackbody with the same flux-weighted mean frequency, $\bar{\nu}$, as the observed

[7] As in the case of starless cores, outer edges of protostellar cores are heated to only 12–14 K by the ISRF (Evans et al. 2001; Shirley et al. 2002; Young et al. 2003).

source SED has (Myers & Ladd 1993):

$$T_{\rm bol} \equiv \frac{\zeta(4)}{4\zeta(5)} \frac{h\bar{\nu}}{k_{\rm B}} = 1.25 \times 10^{-11} \bar{\nu}\,{\rm K\,Hz^{-1}}\,, \tag{4.24}$$

where $\zeta(p) = \sum_{n=1}^{\infty} n^{-p}$ is the Riemann zeta function of argument p, and $\bar{\nu}$ is the ratio of the first and zeroth frequency moments of the spectrum

$$\bar{\nu} \equiv \frac{I_1}{I_0} = \frac{\int \nu S_\nu {\rm d}\nu}{\int S_\nu {\rm d}\nu}\,. \tag{4.25}$$

$L_{\rm bol}$ is calculated by integrating the SED (S_ν) over frequency:

$$L_{\rm bol} = 4\pi d^2 \int_0^\infty S_\nu {\rm d}\nu\,, \tag{4.26}$$

where d is the source distance. As long as the mass of the (infalling) envelope, $M_{\rm env}$, exceeds the mass of the central protostar, $M_\star$, $L_{\rm bol}$ is largely due to mass accretion (radiated outward at the accretion shock front), and thus can be expressed in spherical symmetry as (Adams & Shu 1986; Offner et al. 2009)

$$L_{\rm bol} \equiv L_{\rm acc} = f_{\rm acc} f_{\rm k} \frac{G M_\star \dot{M}_{\rm a}}{R_\star}\,, \tag{4.27}$$

where $f_{\rm acc} \approx 0.5$ is the fraction of the accretion energy that is radiated by an accretion disk (and not to drive a protostellar wind), $f_{\rm k} \approx 0.5$ is the fraction of the kinetic energy of the infalling material radiated by an inner accretion disk (before the material hits the protostellar surface), $\dot{M}_{\rm a}$ is the accretion rate, and $R_\star$ is the radius of the protostar[8]. Another important parameter is the submm luminosity, $L_{\rm sub-mm}$, defined as the integral over the SED for $\lambda \geq 350$ μm:

$$L_{\rm sub-mm} = 4\pi d^2 \int_{350\,\mu{\rm m}}^\infty S_\lambda {\rm d}\lambda = 4\pi d^2 \int_0^{\nu=8.57\times10^{11}\,{\rm Hz}} S_\nu {\rm d}\nu\,. \tag{4.28}$$

The core evolutionary stage can be estimated by comparing the values of $L_{\rm sub-mm}$ and $L_{\rm bol}$ (see below). The advantage of using the $L_{\rm sub-mm}/L_{\rm bol}$ ratio as an evolutionary indicator compared to the value of $T_{\rm bol}$ is that the former is less sensitive to geometrical effects (see below). On the other hand, the value of $T_{\rm bol}$ is less sensitive to the submm envelope emission (Young & Evans 2005; Launhardt et al. 2010).

A useful way to study the evolution from embedded protostars to stars is to compare the $L_{\rm bol} - M_{\rm env}$ and $L_{\rm bol} - T_{\rm bol}$ diagrams with the evolutionary tracks computed by e.g., Saraceno et al. (1996) and Myers et al. (1998). The ratio $M_{\rm env}/L_{\rm bol}^{0.6}$, which is related to the outflow activity and thus decreases with time (Bontemps et al. 1996a, see Paper I), can also be used to constrain the core evolutionary stage.

[8] In general, the total luminosity of an accreting protostar is $L_{\rm bol} = L_{\rm int} + L_{\rm acc} + L_{\rm disk}$, where $L_{\rm int}$ is the interior luminosity, and $L_{\rm disk} = (1 - f_{\rm k}) G M_\star \dot{M}_{\rm a}/R_\star$ is the disk luminosity. Before the protostar joins the zero-age main sequence (ZAMS), $L_{\rm int}$ is due to gravitational contraction and deuterium burning (not due to hydrogen burning).

It should be noted that all emitting matter along the line of sight contributes to the observed SED. Thus, for instance, the derived temperature value represents the so-called "column temperature", which provides an upper limit for the lowest temperature along the line of sight (Shetty et al. 2009). One drawback in the SED-based source classification is that the shape of the SED may strongly depend on the inclination angle of the source (for radiative transfer models, see Whitney et al. 2003; Robitaille et al. 2006; Crapsi et al. 2008). For example, IR emission from a protostar embedded in a circumstellar envelope/disk could be directly detected through the cavity drilled by an outflow when the system is observed face-on (i.e., inclination angle $i = 0°$; cf. Enoch et al. 2009). In such a case, the values of $L_{\rm bol}$ and $T_{\rm bol}$ would be overestimated, and $L_{\rm sub-mm}/L_{\rm bol}$ would appear to be too low. In the case of edge-on system ($i = 90°$), however, IR emission could be hard to detect, and $T_{\rm bol}$ and $L_{\rm bol}$ would thus be underestimated (hence, $L_{\rm sub-mm}/L_{\rm bol}$ ratio is overestimated). As pointed out by e.g., Kenyon et al. (1993) and Sonnhalter et al. (1995), one should try to assess the possible influence of such viewing angle effects before drawing conclusions about the evolutionary stage of an object based on its SED. However, this can be very difficult (or impossible) in practise. In principle, in the case the source is associated with a protostellar outflow, the source inclination can be constrained to some degree with the aid of outflow orientation and morphology (see, e.g., André et al. 1999). For example, if the outflow is lying in the plane of the sky, the source (and its accretion disk) is likely to be seen edge-on (e.g., Chen et al. 2008). In summary, since $T_{\rm bol}$ and $L_{\rm bol}$ both depend on the viewing angle (in contrast to $M_{\rm env}$, see André et al. 2000), the SED-based classification may thus be a result of both the evolutionary stage of the source and its inclination angle.

Next, we describe each evolutionary stage from Class 0 to Class III. Note that the term "protostar" refers to Class 0 and I sources, whereas Class II and III objects are termed "PMS stars". The term "YSO" encompasses both protostars and PMS stars.

4.4.2 Class 0 sources

Prestellar cores discussed in the beginning of this section evolve to Class 0 objects, which represent the earliest protostellar stage[9]. At this stage, a hydrostatic core has formed within the dense core.

There are several observational criteria needed for a core to be classified a Class 0 source (André et al. 1993, 2000):

1. There is a central YSO embedded within the core. This is indicated by, e.g., a compact cm-radio continuum source (see Sect. 4.6), bipolar outflow (see Sect. 4.5), or an internal heating source (embedded IR source).

2. Submm dust continuum emission is extended and centrally peaked. This indicates the presence of a circumstellar envelope (see also Motte & André 2001).

[9]Boss & Yorke (1995) and Masunaga et al. (1998) modelled the early stage of protostar formation and introduced the "first hydrostatic core", or "Class -I" protostar, as a short-lived precursor of Class 0.

3. The ratio of submm to bolometric luminosity is high, $L_{\rm sub-mm}/L_{\rm bol} > 0.005$. As shown by André et al. (1993), this is equivalent to the condition that the envelope mass is far greater than the mass of the central protostar ($M_{\rm env} \gg M_\star$); the newly forming star has accreted less than half of its final mass.

4. Blackbody-like SED corresponds to a bolometric temperature of $T_{\rm bol} < 70$ K.

Moreover, well-known Class 0 sources are characterised by the normalised envelope mass of $M_{\rm env}/L_{\rm bol}^{0.6} \gtrsim 0.4$ $\rm M_\odot/L_\odot^{0.6}$ (Bontemps et al. 1996a; André et al. 2000). Class 0 objects are so deeply embedded within their parent molecular cloud core that they are detectable only at MIR and at longer wavelengths; their SEDs peak in the submm or FIR range[10]. In Paper I, we report the discovery of two new Class 0 candidates in the Orion B9 star-forming region, named SMM 3 and SMM 4. Figure 4.4 shows the 870 μm dust continuum image and the SED of SMM 3.

The Class 0 evolutionary stage is the main mass accretion phase in the formation of a low-mass star. Typical accretion rates of embedded low-mass protostars are $\lesssim 10^{-6}$ $\rm M_\odot$ $\rm yr^{-1}$, but accretion rates are periodic with lower and higher (up to $\sim 10^{-4}$ $\rm M_\odot$ $\rm yr^{-1}$) values, which result in lower and higher luminosities (e.g, Dunham et al. 2010 and references therein). Soon after the accretion starts and a disk forms around the central protostar, very powerful and collimated bipolar outflows develop (e.g., Bachiller 1996; Richer et al. 2000; Königl & Pudritz 2000; Pudritz et al. 2007). Disks around Class 0 protostars have typical masses of about 0.05 $\rm M_\odot$ (Jørgensen et al. 2009). Some Class 0 objects are found to be multiple systems when observed at subarcsecond resolution (e.g., Maury et al. 2010 and references therein).

Class 0 objects are important for low-mass star formation studies because they still retain some memory of their prestellar phase (Ward-Thompson et al. 2007). For example, at the beginning of the Class 0 stage, most of the envelope is so cold, that heavy element-bearing molecules are frozen onto the dust grains, similarly to that in prestellar cores (see Sect. 4.3.2). In Papers I and II, we found that $\rm N_2H^+$ is depleted in the envelope of the Class 0 candidate SMM 4 in Orion B9. However, the duration of the phase of molecular depletion in the Class 0 sources is short due to the central heating (Langer et al. 2000). Regarding the molecular depletion and very large deuteration degrees observed in the envelopes of Class 0 objects (e.g., Emprechtinger et al. 2009) they are virtually indistinguishable from prestellar cores. Similarly to prestellar cores, Emprechtinger et al. (2009) concluded that the $\rm N_2D^+/N_2H^+$ column density ratio can be used to clearly identify the youngest objects among the Class 0 sources. This strengthens the idea that prestellar cores represent the precursors of Class 0 objects (see Ceccarelli et al. 2007). Thus, from a chemical point of view, the most prominent characteristic of the outer envelopes of Class 0 objects is their similarity to prestellar cores. However, unlike prestellar cores the radial intensity profiles of (sub)mm dust continuum emission of the Class 0 objects do not exhibit any flattening in the inner parts (see André et al. 2000).

[10]Because of the surrounding disk (which is optically thick), the peak of the SED of a Class 0 object depends on viewing angle, but the dependence is rather weak (Stamatellos et al. 2005).

On the other hand, warm or hot ($\sim$ 100 K) and dense central parts ($\lesssim$ 100 AU) of Class 0 objects are characterised by a rich chemistry with multitude of complex organic molecules (e.g., Bottinelli et al. 2007). Such Class 0 sources are known as "hot corinos" (see Ceccarelli et al. 2007 for a review), and they resemble their high-mass counterparts, the so-called hot cores around massive protostars. Practically, all radiation emitted from a Class 0 source at $\lambda < 100$ μm comes from the warm/hot central parts (e.g., Emprechtinger et al. 2009).

Recently, in the studies of nearby molecular clouds, Enoch et al. (2009) and Evans et al. (2009) used the relative number of Class 0 and Class I sources to estimate the lifetime of the Class 0 stage; the three-cloud (Perseus, Serpens, Ophiuchus) average yielded a Class 0 lifetime of $\sim 1.0 \times 10^5$ yr. This value is larger than earlier estimates ($\sim 10^4$ yr), and it argues against an extremely rapid accretion as was previously suggested to be characteristic of a Class 0 stage (André & Montmerle 1994; André et al. 2000; Froebrich et al. 2006). However, as discussed by Enoch et al. (2009) and Vorobyov (2010), the accretion rate and thus lifetime may possibly depend on conditions of the parent molecular cloud such as the mean density and the level of turbulence.

As the Class 0 object heats up an increasing amount of radition is emitted at shorter wavelengths. This leads to an increase in both $L_{\rm bol}$ and $T_{\rm bol}$ with time and subsequently the source moves to Class I.

4.4.3 Class I sources

The transition phase between Class 0 and I, commonly designated as Class 0/I, is believed to take place when the envelope mass is about equal to the mass of the central protostar ($M_{\rm env} \simeq M_\star$). Thus, protostars in the Class I stage are relatively evolved objects which have already accumulated the majority of their final stellar mass ($M_{\rm env} < M_\star$; Lada 1987; André & Montmerle 1994). Recently, Evans et al. (2009) estimated for the Class I stage a lifetime of 4.4×10^5 yr, which is somewhat longer than the earlier estimates (typically $\sim 1 - 2 \times 10^5$ yr; Greene et al. 1994).

Class I objects can be detected in the NIR but they are characterised by SEDs that peak in the submm or FIR range as in the case of Class 0 objects. This is due to the fact that Class I protostars are still surrounded by an accretion disk and a circumstellar envelope of gas and dust. The Class I systems are also visible in optical wavelengths when observed along the outflow direction, i.e. when the central protostar is visible. Some Class I objects may look like Class 0 objects when observed edge-on (see Men'shchikov & Henning 1997; André et al. 2000).

Bolometric temperature at this stage is in the range 70 K $< T_{\rm bol} <$ 650 K (e.g., André et al. 2000), and $L_{\rm sub-mm}/L_{\rm bol} < 0.005$. Some infall is still present at this stage. The mass accretion rate is, on average, $\sim$ 2 times lower than in the Class 0 stage (Enoch et al. 2009). However, the luminosity of Class I objects is still mainly due to accretion. Moreover, Enoch et al. (2009) suggested that mass accretion during the Class I stage is episodic[11]. Because of mass accretion outflow activity is still present at Class I stage, but

[11]Enoch et al. (2009) found that $\sim$ 20% of the Class I sources in their sample have $L_{\rm bol} < 0.1$ L$_\odot$.

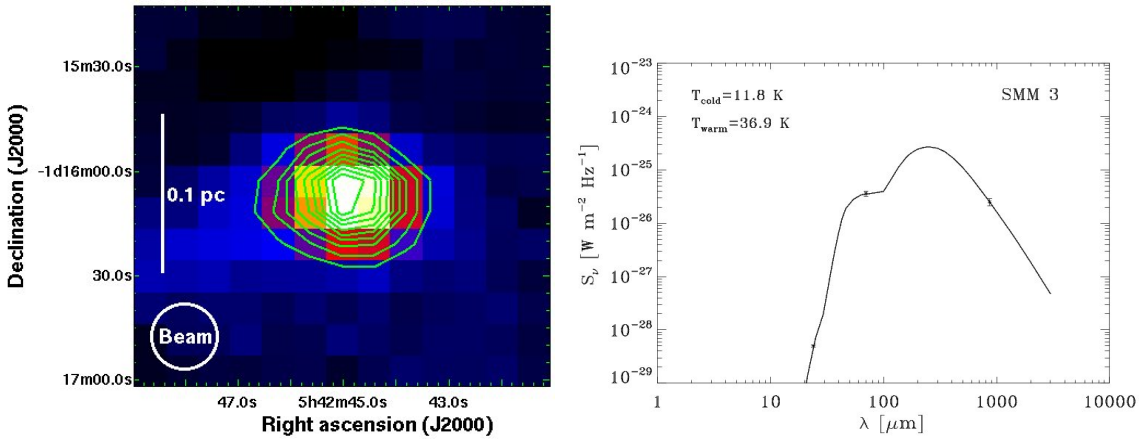

Figure 4.4: **Left:** LABOCA 870 μm dust continuum image of the Class 0 protostellar candidate SMM 3 in the Orion B9 star-forming region (Enlargement of Fig. 1 of Paper I). The contour levels go from 0.2 to 1.0 Jy beam^{-1} in steps of 0.1 Jy beam^{-1}. The beam HPBW (18.6$''$) is shown in the lower left corner. **Right:** A tentative SED of SMM 3 constructed from the Spitzer and LABOCA data. The data were fitted by a two-temperature (cold+warm) composite model. The bolometric temperatures of the cold and warm media are $T_{\rm cold} \simeq 12$ K and $T_{\rm warm} \simeq 37$ K. The total mass and bolometric luminosity resulting from the fit are $\sim 7 \pm 2$ M$_\odot$ and ~ 3.5 L$_\odot$. The temperature of the cold component is in good agreement with the gas kinetic temperature of 11.3 ± 0.8 K derived from NH_3 in Paper II. The $L_{\rm submm}/L_{\rm bol}$ ratio is about 0.1. Adapted from Paper I.

outflows tend to be much less powerful and also less collimated than those emanating from Class 0 objects (e.g., Bontemps et al. 1996a; André et al. 2000).

4.4.4 Class II sources

Class II objects are PMS stars which correspond to classical T Tauri stars (CTTSs). At this stage, there is an optically visible star surrounded by a tenuous disk. Typical masses of Class II disks are only ~ 0.005 $M_\odot$ (Andrews & Williams 2007). There is no more a dense circumstellar envelope, i.e., $M_{\rm env} \approx 0$, because it has either been accreted or dispersed by the outflow (André et al. 2000). Thus, mass accretion continues at a very low rate, typically $\sim 10^{-8}$ $M_\odot$ yr^{-1} (e.g., Furlan et al. 2005), and the star's luminosity is due to the gravitational contraction. Consequently, outflow activity has decreased to a rather weak level, but the object is possibly driving a weakly ionised wind. The SEDs of Class II objects peak at visible or NIR wavelengths, and the disk adds an IR excess to the SED (e.g., Beckwith 1999). Bolometric temperature is in the range 650 K $< T_{\rm bol} <$ 2880 K (e.g., André et al. 2000). We note that the boundary value in $L_{\rm sub-mm}/L_{\rm bol}$ between Class I and II is not defined. The duration of the Class II stage is uncertain, but it is probably $\sim 1 - 3 \times 10^6$ yr (Evans et al. 2009).

There has also been some debate as to whether Class I and II objects really represent different evolutionary stages. These two classes could, in principle, be explained by the inclination angle under which the object is seen (White & Hillenbrand 2004; Eisner et al. 2005). However, the X-ray properties of Class I and II objects are different; Class I objects are more variable in X-rays than Class II objects (Forbrich & Preibisch 2007). This supports the idea that the two types of objects really are in different evolutionary stages.

CTTSs with masses of ~ 1 $M_\odot$ are likely to be good analogues of the conditions that may have prevailed in the early Solar System. Planets are believed to start forming at this stage (see, e.g., Ruden 1999 for a review).

4.4.5 Class III sources

PMS stars in the Class III stage correspond to weak-line T Tauri stars (WTTSs). In these sources, the envelope and disk have largely been accreted/dissipated. Consequently, Class III objects have a simple blackbody SED (Wolk & Walter 1996). Peak emission is in the optical or NIR, and $T_{\rm bol} > 2880$ K (e.g., André et al. 2000).

The ages of Class III objects are estimated to be in the range $\sim 10^6 - 10^8$ yr (e.g., Duvert et al. 2000). Eventually, Class III objects move to the main sequence ($T_{\rm bol} \gtrsim 3000$ K; see Myers et al. 1998; Enoch et al. 2009) and the newly formed star is possibly surrounded by planets.

Such low values can be explained by periods of relative quiescence when $L_{\rm acc}$ is at least an order of magnitude lower than during the active mass accretion.

4.5 Jets and outflows associated with protostellar cores

The early stages of low-mass star formation are characterised by the formation of an accretion disk and the launch of an associated jet/outflow[12]. It is now widely accepted that protostellar jets (or winds) are launched on small scales (< 10 AU), and are driven by magneto-centrifugal processes associated with accretion disks (e.g., Ray et al. 2007; Shang et al. 2007; Pudritz et al. 2007; Machida et al. 2008). The mass of the ejected material is $\sim 10\%$ of that accreted from the disk to the central protostar, and a typical jet velocity is $\sim$ 150 km s^{-1} (Bally et al. 2007; Dunham et al. 2010 and references therein).

Jets from protostars sweep up ambient molecular gas and drive large-scale bipolar molecular outflows, which are one of the first observable signatures of on-going star formation (see Fig. 4.5 for an example). Outflowing gas is revealed via the broad spectral line wings, which indicate that the gas is moving at high velocities with respect to the systemic velocity of the star-forming core (Snell et al. 1980). Outflows typically extend over $0.1 - 1$ pc from the central source, and a typical outflow velocity is $\lesssim 10$ km s^{-1} for low-mass protostars (e.g, Reipurth & Bally 2001; Dunham et al. 2010). Collimation factors (i.e., the ratio between the outflow length and the width) in low-mass outflows range from $\sim 1 - 10$, with a typical value of $\sim 2 - 3$ (see Richer et al. 2000). Mass outflow rates are between $\sim 10^{-8} - 10^{-6}$ M$_\odot$ yr^{-1} depending on the age of the source and it has been estimated that the outflow rates are about $\lesssim 0.1-0.5$ times the accretion rate (e.g., Bontemps et al. 1996a; Königl & Pudritz 2000). Protostellar outflows appear to be most powerful during the early stages of evolution. For instance, Class 0 objects drive outflows that are an order of magnitude more powerful than those from Class I sources (Bontemps et al. 1996a; Bachiller 1996, see also Paper III). Moreover, the outflow opening angle (i.e., collimation) appears to widen with increasing age of the protostar, which is probably caused by the erosion of the envelope by the outflowing gas (see Königl & Pudritz 2000; Arce et al. 2007). Jets from YSOs are usually driven for $\sim 10^5$ yr (e.g., Banerjee et al. 2007).

Protostellar outflows are one of the most important feedback processes in star formation. For example, they are believed to carry away the excess angular momentum from a star-forming system (Königl & Pudritz 2000), and they can remove a large amount of mass from a collapsing core, and thus limit the star formation efficiency (SFE) of the dense gas (see Matzner & McKee 2000; André et al. 2009). Outflows have been proposed to be an important driving source of the turbulence in protostellar cores (e.g., Matzner 2007; Carroll et al. 2009). However, observations such as those presented in Paper II, often show that linewidths in pre- and protostellar cores are very similar. Such results indicate that outflows do not drive significant turbulent gas motions within dense cores. It has also been suggested that outflows drive supersonic turbulence observed in molecular clouds, but this connection is still under debate (Banerjee et al. 2007; Cunningham

[12]Disks and outflows have also been discovered around massive stars and even brown dwarfs (e.g., Morrow et al. 2008; Whelan et al. 2009). This implies that the outflow mechanism is important across the entire stellar mass spectrum (see Pudritz et al. 2007).

et al. 2009; Carroll et al. 2009).

4.5.1 Shock chemistry in outflows[13]

Protostellar outflows produce strong shocks when they ram into the ambient ISM. Shocks in molecular gas can be of type C (continuous) or J (jump), depending on the shock velocity, magnetic field strength, and the degree of ionisation of the preshock gas (e.g., Draine & McKee 1993). The critical velocity between these two types of shocks is typically $\sim 20 - 50$ km s^{-1} (Le Bourlot et al. 2002; Flower & Pineau des Forêts 2003; Guillet et al. 2007, 2009). In most YSOs, a mixture of C- and J-type shocks are likely to occur (van Dishoeck & Blake 1998). Shock waves compress and heat the gas, and thereby affect the chemistry. In particular, molecular chemistry is strongly affected by C-shocks, because they are slow and non-dissociative, and they raise the temperature to only moderate values ($\sim 2000 - 3000$ K) in a thick layer, so that molecules can survive (see van Dishoeck & Blake 1998). The reactions that cannot proceed in cold gas due to energy barriers, can proceed in the C-shock-heated gas. On the other hand, all molecules are destroyed in faster, dissociative J-shocks, where the thin post-shock layer is very hot, $\sim 10^5$ K (Neufeld & Dalgarno 1989; Hollenbach & McKee 1989), and the re-formation of the molecules is a slow process (see Richer et al. 2000). The shock-heated postshock gas is cooled rapidly ($\sim 10^2$ yr) by H_2, CO (and its isotopologues), and H_2O line emission (Kaufman & Neufeld 1996; Gusdorf et al. 2008a). Eventually the high temperature shock-chemistry cannot proceed anymore, and the subsequent chemistry is again dominated by low temperature processes.

Shocks have also impact on dust grains. In C-type shocks, non-thermal sputtering, mainly collisions between H_2 molecules and charged dust grains, injects volatile species from the grain mantles into the gas phase, but the refractory grain cores can also be partially eroded (e.g., Flower & Pineau des Forêts 1994, 1995). In J-shocks, liberation of refractory species is due to destruction of grain cores and thermal sputtering, i.e. the removal of surface atoms by energetic impacts with the most abundant neutral species or ions resulting from thermal motion of the high-temperature gas (Flower et al. 1996). In general, shocks are the dominant destruction mechanism for interstellar dust grains (Draine & McKee 1993; Jones et al. 1994).

After the liberation of species from dust grains into the gas phase there is a chance for some molecules, such as SiO, to be formed (see Richer et al. 2000). SiO can be formed through two different ways by the action of shocks. First, C-type shocks with velocities $v_s \gtrsim 25$ km s^{-1} can form SiO via sputtering of Si from the grain cores (e.g., from the olivine, $MgFeSiO_4$), which then undergoes oxidation through the neutral-neutral gas-phase reactions (Schilke et al. 1997; Gusdorf et al. 2008a,b)

$$\mathrm{Si} + \mathrm{O_2} \rightarrow \mathrm{SiO} + \mathrm{O} \tag{4.29}$$

$$\mathrm{Si} + \mathrm{OH} \rightarrow \mathrm{SiO} + \mathrm{H}\,. \tag{4.30}$$

[13] Although discussed here in the context of low-mass star formation shock chemistry is studied in Paper V which deals with high-mass star-forming regions.

Secondly, SiO can be directly formed through dust destruction by vaporisation in grain-grain collisions (see Guillet et al. 2009 and references therein). In quiescent dark clouds, Si is so heavily depleted onto dust grains that the SiO abundance is only $x(\mathrm{SiO}) \leq 10^{-12}$ (Ziurys et al. 1989). Thus, the detection of SiO emission clearly indicates the presence of shocked gas, and tells of ongoing star formation within the observed region (e.g., Martín-Pintado et al. 1992; Schilke et al. 1997; Gibb et al. 2004; Paper V; Jiménez-Serra et al. 2009), and SiO can exhibit extreme enhancement (by factors of up to $\sim 10^6$) with respect to the quiescent, unperturbed medium. The spectral lines of SiO often present broad wings and are shifted relative to the emission from the ambient gas (see Paper V). SiO is a very useful tracer of shocked gas since the emission is not confused by the ambient cloud component like in the case of the classical outflow tracers like CO. The physical conditions of the shock, such as velocity and density, and/or outflow age, may affect strongly the formation process of SiO. For instance, the terminal shock fronts beyond which the shock becomes subsonic may show only weak SiO emission (see Arce et al. 2007).

In the hot shocked gas, OH becomes abundant through the reaction

$$\mathrm{O} + \mathrm{H_2} \rightarrow \mathrm{OH} + \mathrm{H}\,. \tag{4.31}$$

Subsequently, SiO in converted to $\mathrm{SiO_2}$ in the reaction with OH

$$\mathrm{SiO} + \mathrm{OH} \rightarrow \mathrm{SiO_2} + \mathrm{H}\,, \tag{4.32}$$

which is the limiting factor of the SiO abundance. In Paper V, we suggest that this could possibly explain the decrease of SiO abundance as a function of the gas kinetic temperature because there is more OH available in the warmer gas.

Observations have shown that some outflow regions also exhibit very narrow ($\Delta v \approx 0.5$ km s^{-1}) SiO lines near the systemic velocity (e.g., Jiménez-Serra et al. 2005 and references therein). The abundance of SiO in these cases is only $\sim 10^{-11} - 10^{-10}$, i.e., 2-3 orders of magnitude lower than in the usual broad SiO components. The presence of this "low-velocity SiO" is not well understood. One possibility is that SiO is formed at high velocities but is then decelerated and mixed with the ambient gas (Gusdorf et al. 2008a). Another possibility is that the low-velocity SiO is the signature of a shock precursor component, where neutral gas is only beginning to accelerate and refractory species are just starting to be injected into the gas phase (Jiménez-Serra et al. 2009 and references therein).

Other molecules that are observed to be more abundant (by factors ~ 100) in outflows than in quiescent medium include e.g., $\mathrm{CH_3OH}$, $\mathrm{H_2CO}$, and SO (e.g., Bachiller et al. 2001; Garay et al. 2002; Jørgensen et al. 2004a; Lee et al. 2010). It is likely that the former two species are evaporated directly from the icy dust mantles, whereas SO probably forms via gas phase chemistry of shock released sulfur. Moreover, the above species trace weaker shocks than the SiO emission.

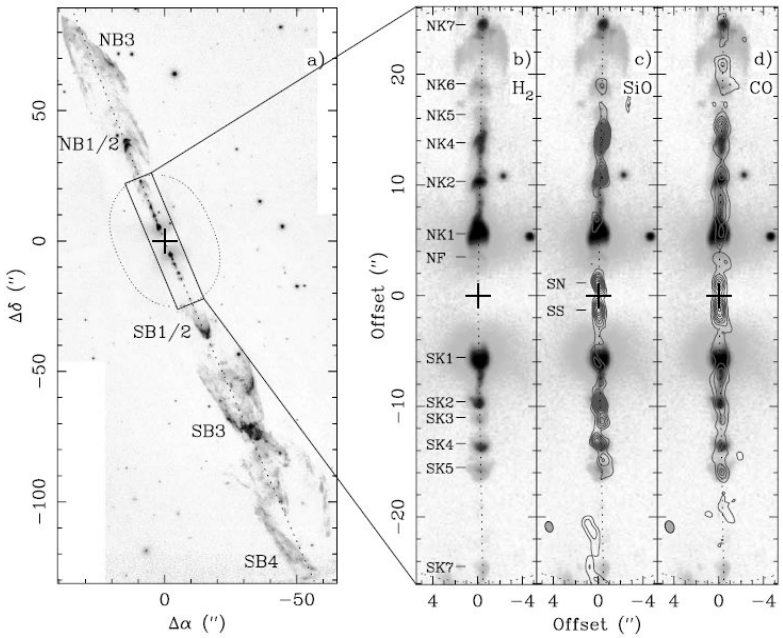

Figure 4.5: (a) and (b) panels show the images of the H_2 $v = 1 - 0$ $S(1)$ line emission at 2.122 μm in the protostellar outflow HH (Herbig-Haro) 212. (c) and (d) panels show the $SiO(8 - 7)$ and $CO(3 - 2)$ emission (tracing the bow shocks) as contours overlaid on the H_2 image. This is one of the most symmetric protostellar outflows found to date. The outflow is driven by the Class 0 source IRAS 05413-0104 (position indicated by the plus sign), which is seen towards the Orion B9 star-forming region (see Papers I and II). The mass, gas kinetic temperature, and non-thermal velocity dispersion of IRAS 05413-0104 are 2.0 ± 0.6 $M_\odot$, 13.4 ± 1.2 K, and 0.18 km s^{-1}, respectively (Paper II). The total flow length is about $240''$ (0.52 pc at 450 pc). Adapted from Lee et al. 2007.

4.6 Radio continuum emission from YSOs

In Paper III, we study the centimetric radio continuum emission from YSOs in the R Coronae Australis molecular cloud. In the following, we give some background to this study.

4.6.1 Thermal radio emission

Most embedded YSOs that drive powerful outflows, are found to be associated with thermal centimetre radio continuum emission (e.g., Rodríguez 1994; Anglada 1995; Rodríguez 1997). This emission is due to free-free radiation from partially ionised material.

Both theoretical and observational results indicate that the ionisation degree in thermal jets is $x(\mathrm{e}) \sim 10\%$ (Rodríguez et al. 1990; Hartigan et al. 1994; Bacciotti et al. 1995). Such a level of ionisation cannot be explained by photoionisation, however, because low-luminosity objects (spectral type later than B) that are detected in radio continuum do not emit UV photons with enough energy for the ionisation (e.g., Rodríguez et al. 1989, 1995; Anglada 1995)[14]. For example, the observed flux densities of the thermal radio jets studied by Anglada et al. (1998) are $2-13$ orders of magnitude higher than those expected from photoionisation. Thus, some other mechanism is needed to explain the ionisation in thermal radio jets. Because low-mass protostars drive molecular outflows, it is believed that the most likely mechanism is provided by the shock-induced ionisation at the base of the outflow. Strong shocks ($v_s \gtrsim 35$ km s^{-1}), that are produced by stellar wind/outflow colliding with the surrounding high density medium at distances of around 10 AU from the central source, produce UV photons that can ionise the gas (e.g., Curiel et al. 1987; Neufeld & Hollenbach 1996; see also Güdel 2002 for a review).

The centimetre radio sources associated with YSOs are, in general, weak and compact. The sources are usually unresolved, except at high angular resolution ($< 1''$). When the radio sources are resolved it has been found that thermal emission is characterised by a low brightness temperature of $T_\mathrm{B} \leq 10^4$ K and that the sources are often elongated along a direction close to the axis of the large-scale molecular outflow (e.g., Anglada 1995; Bontemps et al. 1996b). Curiel et al. (1993) concluded that radio lobes associted with jets could represent some stage prior to the birth of an HH object. Since the "base" of the thermal jet is so close to the central YSO and its circumstellar dust, it is heavily obscured and cannot be detected at optical wavelengths like the large scale jets (e.g., Anglada et al. 1998).

At cm wavelengths, thermal free-free emission is characterised by a flat or positive spectral index, $\alpha \geq -0.1$ (Sect. 3.4). In the case of optically thick ($\tau_\nu \gg 1$) bremsstrahlung, $S_\nu \propto \nu^2$, whereas optically thin ($\tau_\nu \ll 1$) flux density is nearly independent of ν; intermediate values, e.g. $\alpha \sim 1$, indicate partially optically thick plasmas. We note that also thermal dust emission exhibits a positive spectral index, but it dominates at IR and (sub)mm wavelengths only, with only a small contribution expected at

[14] In the case of high-mass protostars, however, the ionisation is due to photoionisation (see Sect. 5.3.2 for a discussion of embedded HII regions).

cm wavelengths: continuum emission from ionised gas dominates the radio emission at wavelengths $\lambda > 3$ mm (e.g., André et al. 1990).

Anglada et al. (1998) showed that the spectral indices between 6 and 3.6 cm for the outflow central sources are, in general, higher than the free-free optically thin value, i.e., $\alpha > -0.1$. This indicates the presence of an optically thick emission component in these sources. Similarly, in Paper III the values of $\alpha_{3\,\mathrm{cm}}^{6\,\mathrm{cm}} \sim 0.1 - 2$ were determined for the majority of the R CrA YSOs. Figure 4.6 (left) shows an example of the 6 cm continuum sources studied in Paper III. The radio spectral indices between 6 and 3 cm of IRS 7A and B shown in the figure are about 0.2 and 0.4, respectively, where the corresponding flux densities were observed simultaneously making the spectral index values independent of time variations. IRS 7B appears to be associated with the bipolar radio jet with the total extent of ~ 0.1 pc.

The predicted spectral index of the so-called standard spherical wind, i.e., a fully ionised, constant velocity, and isotropic stellar wind, is $\alpha = 0.6$ at cm wavelengths (e.g., Panagia & Felli 1975), which is in good agreement with many observations. The models by Reynolds (1986) of free-free emission from a collimated, ionised winds are able to explain the typical observed values of spectral indices. According to the results of Reynolds (1986), it is possible that $\alpha > 0.6$ for an accelerated flow, but a collimated ionised flow produces a flat spectrum with $\alpha < 0.6$. Moreover, the Reynolds (1986) models for a jet of constant temperature, velocity, and ionisation degree, predict that $\alpha = 1.3 - 0.7/\epsilon$, and that the angular size of the source scales with frequence as $\theta_\nu \propto \nu^{-0.7/\epsilon}$, where ϵ depends only on the jet geometry and is the power-law index that describes how the width of the jet depends on the distance from the central driving source ($w \propto r^\epsilon$, where w is the jet half-width, and r is the distance to the jet origin). For a conical, or constant opening angle jet, $\epsilon = 1$ (i.e., $\alpha = 0.6$). If $\epsilon < 1$ ($\alpha < 0.6$), the jet collimation increases with distance out to perhaps hundreds of AU (see also Anglada 1996). González & Cantó (2002) presented a model in which the ionisation, and the radio continuum emission, is caused by internal shocks in the wind (such shocks result from variations in the wind velocity). Their model also predicts flux density and spectral index values that are in good agreement with those observed towards low-mass YSOs.

Radio emission from embedded YSOs can also arise from the ionised region surrounding a protostellar accretion shock (Winkler & Newman 1980; Cassen & Moosman 1981; Neufeld & Hollenbach 1996; Ghavamian & Hartigan 1998), or from an ionised disk wind (e.g., Martin 1996). These two mechanisms, however, produce a much weaker radio emission than collimated jets. Felli et al. (1982) modelled thermal radio emission from an extended, accreting ionised circumstellar envelope. Their model produces a flat spectrum with $\alpha = -0.1$ to 0.1. In Bertout's (1983) model of accretion onto a protostellar core, the radio-emitting region is photoionised by soft X-ray and extreme UV radiation from an accretion shock around a protostellar core. This model is also characterised by a spectral index of $\alpha \simeq 0.6$.

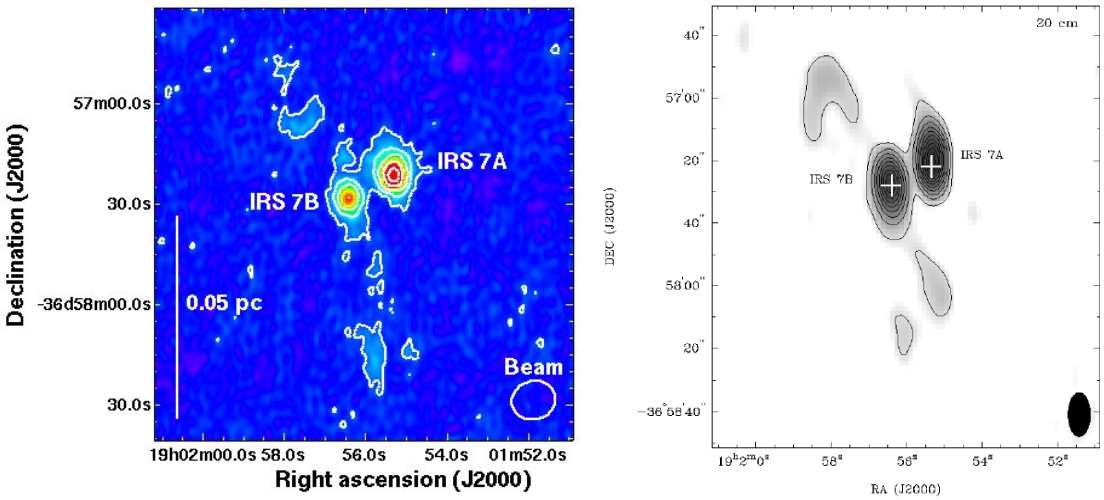

Figure 4.6: **Left:** ATCA 6 cm radio continuum image of the IRS 7A/B pair in the R CrA star-forming region. IRS 7A is probably a Class I protostar, whereas IRS 7B is likely to be in the Class 0/I transitional stage. Note the radio jet emanating from IRS 7B. The contour levels are plotted at 0.15, 0.5, 1.0, 2.0, and 3.0 mJy beam^{-1}. The beam HPBW ($6.5'' \times 5.7''$) is shown in the lower right corner. Modified from Fig. 4 of Paper III. **Right:** Same as in the left panel but at 20 cm wavelength. The radio lobes around IRS 7B are clearly visible at 20 cm, but become weaker at lower wavelengths. The contours go from 0.36 to 3.6 mJy beam^{-1}, in steps of 0.36 mJy beam^{-1}. The beam HPBW ($13.1'' \times 6.6''$) is shown in the lower right corner. Adapted from Paper III.

4.6.2 Non-thermal radio emission

Non-thermal radio continuum emission means that the radiation originates from a particle distribution whose energy distribution is not Maxwellian (see Longair 1981). Non-thermal emission is characterised by negative spectral indices of $\alpha < -0.1$. This can be explained naturally by optically thin gyrosynchrotron emission (Anglada et al. 1998). Gyrosynchrotron emission is produced by mildly relativistic electrons with energies ~ 1 MeV (Lorentz factor $\gamma \lesssim 2-3$) gyrating around the magnetic field lines (Ramaty 1969; Dulk & Marsh 1982). The free-free emission coefficient is proportional to $n(\mathrm{e})^2 T^{-0.5}$, whereas gyrosynchrotron emission goes as $n(\mathrm{e}) T^a B^b$, where $a, b > 1$. Thus, if the electron density is high enough, or if the temperature or the magnetic field strength is low enough, free-free emission is more important than gyrosynchrotron emission (Dulk 1985). The different frequency dependence of the two types of emission mechanisms may also cause the one dominating at lower frequencies and the other at higher frequencies.

There are three observational signatures that, if all detected, clearly indicate that the emission is non-thermal in nature (see André 1996):

1. Variability on timescales of hours to days.
2. Moderate degree of circular polarisation: $P_\mathrm{c} = |V|/I \lesssim 20\%$, where V and I are the Stokes parameters corresponding to flux density of the circularly polarised emission and the total flux density, respectively[15].
3. The brightness temperature is $T_\mathrm{B} \geq 10^7$ K.

The detection of circular polarisation provides direct evidence of circumstellar magnetic activity. The detection of circularly polarised flux at cm wavelengths implies that the magnetic field strength in the source is a few times 10^2 G to ~ 1 kG (Güdel 2002; Choi et al. 2009). For comparison, many theoretical models of protostellar outflows, which are based on the magnetocentrifugal ejection mechanisms, require the presence of dipolar magnetic fields with strength of ~ 1 kG at the protostellar surface (e.g., Camenzind 1990; Shu et al. 1994; see also André 1996).

Circularly polarised radio emission, indicative of gyrosynchrotron emission has been observed towards several PMS stars (e.g., White et al. 1992; Skinner 1993; Rodríguez et al. 1999; Johnston et al. 2003). In particular, Class III YSOs deprived of dense circumstellar envelope/disk are among the most powerful non-thermal radio stars known to date (e.g., Montmerle 1991; André 1996). On the other hand, it is very rare that young protostellar sources have a significant non-thermal emission component. The first reported detection of gyrosynchrotron emission from a protostar was made towards the Class I source IRS 5 in the R Coronae Australis star-forming region by Feigelson et al. (1998). In Paper III, we confirm this detection (see Fig. 4.7). There is also a

[15] To order of magnitude, the fractional circular polarisation amounts to about γ^{-1} (Longair 1981). Thus, P_c for synchrotron radiation is small because of the high energies involved. In one dramatic flare case, also linear polarisation has been observed towards the PMS multiple system HD 283447 in Taurus, which implies electron acceleration to highly relativistic velocities (Phillips et al. 1996).

possible detection of circularly polarised radio emission towards the low-mass (< 0.1 $M_\odot$) protostar L1014-IRS (Shirley et al. 2007). Recently, Choi et al. (2009) detected, for the first time, circularly polarised radio emission towards the Class I protostar IRS 7A in R CrA (see Fig. 4.6 and Sect. 7.3).

The fact that non-thermal radio emission from protostars is not commonly detected may not necessarily mean that they are magnetically inactive. André (1987) argued that YSO winds and ionised circumstellar material are sufficiently dense (optically thick) to free-free *absorb* non-thermal emission produced close to the protostar (see also André et al. 1990, 1992). This conforms with the fact that the non-thermal radio emitting protostar CrA IRS 5, does not appear to be powering an outflow, so its environment should be relatively free of absorbing ionised material (Feigelson & Montmerle 1999). Non-thermal radio emission has also been observed from shocked regions of outflowing gas (though mostly in high-mass star-forming regions). Examples include the Serpens radio jets (Rodríguez et al. 1989; Curiel et al. 1993; Curiel 1995; see also Raga et al. 2000), and radio lobes of a massive protostar IRAS 16547-4247 (Garay et al. 2003; Rodríguez et al. 2005). These observations indicate that electron acceleration can be very efficient in protostellar jets. Shocks associated with jets can accelerate electrons by the first-order Fermi mechanism, the process known as the diffusive shock acceleration (DSA; e.g., Crusius-Wätzel 1990). In this process, electrons are scattered off from the magnetic inhomogeneities, i.e., magnetic mirrors, where the field strength changes along a field line. This changes the direction of the moving electrons, enabling them to traverse the shock several times and to be repeatedly accelerated. In Paper III, we suggest that shock acceleration of electrons is a possible explanation for the observed non-thermal emisssion in the Class 0/I protostar IRS 7B. The radio emission of the lobes associated with IRS 7B decreases at higher frequencies which indicates that the lobes are, at least partly, non-thermal in nature (see Fig. 4.6). We note that some of the non-thermal sources observed in the directions of star-forming regions can also be pulsars or extragalactic objects. The strongest extragalactic sources are non-thermal in nature (see Rohlfs & Wilson 2004).

The magnetic activity in YSOs may originate from a magnetic dynamo generated in the deep convection zones of the stellar interior, i.e., similar to the Sun (note that T Tauri stars have fully convective interiors). However, because YSOs in their early evolutionary stages are surrounded by circumstellar material, magnetic configurations are probably quite complex. These include, for example, star-disk, star-envelope, or disk-disk fields (Feigelson & Montmerle 1999).

Sometimes YSOs show rapid flaring events, but they are much rarer than mid- to long-timescale variability (e.g., Stine et al. 1988). Such outbursts are possibly related to non-steady mass accretion (e.g., Zhu et al. 2009). Feigelson & Montmerle (1985) and White et al. (1992) found gyrosynchrotron radio flares in some YSOs. They were similar in character to those in the Sun, but orders-of-magnitude stronger. The flaring may occur in the stellar magnetosphere, at the star-disk interface, or above a circumstellar disk (Feigelson & Montmerle 1999). Feigelson et al. (1998) found that during the outburst of CrA IRS 5, its circular polarisation was 10% but then jumped to 37% within a day.

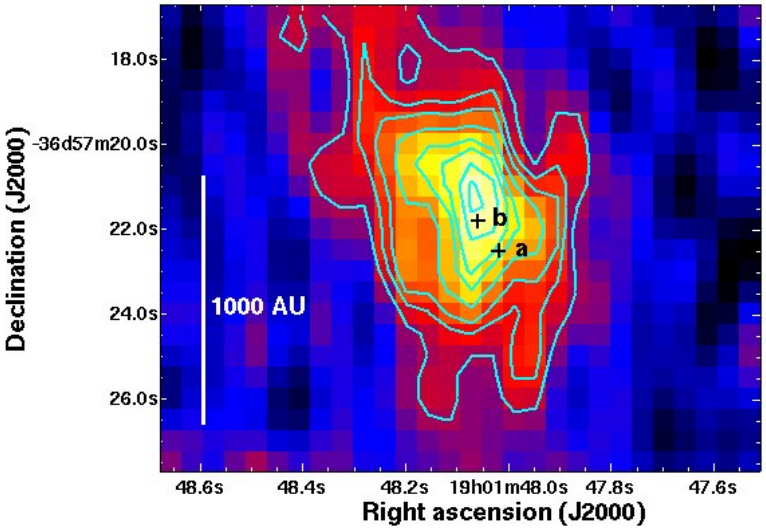

Figure 4.7: Stokes V image of the 3 cm continuum emission of IRS 5 in the R CrA star-forming region (Paper III). IRS 5 is a protobinary system and as a whole it is classified as a Class I source. a and b indicate the positions of IRS 5a and b, respectively (see Paper III and Choi et al. 2009 for details). The contour levels are plotted at 0.05, 0.08, 0.10, 0.13, 0.16, 0.18, 0.21, and 0.23 mJy beam^{-1}. The beam HPBW ($4.4'' \times 3.3''$) is comparable to the source size and is not shown for clarity.

In Paper III, the degree of circular polarisation of IRS 5 was found to be about 33%, which is at the high end of the above range of values, suggesting that the source was in a quiescent state. Feigelson et al. (1998) pointed out that explosive magnetic field reconnection is the only viable way to generate energetic electrons and to produce at the same time the radio variability observed in IRS 5. The CrA IRS 5 is the only known protostellar object which persistently emits a circularly polarised radio flux (Forbrich et al. 2006; Paper III). Thus, this source offers a great opportunity to study the magnetic activity of protostars (Choi et al. 2009).

4.6.3 Connection between the radio continuum emission of a YSO and its evolutionary stage

As proposed by Gibb (1999), there is a possible connection between the radio luminosity of embedded YSOs and their evolutionary stage. A significant fraction of Class 0 sources are associated with thermal radio continuum emission, whereas Class III PMS stars commonly exhibit a variable, non-thermal radio emission (André 1996). What comes to the Class I protostars, they are not always detected at radio wavelengths. For instance, Lucas et al. (2000) detected 4 out of 7 (57%) Class I sources (with outflow activity) in Taurus, while Lehtinen et al. (2003) detected only 1 out of 4 (25%) Class I sources associated with the reflection nebula Cederblad 110 in the Chamaeleon I molecular cloud.

Moreover, the radio detection rate amongst the Class II sources is lower than for the other YSO classes (see Lehtinen et al. 2003).

Gibb (1999) suggested that radio continuum emission can be detected only towards YSOs in their earliest *and* latest evolutionary stages. In the earliest evolutionary stages, free-free emission from ionised jets is dominating. As the mass accretion rate and, consequently, the outflow activity/efficiency, decreases the free-free emission declines. The non-thermal emission becomes observable as the jet emission declines. Finally, the radio emission will be dominated by gyrosynchrotron processes, which arise as a consequence of a magnetic field activity close to the YSO or star-disk interaction region. The above scenario is consistent with the idea that the mass accretion rate and mass ejection both decline with time (Bontemps et al. 1996a; Henriksen et al. 1997). The YSO radio characteristics studied in Paper III are in rough agreement with the scheme that the dominant emission mechanism changes with time. We note, however, that in the ρ Oph cloud, there is no observational evidence to support the idea of a connection between the radio emission and the evolutionary stage of a YSO (see Gibb 1999). Indeed, both the source geometry (i.e., the inclination of the star-disk system with respect to observer), and opacity effects could be responsible for this (possibly) apparent correlation.

Finally, we note that the observed spectral index reflects mainly the source average optical thickness. Thus, it is rather unreliable way to determine the nature of YSO radio emission based solely on the radio spectral index (André 1996; Choi et al. 2008).

4.7 Lifetime of the prestellar phase of core evolution

The duration of the prestellar phase of low-mass core evolution is an important parameter when examining the dominant processes of star formation. From the observational point of view, there are two methods to estimate core lifetimes: (i) using molecular abundances as "chemical clocks", and (ii) the statistical method. The latter approach was used in Papers I and II of this thesis.

Chemical age of the core can be estimated by comparing the observed chemical abundances to those obtained from chemical models (see van Dishoeck et al. 1993; van Dishoeck & Blake 1998; Buckle & Fuller 2003). For example, based on the chemical model of molecular freeze-out, Jørgensen et al. (2005) suggested a timescale of $\sim 10^5$ yr for the dense prestellar phase of core evolution (cf. Eq. (4.15)). Similarly, based on the time-dependent model of deuterium fractionation including the effects of the ortho/para H_2 ratio, Pagani et al. (2009) concluded that the age of the L183 prestellar core is about a few times 10^5 yr. However, chemical age does not necessarily reflect the age of the core since its formation. This is particularly the case for protostellar cores, where chemical clock can be reset if, e.g., fresh carbon is brought into the core by turbulence or outflows (Langer et al. 2000).

The statistical method for estimating prestellar core lifetimes is based on the observed number ratio of starless cores to cores with embedded YSOs, i.e., Class 0 and I objects, $N_{\rm sl}/N_{\rm emb}$. By assuming that the cores are sampled at a random point in time, the relative numbers of objects in distinct evolutionary stages roughly correspond to the relative time

spent in each phase. The duration of the starless phase can then be inferred from the ages of the embedded YSOs, using the following steady-state equation

$$\tau_{\rm sl} = \tau_{\rm emb} \times \frac{N_{\rm sl}}{N_{\rm emb}}\,, \tag{4.33}$$

where $N_{\rm emb} = N_{\rm Class\,0} + N_{\rm Class\,I}$ (e.g., Hatchell et al. 2007; Jørgensen et al. 2007; Enoch et al. 2008; Evans et al. 2009). For instance, Enoch et al. (2008) found that there are approximately equal numbers of starless and protostellar cores in Perseus ($N_{\rm sl}/N_{\rm emb} = 1.0$), and Ophiuchus ($N_{\rm sl}/N_{\rm emb} = 0.8$) but in Serpens, the observed ratio was 0.4[16]. In Paper I, we found that $N_{\rm sl} = N_{\rm emb}$ in the Orion B9 star-forming region. In Paper II we revised those numbers as some of the cores seen towards Orion B9 are likely to be members of the "low-velocity part" of Orion B and not associated with the same cloud volume as the other cores. As a result, the $N_{\rm sl}/N_{\rm emb}$ ratio is likely to be slightly higher. Approximately equal ratios are also seen in numerical simulations of turbulent molecular clouds (e.g., Galván-Madrid et al. 2007). In the case that $N_{\rm sl} \sim N_{\rm emb}$, the lifetime of the prestellar phase should be comparable to the lifetime of embedded protostars, i.e., $\sim 5 \times 10^5$ yr (see Sects. 4.4.2 and 4.4.3)[17]. For typical core densities of $n({\rm H_2}) \sim 10^4 - 10^5$ cm^{-3}, this is only a few times the free-fall time

$$\tau_{\rm ff} \equiv \left(\frac{3\pi}{32 G \bar{\rho}}\right) = 3.4 \times 10^5 \left(\frac{\bar{n}({\rm H_2})}{10^4\,{\rm cm^{-3}}}\right)^{-1/2} {\rm yr}\,, \tag{4.34}$$

where the numerical value is based on the mean core density of $\bar{\rho} = 2.33 m_{\rm H} \bar{n}({\rm H_2})$ (see Fig. 4.8 and Ward-Thompson et al. 2007 for a review). Such short lifetimes suggest a dynamic, rather than slow quasi-static core evolution (see Sects. 4.8 and 6.5), at least after cores have reached high enough densities ($n({\rm H_2}) \gtrsim 10^4$ cm^{-3}) to become visible at sub(mm) wavelengths. For comparison, in numerical simulations where highly turbulent processes dominate the evolution of a molecular cloud, core lifetimes are also only $\approx 1 - 2\tau_{\rm ff}$ (Ballesteros-Paredes et al. 2003; Vázquez-Semadeni et al. 2005). It has been suggested that starless cores may spend an appreciable fraction of their lifetime having (column) density contrasts with the parent molecular cloud too low to be identified as "cores" (Tassis & Mouschovias 2004). Consequently, the value of $N_{\rm sl}$, and thus $\tau_{\rm sl}$, would be underestimated in some dust continuum surveys. However, almost all molecular clouds show signs of star formation, indicating that star formation starts soon after the cloud formation, so the cores within clouds should not have very much time to spend in low-density phase.

The statistical method suffers from the fact that a number of lower mass stars might be missed. For instance, Spitzer IR observations have revealed the presence of extremely

[16] Later, Foster et al. (2009) found that $N_{\rm sl}/N_{\rm emb} = 2$ in isolated regions in Perseus, and 1.4 in clustered regions. The larger ratios compared to those found by Enoch et al. (2008) are mostly due to the larger number of cores (mainly starless) studied by Foster et al. (2009) (and which are not in the sample of Enoch et al. (2008)). Moreover, Foster et al. (2009) used a different method to distinguish between starless and protostellar cores (e.g., the proximity of IR point source to the core).

[17] The lifetime of the protostellar phase can be similarly estimated from the number ratio of protostars to T Tauri stars, and using the age estimates for the T Tauri stars.

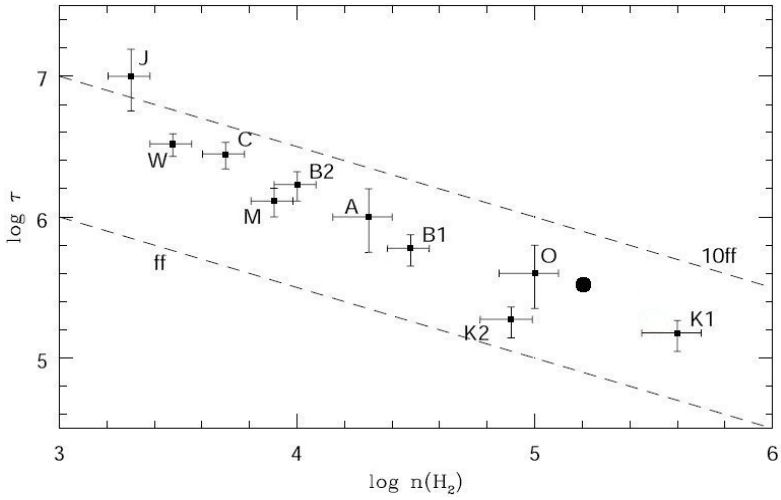

Figure 4.8: A log-log plot of core lifetime as a function of the mean H_2 number density for the starless/prestellar core samples. The dashed lines indicate the free-fall timescale, $\tau_{\rm ff}$ (lower), and $10\tau_{\rm ff}$ (upper). The filled circle indicates the result of Enoch et al. (2008; $\tau_{\rm sl} = 4.5 \times 10^5$ yr for their combined sample). For instance, the core lifetimes in the density range $\sim 2\times10^4 - \sim 2\times10^5$ cm^{-3} appear to be between $\sim 3\times10^5 - \sim 10^6$ yr, i.e., $\sim 4\tau_{\rm ff}$. Figure is modified from Ward-Thompson et al. 2007 (see the references therein).

faint embedded protostars inside some dense cores that were previously believed to be starless (e.g., Dunham et al. 2008 and references therein). On the other hand, an IR source seemingly associated with the core may be, e.g, a background star or a galaxy in the line of sight, though the propability for this is low. As discussed in Sect. 4.1, some of the observed starless cores may dissolve, i.e., they are *not* prestellar. In this case, the number ratio $N_{\rm sl}/N_{\rm emb}$ overestimates the lifetime ratio (Vázquez-Semadeni et al. 2005; Galván-Madrid et al. 2007). Moreover, the statistical fluctuation of the number of objects in time is considered to be an important issue (Galván-Madrid et al. 2007). Finally, in the statistical lifetime estimation it is assumed that the core lifetime does not depend on the core mass. For instance, Hatchell et al. (2005) found, however, that the $N_{\rm sl}/N_{\rm emb}$ ratio decreases with mass (above 12 $M_\odot$, there were no starless cores at all; see also Hatchell & Fuller 2008). This suggests that massive cores evolve faster, i.e., the lifetime of a massive prestellar core is short (cf. Sect. 5.2.1 and Paper IV). An observer is therefore more likely to detect the longest lived objects rather than the ones which evolve rapidly.

4.8 Ambipolar diffusion and the standard model of low-mass star formation

For several years, the "standard model" of low-mass star formation was the one in which molecular cloud cores are initially magnetically supported, and the core collapse ensues after the magnetic support has been removed (Nakano 1984; Shu et al. 1987). Magnetic flux can be removed through the process called ambipolar diffusion (AD), in which neutrals drift quasi-statically (under their own self-gravity) relative to ions and magnetic field. This process was originally proposed by Mestel & Spitzer (1956). As a consequence of AD, an initially magnetically subcritical core will become magnetically supercritical, and dynamical collapse can ensue (e.g., Turner & Heiles 2006). When the core centre collapses, the outer layers lose their pressure support, and also they will fall towards the centre. Thus, the gravitational collapse propagates from inside out and this process leads to the formation of a central star (the so-called "inside-out" collapse). The timescale for quasistatic AD is $\tau_{\rm AD} = r/|v_{\rm D}| \propto \tau_{\rm ff}^2/\tau_{ni}$, where r is the distance from axis of symmetry, $v_{\rm D} \equiv v_i - v_n$ is the drift speed between ions and neutrals, and $\tau_{ni} = (m_i + m_n)/m_i \times 1/(n_i \langle \sigma v \rangle_{in})$ is the neutral-ion collision time (Mouschovias 1991). m_n and m_i are the masses of the neutrals and the ions, respectively, n_i is the number density of ions, and $\langle \sigma v \rangle_{in}$ is the rate coefficient for the momentum transfer between the ions and neutrals (mostly H_2). The AD timescale can be written as (Walmsley et al. 2004)

$$\tau_{\rm AD} \approx \frac{2}{\pi G m_n^2} \sum_i \frac{n_i}{n_n} \frac{m_i m_n}{m_i + m_n} \langle \sigma v \rangle_{in} \,, \tag{4.35}$$

where $n_n = \rho_n/m_n$ is the number density of neutrals, and the summation goes over all ionic species. At low temperatures, the rate coefficient for momentum transfer is (Flower 2000)

$$\langle \sigma v \rangle_{in} = 2\pi e \left(\alpha \frac{m_i + m_n}{m_i m_n} \right)^{1/2} , \tag{4.36}$$

where e is the elementary charge, and α is the polarisability of H_2. Note that $\tau_{\rm AD}$ is proportional to the square root of the reduced mass of the ion-neutral pair, $\mu_{in} \equiv m_i m_n/(m_i + m_n)$.

The AD timescale (4.35) depends strongly on the ionic composition. For instance, $\tau_{\rm AD}$ increases by $\sim 60\%$ as the main ionic species changes from H^+ to HCO^+ (Walmsley et al. 2004; see Sect. 4.3.1). $\tau_{\rm AD}$ depends also on the sizes of dust grains: the smaller the grains are, the shorter $\tau_{\rm AD}$ will be because of the more rapid neutralisation on grain surfaces (Walmsley et al. 2004). On the other hand, AD can redistribute the abundances of dust grains in the core. This is due to the fact that the negatively charged grains are attached to the magnetic field and are thus "left behind" as the neutrals drift inward; also the grain size distribution changes because AD acts more effectively on the larger grains and thus the smaller grains leave behind in the core envelope (Ciolek & Mouschovias 1996, 1998; Ciolek & Basu 2001; Kunz & Mouschovias 2009b).

Because stars form in dark clouds which are efficiently shielded from the ISRF, the ionisation degree is expected to decrease to a level where AD can proceed in a relevant timescale (Shu et al. 1987). The theory of AD-controlled star formation predicts that the timescale to form magnetically supercritical cores is $\tau_{\rm AD} \sim 10 - 20\tau_{\rm ff}$ (e.g., Ciolek & Mouschovias 1995). Thus, according to this scenario, star formation is a slow, quasi-static process, and the precursors of low-mass stars, the starless cores, should be long-lived objects with lifetimes of $\sim \tau_{\rm AD}$ (Nakano 1998). However, if the initial conditions are already near-magnetically critical or marginally subcritical ($\lambda \lesssim 1$), only a small amount of magnetic flux needs to be removed and the time for the core to become magnetically supercritical is significantly shorter, only a few times $\tau_{\rm ff}$ (Nakano 1998; Ciolek & Basu 2001; Hartmann et al. 2001). It is also shown by numerical simulations (e.g., Li & Nakamura 2004; Vázquez-Semadeni et al. 2005; Nakamura & Li 2005), that in the case the gas is initially magnetically supercritical, magnetic fields have a relatively small effect in slowing the star formation rate (SFR). Indeed, observations indicate that, on large scales, molecular clouds are nearly critical, or even slightly supercritical (e.g., McKee 1989; McKee et al. 1993). We note, however, that the AD theory does not require strongly magnetised clouds (Mouschovias et al. 2006). The above timescale is consistent with observations suggesting that the core lifetimes are not much longer than their free-fall times.

4.8.1 Observational support for the AD theory

Star formation controlled by AD is rather an inefficient and slow process. In principle, this is in agreement with the low global SFR (and low SFE; see Sect. 6.4) observed in the Galaxy, i.e., $\sim 3 - 5$ $\rm M_\odot$ $\rm yr^{-1}$ (Prantzos & Aubert 1995). If the molecular gas in the Galaxy would form stars at the free-fall rate, the Galactic SFR would be ~ 10 times higher (see Turner & Heiles 2006). There is also observational support for the AD theory on scales of molecular cloud cores. Some of them are listed below:

1. The AD theory predicts that the mass-to-magnetic flux ratio of dense cores is critical or slightly supercritical ($\lambda \approx 1 - 3$) which is in good agreement with observations (e.g., Mouschovias et al. 2006; see Sect. 4.2.2).

2. Cores within molecular clouds are found in regions of high extinction, i.e., in the cloud interiors, rather than near the cloud surface (e.g., Johnstone et al. 2004; Enoch et al. 2007). This is consistent with the AD process which leads to the formation of magnetically supercritical cores in the cloud interiors.

3. In the prestellar core L1544, $\tau_{\rm AD} \sim \tau_{\rm ff}$ because of the very low ionisation degree (Caselli et al. 2002b). This is consistent with the fact that the core is observed to be nearly magnetically critical and is on the verge of dynamical collapse (Troland & Crutcher 2008).

4. Benson et al. (1998) measured the velocity difference between $\rm N_2H^+$ and neutral species ($\rm C_3H_2$ and CCS) in 60 dense cores. The upper limit on the ion-neutral drift

speed Benson et al. (1998) derived, $v_{\rm D} \leq 30$ m s^{-1}, is comparable to the expected ion-neutral drift speed in cores undergoing AD (e.g., Ciolek & Mouschovias 1995; Ciolek & Basu 2000).

5. The AD theory predicts that the magnetic field strength scales with the gas density as $B \propto \rho^{\kappa}$, with $\kappa \leq 0.5$. Indeed, Crutcher (1999) found that $\kappa = 0.47 \pm 0.08$ for the sample of 15 magnetic field detections in molecular clouds/clumps, consistent with the theoretical prediction (although there is a significant scatter in the fitted data). The value of $\kappa \approx 0.47$ was also found in numerical models of AD driven cloud contraction by Fiedler & Mouschovias (1993).

6. The radial density profiles of prestellar cores are qualitatively consistent with models of magnetically supported cores evolving through AD (e.g., Ciolek & Mouschovias 1995).

4.8.2 Observational evidence against the AD theory

One of the main criticisms against the "standard" scenario of low-mass star formation is that, at the average density of a molecular cloud ($n({\rm H_2}) \sim 100$ cm^{-3}), $\tau_{\rm AD}$ is typically longer than the cloud lifetime (e.g., Mouschovias et al. 2006 and references therein). However, if molecular clouds form in a magnetically supercritical state, the above timescale discrepancy can be avoided. Other results that are in contradiction with the AD theory are the following:

1. The observational estimates of the $\tau_{\rm AD}/\tau_{\rm ff}$ ratios for dense cores typically range from several tens to a few hundred (Caselli et al. 1998; Paper I). These are much longer than the statistical lifetime estimates in typical molecular cloud environments. The latter ones indicate dynamic rather than quasi-static picture of star formation. As mentioned in Sect. 4.7, the observational results could still be consistent with a quasi-static picture, if the cores are only identified in their densest stages ($n({\rm H_2}) \gtrsim 10^4$ cm^{-3}) of a longer scale evolution (extended core-building stage), when they are already magnetically critical to slightly supercritical (Tassis & Mouschovias 2004; Paper I). Also, the process of AD can be accelerated by several mechanisms, e.g., by turbulent fluctuations (see Sect. 6.5 and references therein).

2. In some prestellar cores, spectral lines of several cations (HCO^+, DCO^+, N_2H^+) show infall asymmetry (see Myers et al. 2000). This rules out the AD theory in its most extreme form, in which ions are stationary and the neutrals drift inward.

3. Magnetic support in quasi-equilibrium objects would be expected to produce oblate (flattened) cores. However, isolated dense cores are, statistically, found to be triaxial with a tendency being prolate.

4. According to the idealised AD theory of star formation, the mass-to-magnetic flux ratio should increase from the envelope to core, $[M/\Phi]_{\rm core}/[M/\Phi]_{\rm envelope} > 1$.

However, Crutcher et al. (2009) examined OH Zeeman observations of 4 nearby dense cores, and found that M/Φ *decreases significantly* from the ~ 1 pc envelope to the ~ 0.1 pc core. This is in severe contradiction with the hyphothesis that the cores were formed through AD. We note that the results presented in the Crutcher et al. (2009) paper were strongly criticised by Mouschovias & Tassis (2009) because of e.g., neglecting the spatial variations of the field in the core envelopes (but see Crutcher et al. 2010 for the response).

In summary, the observational data are not consistent with the idea that most cores are born in highly subcritical state, and lose their magnetic flux slowly (over $\sim 10\tau_{\rm ff}$). Obviously, accurate measurements of the magnetic field strengths are needed to determine the importance of AD in the star formation process. An alternative picture for the AD regulated star formation is the one in which molecular cloud evolution is driven by *turbulence*. This will be further discussed in Chapter 6.

Chapter 5

High-mass star formation

Papers IV and V of this thesis deal with the formation of high-mass stars. This chapter gives an overview of this topic.

5.1 Introduction

As was discussed in the previous chapter, the outlines of low-mass star formation are relatively well understood. The formation of intermediate-mass ($\sim 2 - 8$ $M_\odot$) stars, though not much studied yet, is likely to be controlled by the same processes as those effective in the birth of low-mass stars (e.g., Crimier et al. 2010). However, the formation of high mass-stars ($M > 8$ $M_\odot$)[1] is still far from being well understood and is a matter of debate (see Zinnecker & Yorke 2007 for a review). High-mass stars are very important in many sense. For example, high-mass stars dominate the evolution of their parent molecular cloud (and the subsequent nearby star-formation activity) through their powerful winds, ionising UV radiation, and supernova (SN) explosions (e.g., Wada & Norman 2001; Yorke & Bodenheimer 2008). High-mass stars are also the source of the heaviest elements in the universe: Elements heavier than oxygen are synthesised inside massive stars and are ejected in the ISM through winds and SN explosions; elements heavier than iron are made in SNe.

The traditional problem related to the formation of high-mass stars is that they exert such an intense radition pressure on the surrounding material, that their formation should be inhibited (e.g., Kahn 1974; Wolfire & Cassinelli 1987; Jijina & Adams 1996; Yorke & Sonnhalter 2002), whereas for low-mass stars, radiation pressure is negligible. The reason for this is that high-mass stars have Kelvin-Helmholtz timescales, $\tau_{\rm KH} \equiv GM_\star^2/R_\star L_\star$, shorter than the free-fall timescale (see Eq. (4.34)), and thus young high-mass stars begin to burn their nuclear fuel and radiate vast amounts of energy while still gaining mass[2]. There are several possible solutions to overcome the radiation pressure problem, including completely different formation scenarios (see below).

Other reasons why high-mass star formation is poorly understood are the following:

[1] These stars, which are also called OB stars, have luminosities $> 10^3$ $L_\odot$, and spectral types of B3 or earlier.

[2] This is the critical difference between low- and high-mass star formation. Low-mass stars have longer Kelvin-Helmholtz times, and thus they undergo an extensive PMS evolution after accretion has finished. For high-mass stars, there should be no optical PMS phase at all, but they are expected to be born directly on the ZAMS (e.g., Palla 2005) while still embedded, and possibly still accreting.

1. The formation of high-mass stars takes only $\lesssim 10^5$ yr (e.g., Motte et al. 2007), i.e., they form much faster than low-mass stars.

2. High-mass stars and star-forming regions are rare and typically more than a kiloparsec away[3]. The achieved spatial resolution of observations is thus quite low.

3. High-mass star-forming regions are more heavily obscured by dust, and they are more complex (almost always in clustered conditions)[4] than the well-studied regions of low-mass star formation.

4. The energetics of high-mass stars (e.g., luminosities, outflow energies, and accretion rates) are orders of magnitude higher than those associated with low-mass stars and thus the interaction with their environs is very strong (e.g, Arce et al. 2007).

5. The chemistry of high-mass star-forming regions is extremely rich and complex.

Observations have shown that high-mass star-forming cores (or clumps) are typically characterised by sizes ($\sim 0.2-0.5$ pc), masses ($\sim 100-1000$ $M_\odot$), and velocity dispersions ($\sim 1.5-4$ km s^{-1}) that are roughly an order of magnitude larger than those of low-mass cores (e.g., Beuther et al. 2007 and references therein). One of the most important questions related to the formation of high-mass stars is whether they form by a scaled-up version of low-mass star formation, i.e., through accretion with the coupled formation of a disk and bipolar outflow ? Currently, the main competing theories of high-mass star formation are:

1. Monolithic collapse (McKee & Tan 2003)[5].

2. Competitive accretion (Sect. 5.5.1).

3. Stellar collisions and mergers (Sect. 5.5.2).

Another intriguing question is how a massive dense core can collapse into a single high-mass star ? Because of the low temperature and high density of massive cores, the local thermal Jeans mass is low ($M_{\rm J} \propto T^{3/2}\rho^{-1/2}$). In addition, unlike low-mass cores, massive cores are turbulent and thus they are expected to fragment into smaller low-mass condensations (e.g., Dobbs et al. 2005). In high-resolution interferometric studies some of the massive cores are found to be fragmented (e.g., Hennemann et al. 2009; Bontemps et al. 2009). In the McKee & Tan (2003) model of monolithic collapse the level of core fragmentation is reduced (e.g., due to density fluctuations), enabling the collapse into a

[3]The nearest region of high-mass star formation is the Kleinmann-Low (KL) nebula in Orion, at a distance of ~ 420 pc (Kim et al. 2008).

[4]About 4% of massive stars are neither members of clusters nor obvious runaways from clusters, and thus are likely to be truly isolated (de Wit et al. 2005).

[5]This is the turbulent core model, which is an extension of the classic low-mass star formation theory. In this model, very high accretion rates of $\sim 10^{-4}-10^{-3}$ $M_\odot$ yr^{-1} are expected in highly turbulent clumps/cores in which high-mass stars form. Such high accretion rates can overcome the radiation pressure.

single high-mass star. On the other hand, the competitive accretion and merger models are based on collective effects and thus conform with the fact that high-mass stars form in clusters.

Currently, there is no generally accepted scenario for high-mass star formation. However, if it really is a scaled-up version of low-mass star formation one would expect the evolutionary sequence to be the following (Beuther et al. 2007; see also Tan 2008): high-mass starless core (HMSC)→ massive dense core containing accreting low- to intermediate-mass protostars destined to become high-mass protostars → massive core containing high-mass protostar(s), i.e., high-mass protostellar object (HMPO) → final massive star(s). As will be discussed in the next sections, increasing observational evidence supports a picture in which high-mass stars form in a similar way as their lower mass counterparts.

In what follows is an overview of what we have learned about high-mass star formation, the emphasis being in the topics relevant for the present thesis.

5.2 Infrared dark clouds

In recent years it has become evident that the very first steps of high-mass star (and star cluster) formation can be studied in the so-called infrared dark clouds (IRDCs). IRDCs were first discovered by the Infrared Space Observatory (ISO) and the MSX surveys as (often filamentary) dark extinction features against the diffuse Galactic MIR background caused by the polycyclic aromatic hydrocarbon (PAH) emission (particularly at 8 μm), see Fig. 5.1 (Pérault et al. 1996; Egan et al. 1998; Carey et al. 1998; Hennebelle et al. 2001; Simon et al. 2006a).

Studies of IRDCs have shown that they are cold (< 25 K), dense ($n(\mathrm{H_2}) \gtrsim 10^5$ cm^{-3}), and have very high column densities ($N(\mathrm{H_2}) \gtrsim 10^{22}$ cm^{-2})[6] (e.g., Egan et al. 1998; Carey et al. 1998, 2000; Simon et al. 2006a; Rathborne et al. 2006). Typical sizes and masses of IRDCs are $\sim 1-5$ pc and $\sim 10^2 - 10^3$ M$_\odot$, respectively (Simon et al. 2006b; Rathborne et al. 2006; Vasyunina et al. 2009). The possibility that IRDCs represent the earliest stages of high-mass star formation is supported by the fact that their above mentioned physical characteristics are similar to those of warm molecular clumps out of which massive stars/star clusters are supposed to eventually form (cf. Beuther et al. 2002a; Motte et al. 2003; Faúndez et al. 2004; Paper V). Further support is provided by the fact that the peak in the IRDC galactocentric radial distribution corresponds to the Galaxy's 5 kpc molecular ring, which is the Galaxy's most active star-forming structure (Simon et al. 2006a; see also Jackson et al. (2008b) for the association of IRDCs with a Milky Way spiral arm). Rathborne et al. (2009a) estimated that the total SFR within IRDCs is ~ 2 M$_\odot$ yr^{-1}. This value is quite close to the global SFR of the Galaxy.

IRDCs are often found to contain cold dense clumps and cores. This signify that they have begun to fragment (see Sect. 6.1.1 and Paper IV).

[6] Krumholz & McKee (2008) showed that only molecular clouds with column densities of at least 1 g cm^{-2}, i.e., $N(\mathrm{H_2}) \simeq 2.2 \times 10^{23}$ cm^{-2}, can form high-mass stars.

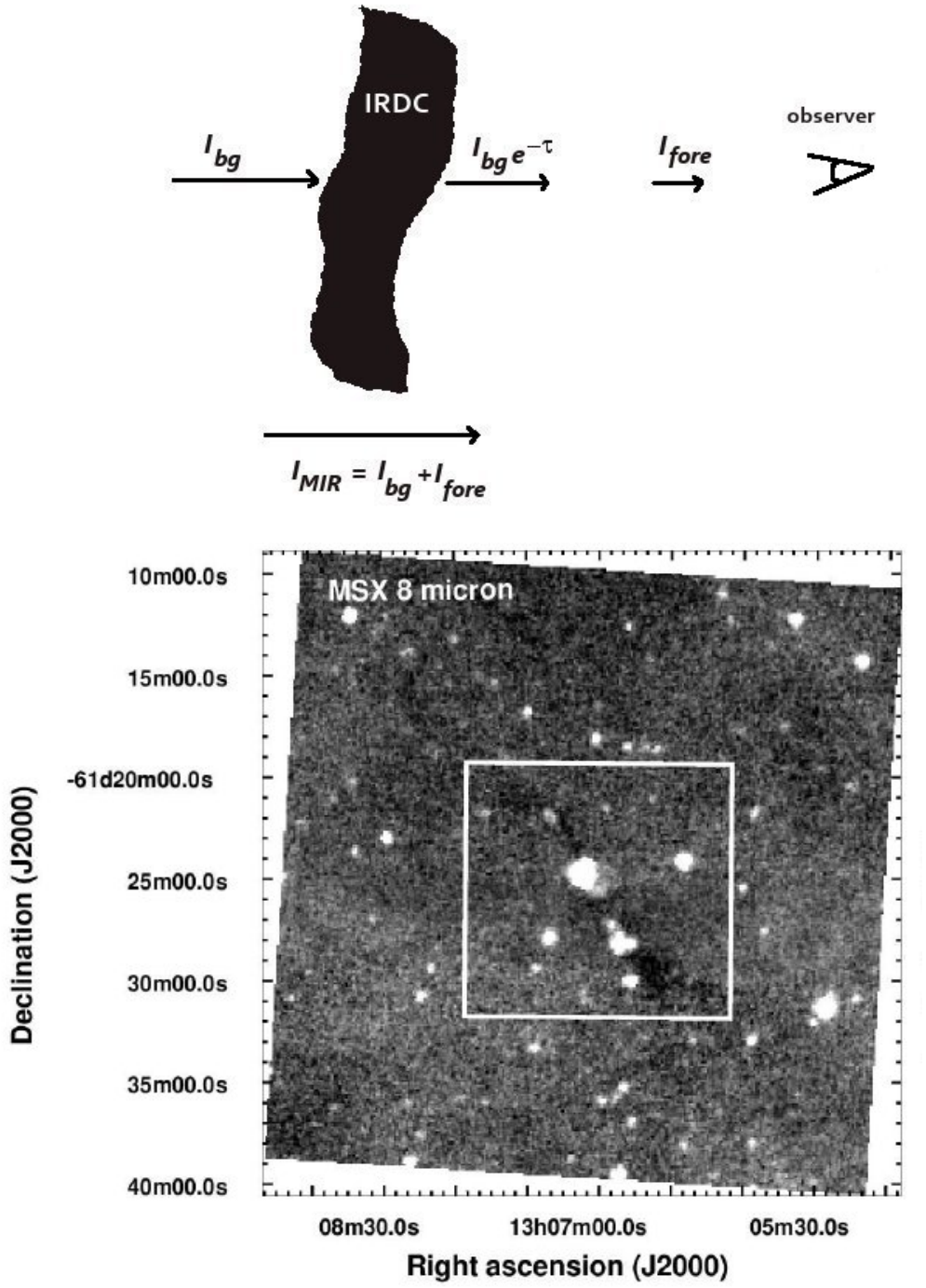

Figure 5.1: **Top:** A sketch showing how IRDCs are seen as dark extinction features against the bright MIR Galactic background radiation ($I_{\rm bg}$). The observed intensity from the cloud is $I^{\rm obs}_{\rm IRDC} = I_{\rm bg}e^{-\tau} + I_{\rm fore}$, where $I_{\rm fore}$ is the intensity contribution from foreground material. The MIR intensity around the cloud is $I_{\rm MIR} = I_{\rm bg}+I_{\rm fore}$ (see Paper IV). **Bottom:** MSX 8 μm image showing the MIR extinction of the IRDC G304.74+01.32. The white rectangle shows the area we mapped in the 870 μm submm dust continuum. Adapted from Paper IV.

5.2.1 Substructures within IRDCs

One of the most important steps towards understanding the formation of high-mass stars is to identify the earliest stages in the process. Submillimetre and millimetre dust continuum observations have shown that IRDCs often contain dense clumps (e.g., Carey et al. 2000; Redman et al. 2003; Garay et al. 2004; Beuther et al. 2005a; Rathborne et al. 2005, 2006; Paper IV). These clumps have typical temperatures of ≈ 15 K, sizes of $\lesssim 0.5$ pc, and masses of ~ 120 $M_\odot$ (Rathborne et al. 2006). Some of the clumps within IRDCs already show signs of ongoing (high-mass) star formation, such as outflows, bright CH_3OH and H_2O masers, hot core chemistry (see Sect. 5.3.1), and bright MIR emission, which presumably arises from heated dust around an embedded protostar(s) (e.g., Carey et al. 2000; Beuther et al. 2005a; Rathborne et al. 2005; Pillai et al. 2006; Wang et al. 2006; Ellingsen 2006; Beuther & Sridharan 2007; Rathborne et al. 2007, 2008; Sanhueza et al. 2010; Rathborne et al. 2010; Paper IV). Some IRDCs, however, appear to give birth only to low- to intermediate-mass stars (see Paper IV). In a few IRDC clumps the degree of deuterium fractionation of the same order of magnitude as in the low-mass dense cores has been detected (e.g., Chen et al. 2010a). Moreover, some clumps contain multiple subcondensations (i.e., cores), which indicate cluster formation (Rathborne et al. 2008; Chambers et al. 2009; Zhang et al. 2009; Beuther & Henning 2009).

Some of the clumps within IRDCs are found to be quiescent (narrow linewidths, low temperatures, no embedded IR sources), and are thus excellent candidates of being HMSCs. They provide the best targets to study the initial conditions of high-mass star formation (Sridharan et al. 2005a; Jackson et al. 2008a; Chambers et al. 2009). Figure 5.2 shows one of the starless IRDC clump candidates studied in Paper IV. Parsons et al. (2009) derived an upper limit of $10^3 - 10^4$ yr for the lifetimes of starless IRDC clumps suggesting that the duration of the high-mass prestellar phase is extremely short.

In summary, some of the dense clumps and cores within IRDCs are excellent candidates of being the cold precursors to HMPOs, and thus their physical and chemical properties provide powerful constraints on the initial conditions of high-mass star formation.

5.3 High-mass protostellar objects

HMPOs can be defined as protostars with masses of $\gtrsim 8$ $M_\odot$; furthermore, at some point they form a detectable hot molecular core (HMC) and hyper-/ultra-compact HII region around themselves.

5.3.1 Hot cores

The so-called HMC is the earliest well-characterised observable phase in the process of high-mass star formation. HMCs are massive ($\sim 10^2$ $M_\odot$), dense ($n(H_2) = 10^6 - 10^8$ cm^{-3}), hot ($100 - 300$ K), and small (diameters $\lesssim 0.1$ pc) condensations around high-mass protostars (e.g., Kurtz et al. 2000; Cesaroni 2005). The nearest and best studied HMC (and the nearest massive protostar, the radio source I) is located in the Orion-KL region (e.g., Beuther & Nissen 2008). However, the Orion Hot Core might represent a

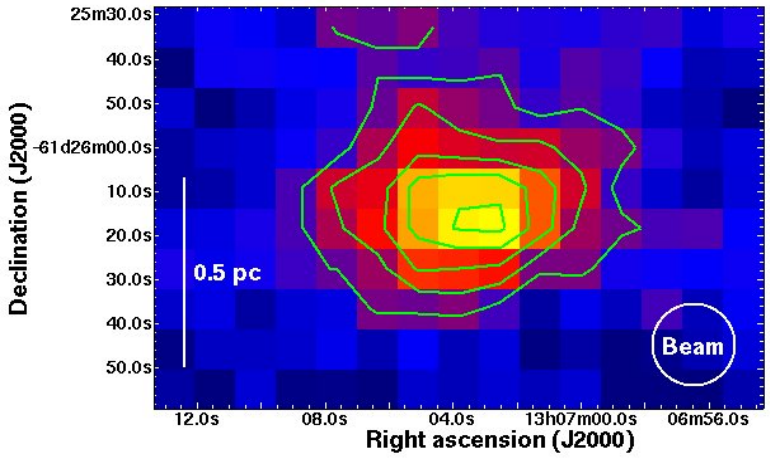

Figure 5.2: LABOCA 870 μm dust continuum image of the MIR dark clump SMM 7 in the IRDC G304.74+01.32. The clump effective radius and mass are 0.35 pc and $\sim$ 50 $M_{\odot}$, respectively. The contour levels are plotted at 0.05, 0.10, 0.15, 0.20, and 0.25 Jy beam^{-1}. The beam HPBW of 18.6$''$ is shown in the lower right corner. Enlargement of Figure 1 (left) of Paper IV.

special case of a HMC as it is possibly externally heated and just the remnant of the core from which the other sources in the region have formed (Beuther et al. 2004; Zapata et al. 2010).

HMCs are characterised by high abundances of complex organic (i.e., C- and O-bearing) molecules, such as CH_3OH, CH_3CN, CH_3OCH_3, C_2H_5OH, and $HCOOCH_3$ (e.g., Blake et al. 1987; Schilke et al. 2001; Mookerjea et al. 2007). The origin of complex molecules in HMCs is not yet clear. They are either formed on the dust grains during the cold phase (i.e., IRDC phase) or such species are formed through high-temperature gas-phase reactions after the precursor molecules are evaporated (see Bisschop et al. 2007 and references therein). Deuterium-bearing species are also detected in HMCs, and they are remnants of a previous cold phase (e.g., Roberts & Millar 2007 and references therein). A few hot cores have been detected in IRDCs, indicating that there is an evolutionary link between the massive IRDC clumps/cores and HMPOs (Rathborne et al. 2007, 2008).

The duration of the HMC phase is believed to last $\sim 10^5$ yr and it may represent a phase prior to the formation of a hypercompact, and furthermore, ultra-compact HII region (but not necessarily in the case of the Orion Hot Core) (e.g., Doty et al. 2006; Beuther et al. 2007). This is supported by the fact that HMCs do not yet show significant free-free radio emission (e.g., Osorio et al. 2009 and references therein).

5.3.2 Hyper- and ultra-compact HII regions

Hypercompact (HC) HII regions are small (diameters $\lesssim 0.01$ pc) and dense ($n(H_2) \gtrsim 10^6$ cm^{-3}) photoionised nebulae produced by strong UV radiation from OB stars (e.g., Kurtz 2005; Beuther et al. 2007; Hoare et al. 2007). They possibly represent the photoevaporating disks associated with individual deeply embedded high-mass stars (Keto 2007; Zinnecker & Yorke 2007). HC HII regions are often found to be in groups of ≥ 2 components (Sewilo et al. 2004), which suggest that they are ionised by a single OB star or possibly a binary system. It is not yet clear whether HC HII regions form after the HMC phase or whether HMCs and HC HII regions co-exist simultaneously (e.g., Beuther et al. 2007; Lizano 2008).

HC HII regions develop to so-called ultra-compact (UC) HII regions, which are $\gtrsim 10$ times larger, ~ 100 times less dense, and less bright than HC HII regions (Kurtz 2002; Churchwell 2002). The radio brightnesses and sizes of UC HII regions indicate that they are ionised by high-mass stars of spectral type earlier than B3 (Peters et al. 2010 and references therein). Some of the UC HII regions may still harbour accreting massive protostars, i.e., are at the end of the HMPO stage, whereas most of them are likely to harbour stars that have already stopped accreting, i.e., are associated with the newly formed stars. The typical lifetime of the UC HII phase is expected to be $< 10^5$ yr (Comeron & Torra 1996; Peters et al. 2010). The luminosity of the central star(s) in UC HII regions is thermally reradiated by the surrounding natal dust cocoon which makes UC HII regions some of the brightest IR sources in the Galaxy.

5.4 Disks and outflows in high-mass star-forming regions

Theoretical/numerical models have suggested that the radiation pressure problem associated with the formation of high-mass stars is most effectively overcome if accretion is not circumstellar but proceeds throug a disk (Jijina & Adams 1996; Yorke & Sonnhalter 2002; Yorke 2004; Krumholz et al. 2005a). Indeed, observational evidence for the presence of such disks is already quite extensive (e.g., Shepherd et al. 2001; Zhang et al. 2002; Beltrán et al. 2004; Chini et al. 2004; Patel et al. 2005; Jiang et al. 2005; Beuther et al. 2005b; Sridharan et al. 2005b; Beltrán et al. 2006; Chini et al. 2006; Jiang et al. 2008; Zapata et al. 2009; Sandell & Wright 2010; see Cesaroni et al. 2007 for a review). Disks around massive stars are found to be massive ($M_{\rm disk} \sim (0.3-0.5) \times M_\star$), extended ($R_{\rm disk} \sim 1000$ AU), rapidly accreting ($\dot{M}_{\rm a} \gtrsim 10^{-4}$ M$_\odot$ yr^{-1}), and strongly gravitationally unstable. Disks are found around stars as massive as early B-type ($\lesssim 25$ M$_\odot$), but no clear evidence for a disk around an early O-type star has been presented to date. In the case of stars with luminosities $> 10^5$ L$_\odot$, corresponding to $\gtrsim 30$ M$_\odot$, only large ($4 - 30 \times 10^3$ AU), massive ($60 - 500$ M$_\odot$), non-equilibrium rotating molecular structures, called "toroids" have been detected (see Cesaroni et al. 2007). In view of the large sizes and high masses of toroids, they may be circum*cluster* rather than circum*stellar* structures. The fact that disks around massive O stars have not been discovered may be due to observational biases as O stars are rare and thus, more distant. On the other

hand, an O star may rapidly destroy the possible disk around it through photoevaporation, making the disk detection a challenge (Hollenbach et al. 1994). Hot cores within IRDCs may be the best targets for detecting high-mass disks because in these sources possible disks are not yet dissipated. Because massive disks are strongly susceptible to fragmentation, they provide a natural explanation for the observed high companion fraction among high-mass stars (e.g., Kratter et al. 2010).

Observations have shown that also molecular outflows are ubiquitous in high-mass star-forming regions (e.g., Shepherd & Churchwell 1996; Beuther et al. 2002b; Zhang et al. 2007; Qiu et al. 2009; Zapata et al. 2009; Ginsburg et al. 2009; see Arce et al. 2007 for a review). However, as in the case of disks, highly collimated outflows have not been clearly detected towards massive YSOs with luminosities $> 10^5$ $L_\odot$ (see Beuther et al. 2007). This may also just be an observational selection effect: O stars form in dense clusters and reach the ZAMS in a few $\times 10^4$ yr, making the detection of collimated outflows difficult (Arce et al. 2007).

Molecular jet/outflow may be revealed by the wing emission of spectral lines such as those of CO (and its isotopologues), HCO^+, and SiO (see Sect. 4.5; Cesaroni et al. 2007). In Paper V, we present observations of SiO wing emission towards several high-mass star-forming regions (see Fig. 5.3)[7]. Outflow detections strongly (but indirectly) support the presence of underlying accretion disks, and consequently, the accretion-based formation scenario in high-mass star formation. Moreover, outflows produce optically thin cavities (dust is sublimated away) through which radiation can escape, significantly (by an order of magnitude) reducing the building up of radiation pressure (Krumholz et al. 2005b). From a theoretical point of view, the turbulent accretion scenario predicts disk and outflow properties that resemble those in low-mass star formation (Yorke & Sonnhalter 2002; McKee & Tan 2003; Krumholz et al. 2007; Keto 2007).

In summary, high-mass star formation, at least up to ~ 30 $M_\odot$, is likely to proceed through accretion, and this process is associated with collimated outflows, resembling the formation of low-mass stars. For more massive stars, however, different formation mechanisms may be needed.

5.5 Alternative formation mechanisms for high-mass stars

As it is unclear whether high-mass (or the highest mass) stars form as a result of a scaled-up version of the low-mass star formation process, two alternative processes have been proposed, namely the competitive accretion and coalescence of lower-mass (proto)stars in dense protoclusters.

[7] A young O5 (proto)star in the G5.89−0.39 UC HII region studied in Paper V possibly drives a collimated outflow, and is thus forming via accretion (Puga et al. 2006). However, the SiO outflow in G5.89−0.39 is not related to the O5 star, but to the 1.3 mm source south-west of it (Sollins et al. 2004; Shepherd 2005). Observations by Puga et al. (2006) show evidence for three outflows in this region.

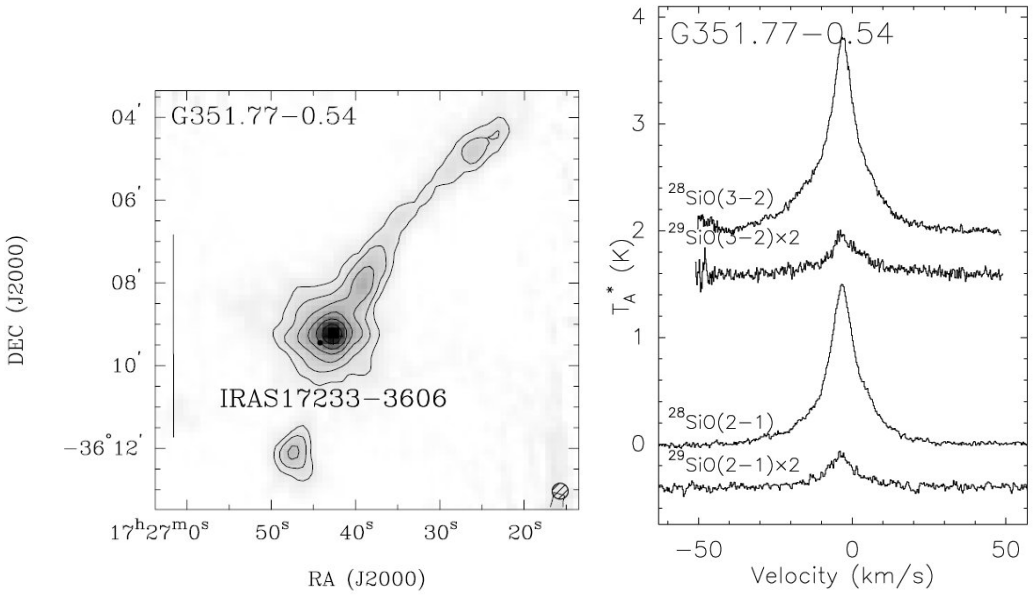

Figure 5.3: **Left:** SEST 1.2 mm dust continuum image of the high-mass star-forming region G351.77-0.54 (IRAS 17233-3606). The scale-bar on the left corresponds to 1 pc, and the beam HPBW of $24''$ is shown in the lower right corner. The contours are plotted at 0.25, 0.5, 1.0, 2.0, 4.0, 8.0, and 16.0 Jy beam^{-1}. **Right:** Spectra of the $J = 2 - 1$ and $J = 3 - 2$ rotational lines of ^{28}SiO and ^{29}SiO towards the strongest mm peak shown in the left panel. The SiO wing emission is evident. The region is recently found to be associated with a large number of molecular outflows. In addition, the region contains several H_2O, CH_3OH, and OH maser spots and HC HII regions (Leurini et al. 2009 and references therein). Adapted from Paper V.

5.5.1 Competitive accretion

In the competitive accretion model, a very low-mass star (~ 0.1 M$_\odot$) forms via gravitational collapse, but then accretes a significant amount of mass that was initially *unbound* to the star, *after* it has accreted its parental core (Bonnell et al. 1997, 2001a; Bonnell & Bate 2006). Thus, different protostars in the common cluster competitively accrete from a common gas reservoir. In this model, all high-mass star formation is associated with cluster formation, which conforms with observations. The mass accretion rate from the initially unbound gas depends on the position of the protostar in the cluster's gravitational potential well. Those protostars that are initially located near the centre of the cluster, accrete at a higher rate (because of the stronger gravititational attraction) and will form high-mass stars. On the other hand, protostars in the lower density outer parts accrete at a much lower rate and will form low-mass stars (Bonnell et al. 2001a). Thus, the model naturally explains the observational fact that high-mass stars are segregated towards the centres of the clusters. The model also produces a two power-law initial mass function (IMF) (many low-mass stars and only a few high-mass stars) (see Sect. 6.2) that is in qualitative agreement with observations (Bonnell et al. 2001b).

The competitive accretion scenario, however, suffers from the fact that the subsequent mass accretion becomes very inefficient for protostellar masses $\gtrsim 10$ M$_\odot$ because of radiation pressure (Edgar & Clarke 2004). So far, this radiative feedback has not been included in any of the simulations of high-mass star formation by competitive accretion. Thus, it is unlikely that competitive accretion can operate above ~ 10 M$_\odot$ (see Beuther et al. 2007). Another drawback is that competitive accretion is likely to be effective only if the virial parameter and mass of the parent molecular clump obey the condition $\alpha_{\rm vir}^2 M \lesssim 10$ M$_\odot$ (Krumholz et al. 2005c), but observations, such as those presented in Paper V, commonly show that this is not the case. Finally, in competitive accretion models, nearly all massive stars have close encounters that will result in the destruction of disks around massive stars (see Bonnell et al. 2007), and thus it is difficult to explain observations of disks and outflows.

5.5.2 Coalescence model

To avoid the effects of radiation pressure, Bonnell et al. (1998) suggested a very different formation mechanism for high-mass stars, i.e., that high-mass stars form via stellar collisions. In this model, lower-mass stars at the centre of embedded clusters merge and form massive stars. However, the model requires extreme stellar densities of $\sim 10^8$ stars pc^{-3}, which is far greater than observed in any Galactic star cluster. Such an ultra-dense region would be very luminous due to the associated massive stars, but such regions have never been observed. On the other hand, in young stellar clusters, the stellar density could be high enough, and the stellar velocity dispersion low enough, for stars to collide and merge with a reasonable probability (e.g., Bonnell & Bate 2002; Freitag 2008). Bonnell & Bate (2005) suggested that binary stars in clusters will evolve towards smaller separations due to mass accretion, and will finally merge. Also, Bally & Zinnecker (2005) suggested stellar mergers to explain the "explosive" nature of the

outflow from the Orion-KL region (see Beuther & Nissen 2008 and references therein). Also in the coalescence model, it is difficult to explain the presence of disks and outflows. This is because the mergers would likely destroy any disks. In the model of Davies et al. (2006), however, a close encounter between a high-mass star and a low-mass PMS star leads to the tidal disruption of the latter one, and to the formation of a massive disk around the high-mass star. The coalescence scenario (combined with accretion) is able to produce the stellar IMF for the high-mass end that is in qualitative agreement with observations (Bonnell & Bate 2002; Beuther et al. 2007).

In general, as it has been shown that also high-mass stars up to ~ 30 $M_{\odot}$ can form via accretion through a disk, the coalescence model needs not to be invoked for such stars. However, mergers, or some other specific processes, still remain a possibility for the most massive stars.

Chapter 6

Issues on turbulence, molecular cloud fragmentation, and control of star formation

In this chapter the topics of the thesis that are related to the "big picture" (or macrophysics) of star formation are briefly introduced. These include the turbulence and molecular cloud fragmentation, clump and core mass distributions, and the star formation efficiency.

6.1 Turbulence and molecular cloud fragmentation – the origin of clumps and cores within molecular clouds

In Chapter 4, we started with the discussion of low-mass star formation from the starless molecular cloud cores. However, the origin of these cores is not yet well understood. On large scales ($\gtrsim$ parsec) practically all molecular clouds are observed to have highly supersonic velocity dispersions ($\sigma_v > c_\mathrm{s}$) which imply the presence of non-thermal turbulent motions, i.e., the gas flow undergoes irregular fluctuations (e.g., Larson 1981; Solomon et al. 1987; see Elmegreen & Scalo 2004 for a review)[1]. Consequently, it has been proposed that supersonic turbulence controls the fragmentation of molecular clouds into dense sheets and filamentary substructures and, furthermore, the formation of dense cores (a process called "turbulent fragmentation"; see Mac Low & Klessen 2004 and Ballesteros-Paredes et al. 2007 for reviews)[2]. This is based on the fact that supersonic turbulent motions carry mass and produce density fluctuations, leading to a clumpy density structure of the medium (see, e.g., Ballesteros-Paredes et al. 2006 and references therein). In particular, turbulence creates a complex network of interacting shocks; it is the stagnation points of converging flows where the formation of density peaks and, furthermore, dense cores, are supposed to take place. Some of these density enhancements are massive and dense enough to become gravitationally unstable and collapse to form stars. However, density fluctuations formed in turbulent velocity fields are highly transient structures. The same random flow that creates the density enhancement can also destroy it. Thus, in order to actually collapse and form stars, density enhancements

[1] The non-thermal supersonic velocity dispersions in molecular clouds are also suggested to be caused primarily by gravitational infall motions and not by random turbulence (see, e.g., Heitsch et al. 2009; Vázquez-Semadeni et al. 2009 and references therein).

[2] Another important role of turbulence is that on large scales, it can support molecular clouds against contraction (the turbulent support increases with the length-scale).

must collapse before another shock passage occurs. Recent results from the *Herschel* Gould Belt Survey by André et al. (2010) and Men'shchikov et al. (2010) are in good agreement with the scenario according to which complex network of filaments form first, possibly as a result of supersonic turbulence, and then the filaments fragment into dense cores through gravitational instability (cf. Paper II).

It is known that, if not continuously driven, supersonic turbulence decays rapidly, in roughly the local crossing time, $\tau_{\rm cross} \equiv D/\sigma_{\rm 3D}$, where D is the diameter of the region, and $\sigma_{\rm 3D} = \sqrt{3}\sigma_{\rm 1D}$ is a three-dimensional velocity dispersion. In typical molecular cloud conditions, turbulence decays on timescales $\leq \tau_{\rm ff}$ (Mac Low et al. 1998; Stone et al. 1998; Mac Low 1999; see also McKee & Ostriker 2007 for a review). Thus, turbulence needs to be continuosly replenished in order to sustain the observed supersonic motions. Because the velocity dispersion in molecular clouds increases up to the largest scales (comparable to the cloud size), and because molecular clouds have self-similar structures, the turbulent motions are probably driven on large scales, i.e., on scales that are comparable to or larger than typical sizes of molecular clouds (e.g., Mac Low & Ossenkopf 2000; Ossenkopf & Mac Low 2002; Brunt 2003; Mac Low & Klessen 2004). Brunt et al. (2009) recently showed that the velocity dispersion-size relation observed in GMCs can be reproduced only if turbulence is driven on large scales. This could be naturally explained if the driving scale itself determines the size of a molecular cloud during its formation (Brunt et al. 2009 and references therein). An alternative for continuously driven turbulence is that most molecular clouds are so young that the initial turbulence (originating from the large-scale flows in the atomic phase that created the cloud) has not yet been completely dissipated (see Schneider et al. 2010 and references therein). Simulations by Klessen et al. (2005) showed that turbulence driven on large scales promotes the formation of quiescent coherent cores, though the number of such cores were smaller than observations suggest (see Paper II). However, this is also in agreement with the idea that molecular cloud turbulence is driven on large scales. Large-scale turbulence leads to a clustered mode of star formation (e.g., Klessen et al. 2000; Klessen & Burkert 2001; Klessen 2001), which is the dominant mode of star formation in the Galaxy.

The possible mechanisms that inject (and maintain) supersonic turbulence into interstellar clouds on large scales include, for example, blast waves and expanding shells from SNe, and density waves associated with galactic spiral arms, the first ones (SNe) being the ones most likely (e.g., Mac Low et al. 2005; de Avillez & Breitschwerdt 2007)[3]. On the other hand, if supersonic motions are driven by gravity (see above), a driving source for turbulence (other than gravity) is no more needed.

6.1.1 Fragmentation of IRDCs

IRDCs are the densest parts of GMCs (Sect. 5.2). One plausible scenario for the origin of IRDCs is that they are formed as a result of shock compression from converging flows driven by large-scale turbulence in GMCs. Indeed, as described in the following sections,

[3]Internal driving is possibly caused by feedback from protostars (e.g., outflows; see Sect. 4.5) and newly formed (massive) stars (stellar winds, radiation, HII regions). However, these are likely to be important only at small (sub-parsec) scales.

several observational facts and modelling results suggest that supersonic turbulence has an important role in the formation of IRDCs and their fragmentation into smaller subunits. For instance, the filamentary shapes of IRDCs (Fig. 5.1), and molecular clouds in general, are consistent with cloud morphologies predicted by numerical models of supersonic turbulence driven on large scales (Paper IV and references therein). Moreover, the fact that star formation in IRDCs takes place in clustered mode suggests that turbulence is driven on large scales.

6.2 Clump and core mass distributions

What determines the observed distribution of stellar masses, i.e., the stellar IMF ? This is one of the main questions to which star-formation studies try to find answers. To shed light on this question, it is useful to study the shape of the prestellar core mass function (CMF), i.e., the number density of cores per mass interval, and how it is related to the IMF, which itself appears to be almost universal over a wide range of star-forming environments[4]. In particular, above a few solar masses, the IMF has a Salpeter-like power-law form $\mathrm{d}N/\mathrm{d}\log M \propto M^{-\Gamma}$, or $\mathrm{d}N/\mathrm{d}M \propto M^{-\alpha}$, where $\alpha = \Gamma + 1 = 2.35$ (Salpeter 1955; see Bastian et al. 2010 for a recent review). The CMF/IMF comparison provides important clues into the origin of the final stellar masses, and is an important test for any model of star formation (see Bonnell et al. 2007 for a review).

Several studies (where also different methods are used) have shown that the CMFs in different molecular clouds are comparable to each other, and moreover, are remarkably similar in shape to the stellar IMF, particularly at the high-mass (> 0.5 $\mathrm{M}_{\odot}$) end (e.g., Motte et al. 1998; Alves et al. 2007; Nutter & Ward-Thompson 2007; Enoch et al. 2008; Sadavoy et al. 2010; André et al. 2010; Könyves et al. 2010; the latter two are recent *Herschel* results). These results suggest that the observed shape of the CMF does not represent a short period in the evolution of a star-forming region (Clark et al. 2007). Nutter & Ward-Thompson (2007) found that the CMF in the northern parts of Orion B is similar to the IMF (see also Goodwin et al. 2008). In Papers I and II, we applied the two-sample Kolmogorov-Smirnov (K-S) test between the core mass distributions in Orion B9 and northern parts of Orion B, and found that they are very likely drawn from the same underlying parent distribution. Thus, the CMF in Orion B9 is also expected to be comparable to the IMF, see Fig. 6.1.

The similarity between the observed CMFs and the stellar IMF suggest that the stellar masses are a direct consequence of the process responsible for the natal molecular cloud fragmentation. There is not, however, a one-to-one relation between the CMF and the IMF, but the observed CMFs are shifted towards higher masses typically by a factor of a few ($\simeq 2-4$) with respect to the IMF. Such a shift indicates that only a small fraction of the core mass converts into stars. Stellar feedback through winds, outflows, and radiation may be important in determining the final stellar masses (e.g., Bonnell

[4]For comparison to the stellar IMF, it is useful to derive the CMF for starless/prestellar cores only, so that it represents the mass initially available to form stars. Protostellar cores have lost some of their mass through outflows and accretion.

et al. 2007). Moreover, molecular cloud cores do not generally produce single stars but multiple systems which further hampers the trivial one-to-one relation between the CMF and the IMF (see also Swift & Williams 2008). Some of the cores may also be gravitationally unbound, and therefore may never form stars. However, the final stellar masses may be *largely* determined already during the core formation process.

In Paper IV, we study the mass distribution of clumps within the IRDC G304.74+01.32. The clump masses in G304.74 are compared with the clump mass spectra from more extensive surveys of IRDCs by Rathborne et al. (2006) and Ragan et al. (2009). We carried out K-S tests between the mass distributions and found that they are likely to represent subsamples of the same parent distribution. The two reference studies showed the following: the mass spectrum of the high-mass ($M \gtrsim 100$ M$_\odot$) IRDC clumps of Rathborne et al. (2006) can be fitted with a power-law $\mathrm{d}N/\mathrm{d}M \propto M^{-2.1\pm0.4}$, which is Salpeter-like. For the clump masses between ~ 30 and 3000 M$_\odot$, Ragan et al. (2009) derived the IRDC clump mass spectrum of the form $\mathrm{d}N/\mathrm{d}M \propto M^{-1.76\pm0.05}$, which is consistent with the mass functions derived for high-mass star-forming regions, and also resembles the mass function of Galactic stellar clusters (see Ragan et al. 2009 and references therein).

Another useful aspect in the CMF is that it provides information on the cloud fragmentation process. Because the shapes of the CMFs/IMFs appear to be quite universal, it has been suggested that the CMF/IMF is determined primarily by turbulent fragmentation because turbulence is observed to be ubiquitous and universal in molecular clouds (e.g., Padoan et al. 1997; Padoan & Nordlund 2002; Heyer & Brunt 2004; Bonnell et al. 2007; Sect. 6.1). Numerical turbulent simulations have been able to reproduce the general shape of the IMF (e.g., Klessen 2001; Padoan & Nordlund 2002; Li et al. 2004; Ballesteros-Paredes et al. 2006). The IRDC clump mass spectra derived by Rathborne et al. (2006) and Ragan et al. (2009) (see above) are comparable to those predicted by turbulent fragmentation models. This supports the idea that the origin of IRDCs, and their subsequent fragmentation, is controlled by supersonic turbulence observed in molecular clouds. We note, however, that simulations of turbulent fragmentation do not produce a universal CMF, but the exact shape of the CMF changes with the wavenumber at which turbulence is driven (e.g., Klessen 2001). The shape of the CMF depends also strongly on the sonic rms Mach number, $M_\mathrm{s} = \sigma_v/c_\mathrm{s}$, of the turbulent flow (Ballesteros-Paredes et al. 2006; see also Ballesteros-Paredes et al. 2007 and Hennebelle & Chabrier 2008). Moreover, Padoan et al. (2007) concluded that the presence of a (weak) magnetic field can be crucial in shaping the CMF/IMF. Recently, Kunz & Mouschovias (2009a) showed that if molecular cloud fragmentation is controlled by AD, the resulting initial CMF is very similar to the IMF.

6.3 Spatial distribution of clumps and cores within molecular clouds

In addition to the clump/core mass distribution, it is also useful to determine how clumps/cores are spatially distributed within the cloud in order to understand the process of cloud fragmentation. For instance, the length scale and strength of energy injection into

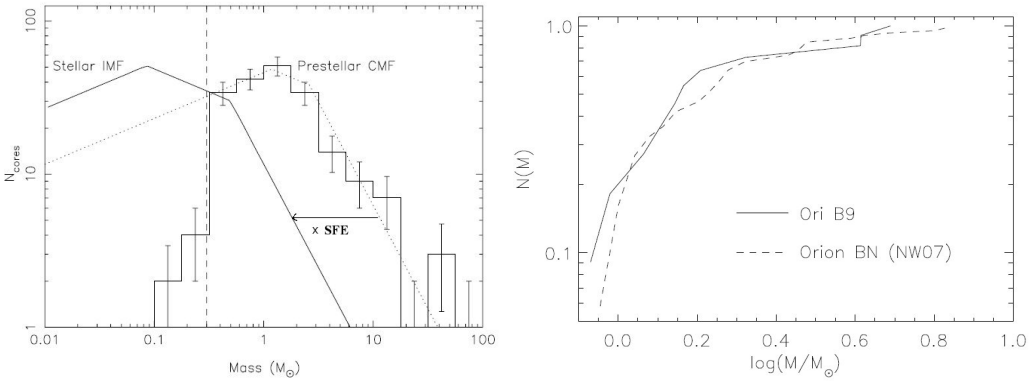

Figure 6.1: **Left:** The combined CMF for the northern parts of Orion A and B. The stellar IMF (normalised to the peak in $N_{\rm core}$ of the CMF) is indicated as a solid line for comparison. The IMF is of the form $M\frac{{\rm d}N}{{\rm d}M} \propto M^{0.3}$, $\propto M^{-0.3}$, and $\propto M^{-1.35}$, at 0.01 $M_\odot < M <$ 0.08 $M_\odot$, 0.08 $M_\odot < M <$ 0.5 $M_\odot$, and $M >$ 0.5 $M_\odot$, respectively. The dotted line has the same slopes as the IMF at 0.4 $M_\odot < M <$ 1.3 $M_\odot$, 1.3 $M_\odot < M <$ 2.4 $M_\odot$, and $M >$ 2.4 $M_\odot$, respectively. The vertical dashed line indicates the average completeness limit of $\sim$ 0.3 $M_\odot$. The CMF is related to the IMF through the core SFE (see Sect. 6.4). Modified from Nutter & Ward-Thompson (2007). **Right:** Normalised cumulative mass functions for the dense cores in Orion B9 (solid line) and in Orion B North (dashed line) studied by Nutter & Ward-Thompson (2007). There is a very high probability ($\sim 95 - 100\%$) that the two CMFs are drawn from the same parent distribution. Adapted from Paper I (see also Paper II).

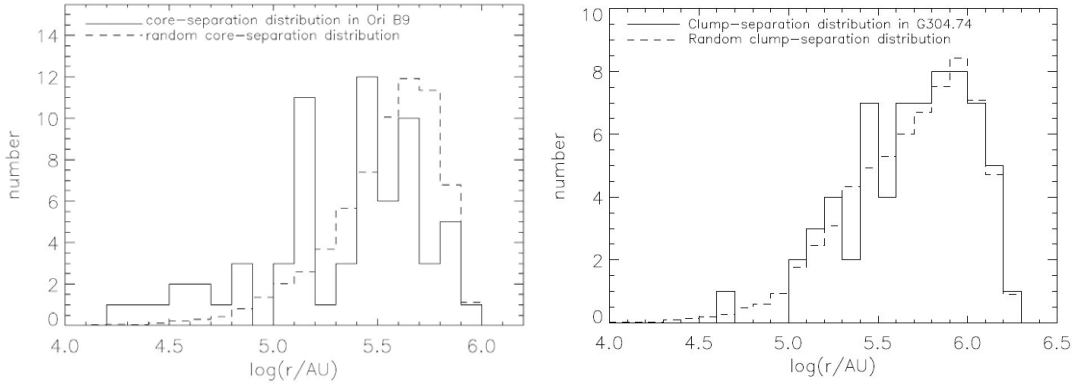

Figure 6.2: **Left:** Observed core-separation distribution (solid line) and the distribution expected for the same number of randomly positioned cores over an identical area (dashed line). The mean values of these two distributions are $\log(r/\mathrm{AU}) = 5.467 \pm 0.037$ and 5.525 ± 0.051, respectively. For comparison, the mean of the core separations in Orion B North studied by Nutter & Ward-Thompson (2007) is $\log(r/\mathrm{AU}) = 5.67 \pm 0.03$. Adapted from Paper II. **Right:** Same as in the left panel but for the clumps in the IRDC G304.74+01.32. The mean values of the observed and model clump-separations are $\log(r/\mathrm{AU}) = 5.690 \pm 0.041$ and 5.674 ± 0.061, respectively. Adapted from Paper IV.

the cloud determine the structure of the turbulent flow and, furthermore, the locations at which substructures form. Thus, the spatial distribution of density enhancements, i.e., clumps and cores, in a molecular cloud is an important constraint on the process of cloud fragmentation. Motived by this, we examined the spatial distribution of dense cores in Orion B9 in Papers I and II, and that of the clumps in the IRDC G304.74+01.32 in Paper IV. Because turbulent motions are stochastic, it cannot be said where (and when) the clumps/cores will form.

In Papers I and II, we showed that the projected core separations in the Orion B9 star-forming region are comparable to those in Orion B North (Nutter & Ward-Thompson 2007) and the mean and median separation distances are comparable also to those of the corresponding random distribution (see Fig. 6.2). However, according to K-S tests, the observed and random distributions are unlikely to be drawn from the same parent distribution (Paper II). In Paper IV, we found that the fragmentation length-scale does not vary much between the studied IRDCs, and that the clump spatial distributions are random-like in most cases. These results are also consistent with the idea that the formation of substructures within IRDCs is determined by turbulent fragmentation.

6.4 Core/star formation efficiency

Another important question related to the "macrophysics" of star formation is that what fraction of the molecular cloud mass is contained in dense cores, i.e., what is the core

formation efficiency ? (e.g., Enoch et al. 2007). This is directly related to the SFE ($\equiv M_{\rm stars}/(M_{\rm stars}+M_{\rm gas})$), which simply tells the fraction of molecular gas mass that is converted into stars. Observations have shown that dense cores typically represent only a few percent ($\sim 1-5\%$) of the mass of their parent molecular cloud (e.g., Johnstone et al. 2004; Nutter et al. 2006; Enoch et al. 2007; Lada et al. 2008; Evans et al. 2009; Paper I). These values are similar to the measured values of the overall SFEs of $\sim 1-5\%$ (see, e.g., Myers et al. 1986; Evans & Lada 1991; Evans 1999; Lada & Lada 2003 and references therein). As demonstrated by the above results, the formation of dense cores and stars in Galactic molecular clouds is a very inefficient process. The reason for this is not yet well understood (see Price & Bate 2009). In principle, the observed low SFE is consistent with the AD controlled star formation. It naturally results from the fact that only a small fraction of the molecular cloud gas is magnetically supercritical, i.e., capable of forming stars. Also theories of turbulence-driven star formation are able to explain (at least to some degree) the low SFEs. This is based on the supporting effect of supersonic turbulence against the global collapse of the cloud, while at the same time turbulence promotes local collapse of density enhancements which account only a small fraction of the cloud mass (Hennebelle & Chabrier 2008). However, SFEs *for individual cores* are typically an order of magnitude higher, $\sim 30-50\%$ (e.g., André et al. 2009; see also Goodwin et al. 2008). The latter values may result from, e.g., core disruption through protostellar outflows (e.g., Matzner & McKee 2000). Note that the CMF and the stellar IMF are related by the core SFE (see Fig. 6.1 and McKee & Ostriker 2007).

6.5 Turbulence versus ambipolar diffusion driven star formation

As described in the previous sections, there are currently two different paradigms of star formation: (i) slow quasi-static contraction based on AD; and (ii) rapid, turbulence regulated star formation. The observational evidence and the results from numerical simulations seem to support the latter scenario. This raises the question about the role of AD. One way to try to distinguish between the above two mechanisms is to study the duration of the prestellar phase of core evolution. In the case that molecular cloud evolution and core formation is controlled primarily by supersonic turbulence, core collapse should be dynamic and take place in only a few times the free-fall time. However, it is difficult to distinguish between different core formation mechanisms based on the core lifetimes only because there appears to be a negative correlation between the lifetime and core density (see Fig. 4.8). Also, observations of magnetic fields can, in principle, provide a strong discriminator between AD and turbulence controlled star formation. Because cores appear to be slightly magnetically supercritical, neither of the extreme-case models can be rule out.

However, because real molecular clouds are known to be both magnetised and turbulent, the theories of star formation need to take both factors into account. Theoretical calculations and numerical simulations indicate that if cores are formed in turbulent medium, the AD timescale is significantly (up to an order of magnitude) shorter due to turbulent fluctuations, and thus the protostellar collapse can rapidly ensue (Zweibel

2002; Fatuzzo & Adams 2002; Heitsch et al. 2004; Li & Nakamura 2004; Nakamura & Li 2005; Kudoh & Basu 2008; Nakamura & Li 2008). The above models also suggest that the observed low SFE is made possible via combination of supersonic turbulence, strong magnetic fields, and AD, where the strong magnetic field prevents the global cloud collapse. Such theoretical considerations are likely to provide the most realistic understanding of the origin of dense cores and star formation process. The relative importance of magnetic fields and turbulence in the formation of cores and stars is one of the main questions in the current star formation studies.

Chapter 7

Summary of the publications

The main results of the papers included in this thesis are summarised in the following sections. The author's contribution to the papers are described at the end of each section.

7.1 Paper I - 'Prestellar and protostellar cores in Orion B9'

In Paper I, we study the Orion B9 star-forming region, which is located in the central part of the Orion B GMC. We mapped the region in the 870 μm submm dust continuum emission using the LABOCA bolometer array on APEX. Selected positions were observed in the spectral lines of $N_2H^+(1-0)$ and $N_2D^+(2-1)$ using the IRAM 30-m telescope. The above data were combined with the Spitzer/MIPS data at 24 and 70 μm. The positions selected for the spectral line observations correspond to the $N_2H^+(1-0)$ emission peaks within the clump associated with IRAS 05405-0117 found by Caselli & Myers (1994), and they were previously examined by Harju et al. (2006) using the $H_2D^+(1_{10}-1_{11})$ observations.

We detected 12 dense cores at 870 μm in the Orion B9 region. Four of them were found to be associated with the previously known IRAS point sources, and eight of them were new submm cores. The Spitzer IR data were used to distinguish between starless and protostellar cores, and we found that there is an equal number of them. Two of the new submm cores with IR counterparts, SMM 3 and SMM 4, turned out to be potential Class 0 candidates, as deduced from their SEDs between 24 and 870 μm. Altogether, SEDs were constructed for six sources, which were detected at three or more wavelengths. The SEDs were fitted with the two-temperature models consisting of a warm/hot ($\sim 40-150$ K) and cold ($\sim 12-20$ K) component. In all cases, the warm component has a negligible contribution to the total mass, but it is required to explain the emission at MIR and FIR wavelengths.

The dense submm cores were found to constitute $\sim$ 4% of the total mass of the Orion B9 region, which is comparable to the low SFEs observed in nearby molecular clouds. According to the K-S test, there is a very high probability that the core mass distribution in Orion B9, and that in the northern part of Orion B, are drawn from the same underlying parent distribution. This suggests that also the CMF for the Orion B9 can give rise to the stellar IMF as is found to be the case for the northern part of Orion B. Also, the mean core-separation distances in these two regions are comparable, suggesting that the fragmentation length-scale is quite similar in these two parts of Orion

B. The random core-separation distribution appeared to show mean and median values comparable to the observed values. The above results suggest that the origin of dense cores in Orion B9, or Orion B in general, could be caused by turbulent fragmentation. The equal numbers of starless and protostellar cores suggest that the prestellar core lifetime is comparable to that of embedded protostars, and should thus be only a few times the free-fall time. Such dynamic evolution is also in agreement with the idea that star formation is driven by supersonic turbulence. Moreover, because star formation in the studied regions is taking place in cluster-like mode, turbulence is likely to be driven on large scales (but see Paper II).

We found a moderate degree of deuteration in the selected positions, i.e., $N(\mathrm{N_2D^+})/N(\mathrm{N_2H^+}) = 0.03 - 0.04$, which are typical values in low-mass cores. We also found evidence of $\mathrm{N_2H^+}$ depletion in the Class 0 candidate SMM 4, suggesting that the protostellar envelope is so dense that even $\mathrm{N_2H^+}$ has disappeared from the gas phase. The ionisation degree and the cosmic-ray ionisation rate of $\mathrm{H_2}$ in the target positions of line observations were estimated to be $x(\mathrm{e}) \sim 10^{-7}$ and $\zeta_{\mathrm{H_2}} \sim 1 - 2 \times 10^{-16}$ s^{-1}, respectively. The analysis also suggested that the most abundant ionic species in these targets is probably $\mathrm{H^+}$ or $\mathrm{HCO^+}$, which is a crucial knowledge when estimating the AD timescale. The relatively high values of $x(\mathrm{e})$ can possibly be explained by the fact that the cores reside in clustered region with an enhanced radiation field. For instance, in the isolated prestellar core L1544, the ionisation degree is found to be only a few $\times 10^{-9}$ (Caselli et al. 2002b). The above values of $\zeta_{\mathrm{H_2}}$ are about an order of magnitude higher than the "standard" value of $\sim 10^{-17}$ s^{-1}. The tentative AD timescales derived for the two target positions were found to be $\sim 70 - 100$ times longer than the free-fall time, much longer than the core lifetime deduced from statistical arguments. A possible explanation for this discrepancy is that submm dust continuum observations are only sensitive to the densest, i.e., dynamically most advanced cores.

Molecular line observations with the IRAM 30-m telescope were made by the author. Moreover, the author was the PI (principal investigator) in the APEX/LABOCA proposal (observations were completed in service mode). The molecular line, submm dust continuum, and Spitzer IR data were reduced by the author, who also performed most of the analysis. The NIR extinction map of Orion B9 and the total mass in the region were determined by J. Kainulainen. The author wrote most parts of the paper. Section 4.4 (Ionisation degree and cosmic-ray ionisation rate) was mostly written by J. Harju, who also wrote the original versions of the IDL programmes for analysing the core mass and spatial distributions.

7.2 Paper II - 'Physical properties of dense cores in Orion B9'

Paper II is a follow-up study of Paper I. To determine the gas kinetic temperature, kinematics, and the dynamical state of the cores, we performed pointed observations of the $\mathrm{NH_3}(1, 1)$ and $(2, 2)$ inversion lines, and $\mathrm{N_2H^+}(3 - 2)$ rotational lines towards the core submm peak positions with the Effelsberg 100-m and APEX telescopes, respectively. These line observations were combined with our previous 870 μm submm dust continuum

data of the region.

The gas kinetic temperature in the cores is between $T_{\rm kin} \sim 9.4 - 13.9$ K, with an average value of about 12 K. The cores are characterised by subsonic, or at most transonic, non-thermal turbulent motions. The non-thermal linewidth in protostellar cores appears to increase with increasing bolometric luminosity as $\Delta v_{\rm NT} \propto L_{\rm bol}^{0.25\pm0.11}$. In Paper II, the derived temperatures were used to recalculate the temperature-dependent core parameters presented in Paper I. For instance, the core masses were found to be in the range of $\sim 2 - 8$ M$_\odot$, H_2 column densities between $\sim 1 - 8 \times 10^{22}$ cm^{-2}, and H_2 number densities of $\sim 2 \times 10^4 - 1 \times 10^5$ cm^{-3}. The virial-parameter analysis showed that the starless cores in the region are likely to be gravitationally bound, and thus prestellar. The fractional abundances of NH_3 and N_2H^+ in the cores are $\sim 1.5 - 9.8 \times 10^{-8}$ and $\sim 0.2 - 5.9 \times 10^{-10}$, respectively. We found a trend of decreasing NH_3 abundance with increasing H_2 column and number densities, suggesting that NH_3 freeze out at the highest densities (see Fig. 4.2). The NH_3/N_2H^+ column density ratio is larger in starless cores than in cores with embedded protostars, a trend which has also been observed in other star-forming regions.

The core population in Orion B9 is comparable in physical properties to those in nearby low-mass star-forming regions. The Orion B9 cores also seem to resemble cores found in isolation rather than those associated with clusters. Some of the cores have a lower radial velocity than the systemic velocity of the region. This suggests that they are members of the "low-velocity part" of Orion B which is likely to originate from the feedback from the nearby Ori OB 1b group. This brings into question the statistical analyses presented in Paper I, and thus they were re-analysed in Paper II. For example, the cores may not be randomly distributed within the region, and the number ratio between starless and protostellar cores appears to be somewhat larger. Thus, it is unclear if the the origin of cores could be explained by turbulent fragmentation. On the other hand, many of the core properties conform with the picture of dynamic core evolution. Because the distances between the nearest-neighbours are comparable to the thermal Jeans length, the fragmentation of the parental cloud region into cores could be caused by gravitational instability.

The author was the PI in the APEX proposal, and made the NH_3 observations with the Effelsberg 100-m telescope together with J. Harju. The data were calibrated, reduced, and analysed by the author, who also completely wrote the first draft of the paper. Part of the text was modified by the co-authors.

7.3 Paper III - 'Radio continuum imaging of the R Coronae Austrinae star-forming region with the ATCA'

The Coronae Austrinae (or Corona Australis) star-forming region is one of the nearest and most active regions of recent and ongoing low- to intermediate-mass star formation. In particular, the Coronet cluster in the region contains a very compact group of protostars in early evolutionary stages. In Paper III, we investigated the nature and evolutionary stages of radio-emitting YSOs within the the R CrA star-forming region. The

region was imaged at 3, 6, and 20 cm wavelengths using the ATCA radio interferometer.

Altogether, eight sources were detected in the region[1]. Seven of them can be assigned to YSOs in different stages of evolution but the nature of one of the sources (Brown 5) is uncertain. We examined the radio spectral indices, variability, and polarisation to gain information on possible emission mechanisms in the sources. The spectral indices of the youngest protostars in the region, Brown 9 (Class 0 candidate) and IRS 7B (Class 0/I transition object) were found to be consistent with free-free emission from a collimated jet[2]. IRS 7B was found to be associated with extended radio lobes at 6 and 20 cm (see Fig. 4.6). The lobes may have a gyrosynchrotron emission component which suggests that energetic jets from protostars can give rise to non-thermal emission via shock acceleration.

The three Class I protostars detected in this survey, IRS 1, IRS 5, and IRS 7A, have very different radio characteristics. The spectral indices of IRS 1 and IRS 7A are consistent with free-free emission, with the distinction that emission from IRS 1 is optically thick, possibly originating in shocks, whereas emission from IRS 7A is optically thin, suggesting a collimated jet[3]. Radio emission from the wide binary protostar IRS 5 was found to have a substantial non-thermal component indicated by a negative spectral index, rapid variability, and a high degree of circular polarisation with $P_{\rm c} \approx 33$ % on one of the days of observation (see Fig. 4.7). These characteristics are signs of magnetic activity in the system[4]. The Herbig Ae star R CrA, and the Class II source IRS 6, showed only weak radio emission. The radio characteristics of the detected YSOs are in rough agreement with the scheme presented by Gibb (1999), i.e., that the dominant emission mechanism changes with the evolutionary stage of the source.

Observations presented in Paper III were carried out by the co-authors. The data reduction was performed by the author under the guidance of J. Harju. The author was

[1] After the publication of Paper III, Choi et al. (2008) detected radio emission also from the Herbig Ae star T CrA, and the Class I source WMB 55 (embedded in the submm core SMM 2; Nutter et al. 2005), for the first time. The mechanisms producing radio emission in these sources are not yet known.

[2] Choi et al. (2008) resolved Brown 9 (B9) into two sources with a separation of $0.5''$ (see their Fig. 6). Both of them show clearly negative spectral indices between 6.2 and 3.5 cm (B9a: -0.35 ± 0.09, B9b: -0.9 ± 0.4), indicating that, at least partially, the cm-emission is non-thermal in nature. However, in Paper III, we reported a positive spectral index for B9 between 6 and 3 cm (0.4 ± 0.2). This suggests that either the non-thermal component is highly variable or our flux density determination included a significant contribution from the extended thermal emission source. Choi et al. (2008) suggested that the B9 complex may be a multiple-protostar system that is driving at least two outflows.

[3] Interestingly, the 3.5 cm image of IRS 7A from February 3, 2005 presented by Choi et al. (2008; Fig. 6 therein), i.e., about 5 yr later than our observations, shows a newly appearing subcomponent at $0.85''$ ($\sim$ 110 AU at 130 pc) southeast of the main peak. It may be a bright knot of recently ejected material.

[4] Choi et al. (2009) showed that while IRS 5a and 5b have comparable Stokes I flux densities, all the detectable Stokes V flux density can be attributed to IRS 5b (see their Fig. 2 and Fig. 4.7 of this thesis). This may be due to source geometry, i.e., inclination angle of the system. Also, for the first time, Choi et al. (2009) detected circularly polarised radio emission towards IRS 7A and Brown 5 (B5) (see their Figs. 5 and 6). B5 was in an outburst when the Stokes V flux was detected, but the nature of the source is still unclear.

responsible for analysing the data and had a leading role in writing the paper.

7.4 Paper IV - 'LABOCA mapping of the infrared dark cloud MSXDC G304.74+01.32'

In Paper IV, we study the physical properties and spatial distribution of dense clumps in the IRDC MSXDC G304.74+01.32 (G304.74). At the distance of 2.4 kpc, this is one of the nearest IRDC to the Sun. The cloud was mapped in the 870 μm dust continuum with the LABOCA bolometer on APEX telescope. The submm data were used in conjunction with the archival IR data from MSX and IRAS, which were used to examine the nature and properties of the submm clumps within the cloud. In particular, the H_2 column densities were determined using both the 870 μm dust emission and the MSX 8 μm extinction data.

By using the 2D version of the Clumpfind algorithm, we identified 12 clumps from the 870 μm map. Three clumps are associated with the MSX and IRAS point sources. Moreover, one of the clumps (SMM 6) is associated with two 8 μm point-like sources. These are clear signs of star formation within the cloud. The SEDs of two of the IRAS sources indicated bolometric luminosities in the range $\sim 1.5 - 2 \times 10^3$ $L_\odot$. On the other hand, there are 8 clumps within G304.74 which are not associated with MIR emission. The masses of these candidate starless clumps ($\sim 40 - 200$ $M_\odot$) are sufficiently large to enable high-mass star formation. The H_2 column densities of the clumps derived from the dust continuum and extinction data were found to be quite similar, suggesting that the dust parameters used in the calculations are reasonable (e.g., $T_{\rm dust} = 15$ K). The clump masses in G304.74 were compared with the clump mass distributions from more extensive IRDC surveys by Rathborne et al. (2006) and Ragan et al. (2009). According to the K-S test, the G304.74 clump masses and those from the above reference studies are likely to represent subsamples of the same underlying parent distribution. In addition, the clump spatial distributions in different IRDCs were found to be comparable to each other, and also to the corresponding random distributions (see Fig. 6.2). This suggests that the fragmentation length-scale (at the scale of clumps) does not vary much between different IRDCs.

Some of the MIR dark clumps found in Paper IV are good candidates of being/harbouring HMSCs. The fact that the clump mass and spatial distributions seem to be comparable between different IRDCs, supports the idea that the origin of IRDCs, and their further fragmentation into smaller subunits is driven by supersonic turbulence.

The author was the PI in the APEX/LABOCA proposal. Most of the data reductions, analyses, and paper writing were performed by the author. The analysis presented in Sect. 5.4 (Extinction estimates with 2MASS) and writing that section were mostly done by J. Harju who also helped in writing the IDL scripts used in the statistical analysis of the clump properties.

7.5 Paper V - 'SiO and CH_3CCH abundances and dust emission in high-mass star-forming cores'

In Paper V, we study the physical and chemical properties of 15 high-mass star-forming cores[5] by means of SiO and CH_3CCH spectral lines and 1.2 mm dust continuum emission. The observations were completed with the SEST telescope. The source sample, which was drawn from the SiO survey by Harju et al. (1998; sources showing the brightest SiO emission), represents typical high-mass star-forming cores with associated OH, H_2O, and CH_3OH masers, and UC HII regions.

The gas kinetic temperatures and the CH_3CCH column densities in the cores were derived through the rotational diagram method in the LTE approximation. The following core properties were derived: $T_{\rm kin} \approx 25-39$ K, $M \sim 120-8100$ $M_\odot$, $R = 0.03-0.7$ pc, $N(H_2) \sim 5\times10^{22}-1.6\times10^{23}$ cm^{-2}, and $n(H_2) \sim 3\times10^4-2.5\times10^7$ cm^{-3}. The fractional CH_3CCH abundances were found to be $\sim 3-18\times10^{-9}$. Typically, half of the integrated intensity of the SiO spectral lines came from the velocity range with detectable CH_3CCH emission. The fractional SiO abundances in this "quiescent" gas component were found to be $\sim 1-7\times10^{-10}$.

CH_3CCH abundance was found to exhibit a shallow, positive correlation with the gas kinetic temperature, whereas SiO showed the opposite trend. We suggested that the high CH_3CCH abundance, and its possible increase as a function of $T_{\rm kin}$, is related to the intensified desorption of the precursor molecules, such as C_2H_4, from the icy mantles of dust grains. A possible explanation for the decreasing SiO abundance as a function of $T_{\rm kin}$ is that warmer cores are in later stage of evolution and that highly energetic protostellar outflows releasing SiO into the gas phase are less frequent. In addition, rapid post-shock chemical processing may have led to a diminished SiO abundance. Because all the high-mass star-forming cores studied in Paper V show broad SiO-line wings, indicating the presence of bipolar outflows, the results of this study support the idea that high-mass star formation proceeds through disk accretion, although the resolution of the single-dish observations is not sufficient to resolve whether the embedded HMPOs are actually driving these outflows[6].

Observations presented in Paper V were made by J. Harju and L. K. Haikala. The

[5] Clumps according to the terminology used in Paper IV.

[6] The sample includes one of the most spectacular regions of high-mass star formation in the Galaxy, NGC 6334. For a recent review of NGC 6334, see Persi & Tapia (2008). Since the publication of Paper V, NGC 6334 has been the target of several studies. For example, Beuther et al. (2008) detected outflow signatures in NGC 6334I. Persi et al. (2009) found a new centre of high-mass star formation in NGC 6334 IV, and Brogan et al. (2009) showed that the massive protocluster NGC 6334I(N) is giving birth to several high-mass stars, where also signs of multiple outflows were detected (cf. Fig. 1 of Paper V). A few other sources of our sample have also been studied recently. Leurini et al. (2009) found signs of multiple outflows driven by high-mass YSOs in the IRAS 17233-3606 region (see Fig. 5.3). Hunter et al. (2008) resolved the G5.89-0.39 clump into several discrete sources at subarcsec resolution in the 875 μm dust continuum image (their Fig. 1; cf. our 1.2 mm image in Fig. 1 of Paper V). They also discovered outflow signatures in the region. Garay et al. (2010) found that the CS and SiO line profiles of IRAS 16060-5146 show wide velocity components, indicating mass outflows.

dust continuum observations were reduced by L. K. Haikala, whereas the spectral line observations were reduced by the author. J. Harju wrote the Fortran and IDL programmes for the rotational diagram method. The author performed the data analysis and wrote the paper with guidance from the supervisors, J. Harju and L. K. Haikala (Paper V is based on the author's M.Sc. Thesis), with the exception of Sect. 2.2 (Continuum observations) and part of Sect. 5.1 (SiO and CH_3CCH abundances), which were written by L. K. Haikala and J. Harju, respectively.

Chapter 8

Concluding remarks

In the present thesis we have carried out studies of Galactic star-forming molecular clouds in order to characterise their physical and chemical properties. We have concentrated on dense clumps and cores which are either collapsing or likely to collapse in the future to form stars. The characteristics investigated include the mass, the gas column and number densities, temperature, velocity dispersion, degree of ionisation, and the fractional abundances of several molecular species and their isotopic variants. These parameters are needed to understand the mechanisms and timescales related the formation of clumps and cores, which in turn represent conditions leading to protostellar collapse.

The investigation has been primarily performed through molecular line and dust continuum observations at (sub)millimetre and radio wavelengths. Additional infrared data were needed (in Papers I and IV) to detect and characterise young protostars deeply embedded in their natal molecular cloud cores. We also used centimetre radio continuum emission from young stellar objects (YSOs) in order to study their nature and evolutionary stage (Paper III).

The results of this thesis can be summarised as follows:

- While the observational results agree with the idea that supersonic turbulence in molecular clouds gives rise to filamentary structures, the situation concerning the further fragmentation of filaments to clumps and cores is less clear. In the Orion B9 star-forming region, most of the cores have subsonic non-thermal velocity dispersions and the typical core separation distance is comparable to the Jeans length. These characteristics point towards gravitational collapse of thermally supported natal clumps.

- The core evolution in Orion B9 appears to be dynamic. This suggests that the role of ambipolar diffusion (AD) in the formation and collapse of the cores, due to the very long timescale associated with the process, may not be significant.

- The dominant mechanism of centimetric radio emission from a YSO is likely to change with its evolutionary stage. In the R CrA star-forming region the radio properties of the YSOs roughly conform with the scenario where the emission at the early stages is caused by free-free radiation from an ionised jet, whereas at the later stages it is due to non-thermal gyrosynchrotron processes. Moreover, the case of IRS 7B in R CrA suggests that the non-thermal radio emission from young protostars can be caused by shock acceleration in protostellar jets.

- The infrared dark cloud (IRDC) G304.74+01.32 contains candidate high-mass starless cores. These objects may represent the very first steps of high-mass star and star cluster formation.

- SiO outflow signatures are seen in several high-mass star-forming regions, such as IRAS 15520-5234 and IRAS 17233-3606. This supports the idea that high-mass stars, at least up to several tens of solar masses, form in a similar way as their low-mass counterparts, i.e., via disk accretion.

In order to discriminate between the main physical drivers of the star formation process, the relative role played by turbulence, magnetic field, and AD needs to be clarified. A scenario including both the supersonic turbulence and magnetic field is likely to be the most realistic one, and could thus provide the possible solution: initially, turbulence generates the seeds of dense cores that eventually become gravitationally unstable and collapse. The process can be modified by magnetic fields through AD or magnetic instabilities.

The combination of (sub)millimetre and far-infrared continuum maps with molecular spectroscopy has turned out to be an efficient means to investigate the structure of molecular clouds and to identify cores at various stages of evolution within them. Clearly, more observational work both with large samples and individual sources are needed. A high angular resolution and the possibility to measure polarisation would seem especially useful in conjunction with detailed numerical models of the protostellar collapse. The nearby star-forming complexes, R CrA and Orion B9, the nearby IRDC G304.74, and the massive GMC cores studied in this thesis provide excellent targets for high-resolution interferometric observations with ALMA. Detailed investigations of these regions seem particularly worth while as they can improve our knowledge of the formation of stellar clusters and high-mass stars.

Bibliography

Adams, F. C., Lada, C. J., & Shu, F. H. 1987, ApJ, 312, 788

Adams, F. C. & Shu, F. H. 1986, ApJ, 308, 836

Aikawa, Y., Herbst, E., Roberts, H., & Caselli, P. 2005, ApJ, 620, 330

Aikawa, Y., Ohashi, N., & Herbst, E. 2003, ApJ, 593, 906

Aikawa, Y., Ohashi, N., Inutsuka, S.-i., Herbst, E., & Takakuwa, S. 2001, ApJ, 552, 639

Aikawa, Y., Wakelam, V., Garrod, R. T., & Herbst, E. 2008, ApJ, 674, 984

Akyilmaz, M., Flower, D. R., Hily-Blant, P., Pineau des Forêts, G., & Walmsley, C. M. 2007, A&A, 462, 221

Alves, J., Lombardi, M., & Lada, C. J. 2007, A&A, 462, L17

Alves, J. F., Lada, C. J., & Lada, E. A. 2001, Nature, 409, 159

André, P. 1987, in *Protostars and Molecular Clouds*, ed. T. Montmerle & C. Bertout (Saclay: CEA/Doc), p. 143

André, P. 1996, in ASPCS, Vol. 93, *Radio Emission from the Stars and the Sun*, ed. A. R. Taylor & J. M. Paredes, p. 273

André, P., Basu, S., & Inutsuka, S.-i. 2009, in *Structure Formation in Astrophysics*, ed. G. Chabrier (Cambridge: Cambridge Univ. Press), p. 254

André, P., Belloche, A., Motte, F., & Peretto, N. 2007, A&A, 472, 519

André, P., Deeney, B. D., Phillips, R. B., & Lestrade, J.-F. 1992, ApJ, 401, 667

André, P., Men'shchikov, A., Bontemps, S., et al. 2010, A&A, 518, L102

André, P. & Montmerle, T. 1994, ApJ, 420, 837

André, P., Montmerle, T., Feigelson, E. D., & Steppe, H. 1990, A&A, 240, 321

André, P., Motte, F., & Bacmann, A. 1999, ApJL, 513, L57

André, P., Ward-Thompson, D., & Barsony, M. 1993, ApJ, 406, 122

André, P., Ward-Thompson, D., & Barsony, M. 2000, in *Protostars and Planets IV*, ed. V. Mannings, A. P. Boss, & S. S. Russell (Tuscon, AZ: Univ. Arizona Press), p. 59

Andrews, S. M. & Williams, J. P. 2007, ApJ, 671, 1800

Anglada, G. 1995, in RMxAC, Vol. 1, *Circumstellar Disks, Outflows and Star Formation*, ed. S. Lizano & J. M. Torrelles, p. 67

Anglada, G. 1996, in ASPCS, Vol. 93, *Radio Emission from the Stars and the Sun*, ed. A. R. Taylor & J. M. Paredes, p. 3

Anglada, G., Villuendas, E., Estalella, R., et al. 1998, AJ, 116, 2953

Arce, H. G., Shepherd, D., Gueth, F., et al. 2007, in *Protostars and Planets V*, ed. B. Reipurth, D. Jewitt, & K. Keil (Tuscon, AZ: Univ. Arizona Press), p. 245

Arons, J. & Max, C. E. 1975, ApJL, 196, L77

Bacciotti, F., Chiuderi, C., & Oliva, E. 1995, A&A, 296, 185

Bachiller, R. 1996, ARA&A, 34, 111

Bachiller, R., Pérez Gutiérrez, M., Kumar, M. S. N., & Tafalla, M. 2001, A&A, 372, 899

Bacmann, A., André, P., Puget, J.-L., et al. 2000, A&A, 361, 555

Bacmann, A., Lefloch, B., Ceccarelli, C., et al. 2002, A&A, 389, L6

Bacmann, A., Lefloch, B., Ceccarelli, C., et al. 2003, ApJL, 585, L55

Ballesteros-Paredes, J., Gazol, A., Kim, J., et al. 2006, ApJ, 637, 384

Ballesteros-Paredes, J., Klessen, R. S., Mac Low, M.-M., & Vazquez-Semadeni, E. 2007, in *Protostars and Planets V*, ed. B. Reipurth, D. Jewitt, & K. Keil (Tuscon, AZ: Univ. Arizona Press), p. 63

Ballesteros-Paredes, J., Klessen, R. S., & Vázquez-Semadeni, E. 2003, ApJ, 592, 188

Bally, J., Reipurth, B., & Davis, C. J. 2007, in *Protostars and Planets V*, ed. B. Reipurth, D. Jewitt, & K. Keil (Tuscon, AZ: Univ. Arizona Press), p. 215

Bally, J. & Zinnecker, H. 2005, AJ, 129, 2281

Banerjee, R., Klessen, R. S., & Fendt, C. 2007, ApJ, 668, 1028

Bastian, N., Covey, K. R., & Meyer, M. R. 2010, ARA&A, 48, 339

Beckwith, S. V. W. 1999, in NATO ASIC Proc. 540: *The Origin of Stars and Planetary Systems*, ed. C. J. Lada & N. D. Kylafis, p. 579

Beichman, C. A., Myers, P. C., Emerson, J. P., et al. 1986, ApJ, 307, 337

Belloche, A. & André, P. 2004, A&A, 419, L35

Beltrán, M. T., Cesaroni, R., Codella, C., et al. 2006, Nature, 443, 427

Beltrán, M. T., Cesaroni, R., Neri, R., et al. 2004, ApJL, 601, L187

Benson, P. J., Caselli, P., & Myers, P. C. 1998, ApJ, 506, 743

Bergin, E. A., Alves, J., Huard, T., & Lada, C. J. 2002, ApJL, 570, L101

Bergin, E. A., Ciardi, D. R., Lada, C. J., Alves, J., & Lada, E. A. 2001, ApJ, 557, 209

Bergin, E. A. & Langer, W. D. 1997, ApJ, 486, 316

Bergin, E. A. & Tafalla, M. 2007, ARA&A, 45, 339

Bertoldi, F. & McKee, C. F. 1992, ApJ, 395, 140

Bertout, C. 1983, A&A, 126, L1

Bertout, C., Basri, G., & Bouvier, J. 1988, ApJ, 330, 350

Beuther, H., Churchwell, E. B., McKee, C. F., & Tan, J. C. 2007, in *Protostars and Planets V*, ed. B. Reipurth, D. Jewitt, & K. Keil (Tuscon, AZ: Univ. Arizona Press), p. 165

Beuther, H. & Henning, T. 2009, A&A, 503, 859

Beuther, H. & Nissen, H. D. 2008, ApJL, 679, L121

Beuther, H., Schilke, P., Menten, K. M., et al. 2002a, ApJ, 566, 945

Beuther, H., Schilke, P., Sridharan, T. K., et al. 2002b, A&A, 383, 892

Beuther, H. & Sridharan, T. K. 2007, ApJ, 668, 348

Beuther, H., Sridharan, T. K., & Saito, M. 2005a, ApJL, 634, L185

Beuther, H., Walsh, A. J., Thorwirth, S., et al. 2008, A&A, 481, 169

Beuther, H., Zhang, Q., Greenhill, L. J., et al. 2004, ApJL, 616, L31

Beuther, H., Zhang, Q., Sridharan, T. K., & Chen, Y. 2005b, ApJ, 628, 800

Bisschop, S. E., Fraser, H. J., Öberg, K. I., van Dishoeck, E. F., & Schlemmer, S. 2006, A&A, 449, 1297

Bisschop, S. E., Jørgensen, J. K., van Dishoeck, E. F., & de Wachter, E. B. M. 2007, A&A, 465, 913

Blake, G. A., Sutton, E. C., Masson, C. R., & Phillips, T. G. 1987, ApJ, 315, 621

Blitz, L. 1993, in *Protostars and Planets III*, ed. E. H. Levy & J. I. Lunine (Tuscon, AZ: Univ. Arizona Press), p. 125

Bonnell, I. A. & Bate, M. R. 2002, MNRAS, 336, 659

Bonnell, I. A. & Bate, M. R. 2005, MNRAS, 362, 915

Bonnell, I. A. & Bate, M. R. 2006, MNRAS, 370, 488

Bonnell, I. A., Bate, M. R., Clarke, C. J., & Pringle, J. E. 1997, MNRAS, 285, 201

Bonnell, I. A., Bate, M. R., Clarke, C. J., & Pringle, J. E. 2001a, MNRAS, 323, 785

Bonnell, I. A., Bate, M. R., & Zinnecker, H. 1998, MNRAS, 298, 93

Bonnell, I. A., Clarke, C. J., Bate, M. R., & Pringle, J. E. 2001b, MNRAS, 324, 573

Bonnell, I. A., Larson, R. B., & Zinnecker, H. 2007, in *Protostars and Planets V*, ed. B. Reipurth, D. Jewitt, & K. Keil (Tuscon, AZ: Univ. Arizona Press), p. 149

Bonnor, W. B. 1956, MNRAS, 116, 351

Bontemps, S., André, P., Terebey, S., & Cabrit, S. 1996a, A&A, 311, 858

Bontemps, S., Motte, F., Csengeri, T., & Schneider, N. 2009, ArXiv e-prints

Bontemps, S., Ward-Thompson, D., & André, P. 1996b, A&A, 314, 477

Boss, A. P. & Yorke, H. W. 1995, ApJL, 439, L55

Bottinelli, S., Ceccarelli, C., Williams, J. P., & Lefloch, B. 2007, A&A, 463, 601

Brogan, C. L., Hunter, T. R., Cyganowski, C. J., et al. 2009, ApJ, 707, 1

Brunt, C. M. 2003, ApJ, 583, 280

Brunt, C. M., Heyer, M. H., & Mac Low, M. 2009, A&A, 504, 883

Buckle, J. V. & Fuller, G. A. 2003, A&A, 399, 567

Camenzind, M. 1990, in Reviews in Modern Astronomy, Vol. 3, *Accretion and winds*, ed. G. Klare, p. 234

Carey, S. J., Clark, F. O., Egan, M. P., et al. 1998, ApJ, 508, 721

Carey, S. J., Feldman, P. A., Redman, R. O., et al. 2000, ApJL, 543, L157

Carroll, J. J., Frank, A., Blackman, E. G., Cunningham, A. J., & Quillen, A. C. 2009, ApJ, 695, 1376

Caselli, P. 2002, Ap&SS, 50, 1133

Caselli, P., Benson, P. J., Myers, P. C., & Tafalla, M. 2002a, ApJ, 572, 238

Caselli, P., Hartquist, T. W., & Havnes, O. 1997, A&A, 322, 296

Caselli, P. & Myers, P. C. 1994, in ASPCS, Vol. 65, *Clouds, Cores, and Low Mass Stars*, ed. D. P. Clemens & R. Barvainis, p. 52

Caselli, P. & Myers, P. C. 1995, ApJ, 446, 665

Caselli, P., van der Tak, F. F. S., Ceccarelli, C., & Bacmann, A. 2003, A&A, 403, L37

Caselli, P., Walmsley, C. M., Tafalla, M., Dore, L., & Myers, P. C. 1999, ApJL, 523, L165

Caselli, P., Walmsley, C. M., Terzieva, R., & Herbst, E. 1998, ApJ, 499, 234

Caselli, P., Walmsley, C. M., Zucconi, A., et al. 2002b, ApJ, 565, 344

Cassen, P. & Moosman, A. 1981, Icarus, 48, 353

Castets, A., Ceccarelli, C., Loinard, L., Caux, E., & Lefloch, B. 2001, A&A, 375, 40

Ceccarelli, C. 2004, in ASPCS, Vol. 323, *Star Formation in the Interstellar Medium: In Honor of David Hollenbach*, ed. D. Johnstone, F. C. Adams, D. N. C. Lin, D. A. Neufeeld, & E. C. Ostriker, p. 195

Ceccarelli, C., Caselli, P., Herbst, E., Tielens, A. G. G. M., & Caux, E. 2007, in *Protostars and Planets V*, ed. B. Reipurth, D. Jewitt, & K. Keil (Tuscon, AZ: Univ. Arizona Press), p. 47

Cesaroni, R. 2005, in IAU Symposium, Vol. 227, *Massive Star Birth: A Crossroads of Astrophysics*, ed. R. Cesaroni, M. Felli, E. Churchwell, & M. Walmsley, p. 59

Cesaroni, R., Galli, D., Lodato, G., Walmsley, C. M., & Zhang, Q. 2007, in *Protostars and Planets V*, ed. B. Reipurth, D. Jewitt, & K. Keil (Tuscon, AZ: Univ. Arizona Press), p. 197

Chambers, E. T., Jackson, J. M., Rathborne, J. M., & Simon, R. 2009, ApJS, 181, 360

Chen, H., Liu, S., Su, Y., & Zhang, Q. 2010a, ApJL, 713, L50

Chen, H., Myers, P. C., Ladd, E. F., & Wood, D. O. S. 1995, ApJ, 445, 377

Chen, J., Evans, N. J., Lee, J., & Bourke, T. L. 2009, ApJ, 705, 1160

Chen, X., Arce, H. G., Zhang, Q., et al. 2010b, ApJ, 715, 1344

Chen, X., Launhardt, R., Bourke, T. L., Henning, T., & Barnes, P. J. 2008, ApJ, 683, 862

Chini, R., Hoffmeister, V., Kimeswenger, S., et al. 2004, Nature, 429, 155

Chini, R., Hoffmeister, V. H., Nielbock, M., et al. 2006, ApJL, 645, L61

Choi, M., Hamaguchi, K., Lee, J.-E., & Tatematsu, K. 2008, ApJ, 687, 406

Choi, M., Tatematsu, K., Hamaguchi, K., & Lee, J.-E. 2009, ApJ, 690, 1901

Churchwell, E. 2002, ARA&A, 40, 27

Ciolek, G. E. & Basu, S. 2000, ApJ, 529, 925

Ciolek, G. E. & Basu, S. 2001, ApJ, 547, 272

Ciolek, G. E. & Mouschovias, T. C. 1994, ApJ, 425, 142

Ciolek, G. E. & Mouschovias, T. C. 1995, ApJ, 454, 194

Ciolek, G. E. & Mouschovias, T. C. 1996, ApJ, 468, 749

Ciolek, G. E. & Mouschovias, T. C. 1998, ApJ, 504, 280

Clark, P. C., Klessen, R. S., & Bonnell, I. A. 2007, MNRAS, 379, 57

Comeron, F. & Torra, J. 1996, A&A, 314, 776

Condon, E. U. & Shortley, G. H. 1935, *The Theory of Atomic Spectra* (Cambridge: Cambridge Univ. Press)

Crapsi, A., Caselli, P., Walmsley, C. M., et al. 2005, ApJ, 619, 379

Crapsi, A., Caselli, P., Walmsley, C. M., et al. 2004, A&A, 420, 957

Crapsi, A., Caselli, P., Walmsley, M. C., & Tafalla, M. 2007, A&A, 470, 221

Crapsi, A., van Dishoeck, E. F., Hogerheijde, M. R., Pontoppidan, K. M., & Dullemond, C. P. 2008, A&A, 486, 245

Crimier, N., Ceccarelli, C., Alonso-Albi, T., et al. 2010, A&A, 516, A102

Crusius-Wätzel, A. R. 1990, ApJL, 361, L49

Crutcher, R. 2005, in *The Magnetized Plasma in Galaxy Evolution*, ed. K. T. Chyzy, K. Otmianowska-Mazur, M. Soida, & R.-J. Dettmar, p. 103

Crutcher, R. M. 1999, ApJ, 520, 706

Crutcher, R. M., Hakobian, N., & Troland, T. H. 2009, ApJ, 692, 844

Crutcher, R. M., Hakobian, N., & Troland, T. H. 2010, MNRAS, L4

Crutcher, R. M., Nutter, D. J., Ward-Thompson, D., & Kirk, J. M. 2004, ApJ, 600, 279

Cunningham, A. J., Frank, A., Carroll, J., Blackman, E. G., & Quillen, A. C. 2009, ApJ, 692, 816

Curiel, S. 1995, in RMxAC, Vol. 1, *Circumstellar Disks, Outflows and Star Formation*, ed. S. Lizano & J. M. Torrelles, p. 59

Curiel, S., Canto, J., & Rodriguez, L. F. 1987, RMxAA, 14, 595

Curiel, S., Rodriguez, L. F., Moran, J. M., & Canto, J. 1993, ApJ, 415, 191

Dalgarno, A. 2006, Proceedings of the National Academy of Science, 103, 12269

Dalgarno, A. & Lepp, S. 1984, ApJL, 287, L47

Davies, M. B., Bate, M. R., Bonnell, I. A., Bailey, V. C., & Tout, C. A. 2006, MNRAS, 370, 2038

de Avillez, M. A. & Breitschwerdt, D. 2007, ApJL, 665, L35

de Wit, W. J., Testi, L., Palla, F., & Zinnecker, H. 2005, A&A, 437, 247

di Francesco, J., André, P., & Myers, P. C. 2004, ApJ, 617, 425

di Francesco, J., Evans, II, N. J., Caselli, P., et al. 2007, in *Protostars and Planets V*, ed. B. Reipurth, D. Jewitt, & K. Keil (Tuscon, AZ: Univ. Arizona Press), p. 17

Dobbs, C. L., Bonnell, I. A., & Clark, P. C. 2005, MNRAS, 360, 2

Doty, S. D., van Dishoeck, E. F., & Tan, J. C. 2006, A&A, 454, L5

Doty, S. D., van Dishoeck, E. F., van der Tak, F. F. S., & Boonman, A. M. S. 2002, A&A, 389, 446

Draine, B. T., Dale, D. A., Bendo, G., et al. 2007, ApJ, 663, 866

Draine, B. T. & McKee, C. F. 1993, ARA&A, 31, 373

Draine, B. T. & Sutin, B. 1987, ApJ, 320, 803

Duchêne, G., Delgado-Donate, E., Haisch, Jr., K. E., Loinard, L., & Rodríguez, L. F. 2007, in *Protostars and Planets V*, ed. B. Reipurth, D. Jewitt, & K. Keil (Tuscon, AZ: Univ. Arizona Press), p. 379

Dulk, G. A. 1985, ARA&A, 23, 169

Dulk, G. A. & Marsh, K. A. 1982, ApJ, 259, 350

Dunham, M. M., Crapsi, A., Evans, II, N. J., et al. 2008, ApJS, 179, 249

Dunham, M. M., Evans, N. J., Terebey, S., Dullemond, C. P., & Young, C. H. 2010, ApJ, 710, 470

Dunne, L. & Eales, S. A. 2001, MNRAS, 327, 697

Duvert, G., Guilloteau, S., Ménard, F., Simon, M., & Dutrey, A. 2000, A&A, 355, 165

Ebert, R. 1955, ZAp, 37, 217

Edgar, R. & Clarke, C. 2004, MNRAS, 349, 678

Egan, M. P., Shipman, R. F., Price, S. D., et al. 1998, ApJL, 494, L199

Eisner, J. A., Hillenbrand, L. A., Carpenter, J. M., & Wolf, S. 2005, ApJ, 635, 396

Ellingsen, S. P. 2006, ApJ, 638, 241

Elmegreen, B. G. & Scalo, J. 2004, ARA&A, 42, 211

Emprechtinger, M., Caselli, P., Volgenau, N. H., Stutzki, J., & Wiedner, M. C. 2009, A&A, 493, 89

Enoch, M. L., Evans, II, N. J., Sargent, A. I., & Glenn, J. 2009, ApJ, 692, 973

Enoch, M. L., Evans, II, N. J., Sargent, A. I., et al. 2008, ApJ, 684, 1240

Enoch, M. L., Glenn, J., Evans, II, N. J., et al. 2007, ApJ, 666, 982

Evans, II, N. J. 1999, ARA&A, 37, 311

Evans, II, N. J., Dunham, M. M., Jørgensen, J. K., et al. 2009, ApJS, 181, 321

Evans, II, N. J. & Lada, E. A. 1991, in IAU Symposium, Vol. 147, *Fragmentation of Molecular Clouds and Star Formation*, ed. E. Falgarone, F. Boulanger, & G. Duvert, p. 293

Evans, II, N. J., Rawlings, J. M. C., Shirley, Y. L., & Mundy, L. G. 2001, ApJ, 557, 193

Falgarone, E., Troland, T. H., Crutcher, R. M., & Paubert, G. 2008, A&A, 487, 247

Fatuzzo, M. & Adams, F. C. 2002, ApJ, 570, 210

Faúndez, S., Bronfman, L., Garay, G., et al. 2004, A&A, 426, 97

Feigelson, E. D., Carkner, L., & Wilking, B. A. 1998, ApJL, 494, L215

Feigelson, E. D., Martin, A. L., McNeill, C. J., Broos, P. S., & Garmire, G. P. 2009, AJ, 138, 227

Feigelson, E. D. & Montmerle, T. 1985, ApJL, 289, L19

Feigelson, E. D. & Montmerle, T. 1999, ARA&A, 37, 363

Felli, M., Gahm, G. F., Harten, R. H., Liseau, R., & Panagia, N. 1982, A&A, 107, 354

Fich, M., Blitz, L., & Stark, A. A. 1989, ApJ, 342, 272

Fiedler, R. A. & Mouschovias, T. C. 1993, ApJ, 415, 680

Flower, D. R. 2000, MNRAS, 313, L19

Flower, D. R. & Pineau des Forêts, G. 1994, MNRAS, 268, 724

Flower, D. R. & Pineau des Forêts, G. 1995, MNRAS, 275, 1049

Flower, D. R. & Pineau des Forêts, G. 2003, MNRAS, 343, 390

Flower, D. R., Pineau des Forêts, G., Field, D., & May, P. W. 1996, MNRAS, 280, 447

Flower, D. R., Pineau des Forêts, G., & Walmsley, C. M. 2004, A&A, 427, 887

Flower, D. R., Pineau des Forêts, G., & Walmsley, C. M. 2005, A&A, 436, 933

Flower, D. R., Pineau des Forêts, G., & Walmsley, C. M. 2006a, A&A, 456, 215

Flower, D. R., Pineau des Forêts, G., & Walmsley, C. M. 2006b, A&A, 449, 621

Flower, D. R., Pineau des Forêts, G., & Walmsley, C. M. 2007, A&A, 474, 923

Fontani, F., Caselli, P., Crapsi, A., et al. 2006, A&A, 460, 709

Forbrich, J. & Preibisch, T. 2007, A&A, 475, 959

Forbrich, J., Preibisch, T., & Menten, K. M. 2006, A&A, 446, 155

Foster, J. B., Rosolowsky, E. W., Kauffmann, J., et al. 2009, ApJ, 696, 298

Freitag, M. 2008, in ASPCS, Vol. 387, *Massive Star Formation: Observations Confront Theory*, ed. H. Beuther, H. Linz, & T. Henning, p. 247

Frerking, M. A., Langer, W. D., & Wilson, R. W. 1982, ApJ, 262, 590

Friesen, R. K., Di Francesco, J., Shimajiri, Y., & Takakuwa, S. 2010, ApJ, 708, 1002

Froebrich, D., Schmeja, S., Smith, M. D., & Klessen, R. S. 2006, MNRAS, 368, 435

Furlan, E., Calvet, N., D'Alessio, P., et al. 2005, ApJL, 628, L65

Galli, D., Walmsley, M., & Gonçalves, J. 2002, A&A, 394, 275

Galván-Madrid, R., Vázquez-Semadeni, E., Kim, J., & Ballesteros-Paredes, J. 2007, ApJ, 670, 480

Garay, G., Brooks, K. J., Mardones, D., & Norris, R. P. 2003, ApJ, 587, 739

Garay, G., Faúndez, S., Mardones, D., et al. 2004, ApJ, 610, 313

Garay, G., Mardones, D., Bronfman, L., et al. 2010, ApJ, 710, 567

Garay, G., Mardones, D., Rodríguez, L. F., Caselli, P., & Bourke, T. L. 2002, ApJ, 567, 980

Ghavamian, P. & Hartigan, P. 1998, ApJ, 501, 687

Gibb, A. G. 1999, MNRAS, 304, 1

Gibb, A. G., Richer, J. S., Chandler, C. J., & Davis, C. J. 2004, ApJ, 603, 198

Ginsburg, A. G., Bally, J., Yan, C., & Williams, J. P. 2009, ApJ, 707, 310

Goicoechea, J. R., Pety, J., Gerin, M., Hily-Blant, P., & Le Bourlot, J. 2009, A&A, 498, 771

Goldsmith, P. F. 2001, ApJ, 557, 736

Goldsmith, P. F. & Langer, W. D. 1978, ApJ, 222, 881

González, R. F. & Cantó, J. 2002, Apj, 580, 459

Goodman, A. A., Benson, P. J., Fuller, G. A., & Myers, P. C. 1993, ApJ, 406, 528

Goodwin, S. P. & Kroupa, P. 2005, A&A, 439, 565

Goodwin, S. P., Kroupa, P., Goodman, A., & Burkert, A. 2007, in *Protostars and Planets V*, ed. B. Reipurth, D. Jewitt, & K. Keil (Tuscon, AZ: Univ. Arizona Press), p. 133

Goodwin, S. P., Nutter, D., Kroupa, P., Ward-Thompson, D., & Whitworth, A. P. 2008, A&A, 477, 823

Goodwin, S. P., Ward-Thompson, D., & Whitworth, A. P. 2002, MNRAS, 330, 769

Greene, T. P., Wilking, B. A., Andre, P., Young, E. T., & Lada, C. J. 1994, ApJ, 434, 614

Güdel, M. 2002, ARA&A, 40, 217

Guélin, M., Langer, W. D., & Wilson, R. W. 1982, A&A, 107, 107

Guillet, V., Jones, A. P., & Pineau des Forêts, G. 2009, A&A, 497, 145

Guillet, V., Pineau des Forêts, G., & Jones, A. P. 2007, A&A, 476, 263

Gusdorf, A., Cabrit, S., Flower, D. R., & Pineau des Forêts, G. 2008a, A&A, 482, 809

Gusdorf, A., Pineau des Forêts, G., Cabrit, S., & Flower, D. R. 2008b, A&A, 490, 695

Harju, J., Haikala, L. K., Lehtinen, K., et al. 2006, A&A, 454, L55

Harju, J., Juvela, M., Schlemmer, S., et al. 2008, A&A, 482, 535

Harju, J., Lehtinen, K., Booth, R. S., & Zinchenko, I. 1998, A&AS, 132, 211

Hartigan, P., Morse, J. A., & Raymond, J. 1994, ApJ, 436, 125

Hartmann, L., Ballesteros-Paredes, J., & Bergin, E. A. 2001, ApJ, 562, 852

Hatchell, J. & Fuller, G. A. 2008, A&A, 482, 855

Hatchell, J., Fuller, G. A., Richer, J. S., Harries, T. J., & Ladd, E. F. 2007, A&A, 468, 1009

Hatchell, J., Richer, J. S., Fuller, G. A., et al. 2005, A&A, 440, 151

Heiles, C. & Crutcher, R. 2005, in Lecture Notes in Physics, Berlin Springer Verlag, Vol. 664, *Cosmic Magnetic Fields*, ed. R. Wielebinski & R. Beck, p. 137

Heitsch, F., Ballesteros-Paredes, J., & Hartmann, L. 2009, ApJ, 704, 1735

Heitsch, F., Zweibel, E. G., Slyz, A. D., & Devriendt, J. E. G. 2004, ApJ, 603, 165

Hennebelle, P. & Chabrier, G. 2008, ApJ, 684, 395

Hennebelle, P., Pérault, M., Teyssier, D., & Ganesh, S. 2001, A&A, 365, 598

Hennemann, M., Birkmann, S. M., Krause, O., et al. 2009, ApJ, 693, 1379

Henriksen, R., Andre, P., & Bontemps, S. 1997, A&A, 323, 549

Herbst, E. & Klemperer, W. 1973, ApJ, 185, 505

Heyer, M. H. & Brunt, C. M. 2004, ApJL, 615, L45

Hirota, T., Maezawa, H., & Yamamoto, S. 2004, ApJ, 617, 399

Hoare, M. G., Kurtz, S. E., Lizano, S., Keto, E., & Hofner, P. 2007, in *Protostars and Planets V*, ed. B. Reipurth, D. Jewitt, & K. Keil (Tuscon, AZ: Univ. Arizona Press), p. 181

Hollenbach, D., Johnstone, D., Lizano, S., & Shu, F. 1994, ApJ, 428, 654

Hollenbach, D. & McKee, C. F. 1989, ApJ, 342, 306

Hunter, T. R., Brogan, C. L., Indebetouw, R., & Cyganowski, C. J. 2008, ApJ, 680, 1271

Ikeda, N., Sunada, K., & Kitamura, Y. 2007, ApJ, 665, 1194

Jackson, J. M., Chambers, E. T., Rathborne, J. M., Simon, R., & Zhang, Q. 2008a, in ASPCS, Vol. 387, *Massive Star Formation: Observations Confront Theory*, ed. H. Beuther, H. Linz, & T. Henning, p. 44

Jackson, J. M., Finn, S. C., Rathborne, J. M., Chambers, E. T., & Simon, R. 2008b, ApJ, 680, 349

Jiang, Z., Tamura, M., Fukagawa, M., et al. 2005, Nature, 437, 112

Jiang, Z., Tamura, M., Hoare, M. G., et al. 2008, ApJL, 673, L175

Jijina, J. & Adams, F. C. 1996, ApJ, 462, 874

Jijina, J., Myers, P. C., & Adams, F. C. 1999, ApJS, 125, 161

Jiménez-Serra, I., Martín-Pintado, J., Caselli, P., Viti, S., & Rodríguez-Franco, A. 2009, ApJ, 695, 149

Jiménez-Serra, I., Martín-Pintado, J., Rodríguez-Franco, A., & Martín, S. 2005, ApJL, 627, L121

Johnston, K. J., Gaume, R. A., Fey, A. L., de Vegt, C., & Claussen, M. J. 2003, AJ, 125, 858

Johnstone, D., di Francesco, J., & Kirk, H. 2004, ApJL, 611, L45

Jones, A. P., Tielens, A. G. G. M., Hollenbach, D. J., & McKee, C. F. 1994, ApJ, 433, 797

Jones, C. E., Basu, S., & Dubinski, J. 2001, ApJ, 551, 387

Jørgensen, J. K. 2004, A&A, 424, 589

Jørgensen, J. K., Hogerheijde, M. R., Blake, G. A., et al. 2004a, A&A, 415, 1021

Jørgensen, J. K., Johnstone, D., Kirk, H., & Myers, P. C. 2007, ApJ, 656, 293

Jørgensen, J. K., Johnstone, D., van Dishoeck, E. F., & Doty, S. D. 2006, A&A, 449, 609

Jørgensen, J. K., Schöier, F. L., & van Dishoeck, E. F. 2004b, A&A, 416, 603

Jørgensen, J. K., Schöier, F. L., & van Dishoeck, E. F. 2005, A&A, 435, 177

Jørgensen, J. K., van Dishoeck, E. F., Visser, R., et al. 2009, A&A, 507, 861

Kahn, F. D. 1974, A&A, 37, 149

Kandori, R., Nakajima, Y., Tamura, M., et al. 2005, AJ, 130, 2166

Kaufman, M. J. & Neufeld, D. A. 1996, ApJ, 456, 611

Kenyon, S. J., Calvet, N., & Hartmann, L. 1993, ApJ, 414, 676

Keto, E. 2007, ApJ, 666, 976

Keto, E. & Caselli, P. 2008, ApJ, 683, 238

Keto, E. & Caselli, P. 2010, MNRAS, 402, 1625

Kim, M. K., Hirota, T., Honma, M., et al. 2008, PASJ, 60, 991

Kirk, H., Johnstone, D., & Tafalla, M. 2007, ApJ, 668, 1042

Kirk, J. M., Crutcher, R. M., & Ward-Thompson, D. 2009, ApJ, 701, 1044

Kirk, J. M., Ward-Thompson, D., & André, P. 2005, MNRAS, 360, 1506

Kirk, J. M., Ward-Thompson, D., & Crutcher, R. M. 2006, MNRAS, 369, 1445

Klessen, R. S. 2001, ApJ, 556, 837

Klessen, R. S., Ballesteros-Paredes, J., Vázquez-Semadeni, E., & Durán-Rojas, C. 2005, ApJ, 620, 786

Klessen, R. S. & Burkert, A. 2001, ApJ, 549, 386

Klessen, R. S., Heitsch, F., & Mac Low, M.-M. 2000, ApJ, 535, 887

Königl, A. & Pudritz, R. E. 2000, in *Protostars and Planets IV*, ed. V. Mannings, A. P. Boss, & S. S. Russell (Tuscon, AZ: Univ. Arizona Press), p. 759

Könyves, V., André, P., Men'shchikov, A., et al. 2010, A&A, 518, L106

Kramer, C., Alves, J., Lada, C. J., et al. 1999, A&A, 342, 257

Kratter, K. M., Matzner, C. D., Krumholz, M. R., & Klein, R. I. 2010, ApJ, 708, 1585

Krumholz, M. R., Klein, R. I., & McKee, C. F. 2005a, in IAU Symposium, Vol. 227, *Massive Star Birth: A Crossroads of Astrophysics*, ed. R. Cesaroni, M. Felli, E. Churchwell, & M. Walmsley, p. 231

Krumholz, M. R., Klein, R. I., & McKee, C. F. 2007, ApJ, 656, 959

Krumholz, M. R. & McKee, C. F. 2008, Nature, 451, 1082

Krumholz, M. R., McKee, C. F., & Klein, R. I. 2005b, ApJL, 618, L33

Krumholz, M. R., McKee, C. F., & Klein, R. I. 2005c, Nature, 438, 332

Kudoh, T. & Basu, S. 2008, ApJL, 679, L97

Kulsrud, R. & Pearce, W. P. 1969, ApJ, 156, 445

Kunz, M. W. & Mouschovias, T. C. 2009a, MNRAS, 399, L94

Kunz, M. W. & Mouschovias, T. C. 2009b, ApJ, 693, 1895

Kurtz, S. 2002, in ASPCS, Vol. 267, *Hot Star Workshop III: The Earliest Phases of Massive Star Birth*, ed. P. Crowther, p. 81

Kurtz, S. 2005, in IAU Symposium, Vol. 227, *Massive Star Birth: A Crossroads of Astrophysics*, ed. R. Cesaroni, M. Felli, E. Churchwell, & M. Walmsley, p. 111

Kurtz, S., Cesaroni, R., Churchwell, E., Hofner, P., & Walmsley, C. M. 2000, in *Protostars and Planets IV*, ed. V. Mannings, A. P. Boss, & S. S. Russell (Tuscon, AZ: Univ. Arizona Press), p. 299

Lada, C. J. 1987, in IAU Symposium, Vol. 115, *Star Forming Regions*, ed. M. Peimbert & J. Jugaku, p. 1

Lada, C. J. & Lada, E. A. 2003, ARA&A, 41, 57

Lada, C. J., Muench, A. A., Rathborne, J., Alves, J. F., & Lombardi, M. 2008, ApJ, 672, 410

Lada, C. J. & Wilking, B. A. 1984, ApJ, 287, 610

Langer, W. D., van Dishoeck, E. F., Bergin, E. A., et al. 2000, in *Protostars and Planets IV*, ed. V. Mannings, A. P. Boss, & S. S. Russell (Tuscon, AZ: Univ. Arizona Press), p. 29

Larson, R. B. 1981, MNRAS, 194, 809

Launhardt, R., Nutter, D., Ward-Thompson, D., et al. 2010, ApJS, 188, 139

Le Bourlot, J., Pineau des Forêts, G., Flower, D. R., & Cabrit, S. 2002, MNRAS, 332, 985

Lee, C., Hasegawa, T. I., Hirano, N., et al. 2010, ApJ, 713, 731

Lee, C., Ho, P. T. P., Hirano, N., et al. 2007, ApJ, 659, 499

Lee, C. W., Myers, P. C., & Tafalla, M. 1999, ApJ, 526, 788

Lee, J.-E., Evans, II, N. J., Shirley, Y. L., & Tatematsu, K. 2003, ApJ, 583, 789

Léger, A. 1983, A&A, 123, 271

Léger, A., Jura, M., & Omont, A. 1985, A&A, 144, 147

Lehtinen, K., Harju, J., Kontinen, S., & Higdon, J. L. 2003, A&A, 401, 1017

Leurini, S., Codella, C., Zapata, L. A., et al. 2009, A&A, 507, 1443

Li, P. S., Norman, M. L., Mac Low, M.-M., & Heitsch, F. 2004, ApJ, 605, 800

Li, Z.-Y. & Nakamura, F. 2004, ApJL, 609, L83

Li, Z.-Y. & Shu, F. H. 1996, ApJ, 472, 211

Linsky, J. L., Draine, B. T., Moos, H. W., et al. 2006, ApJ, 647, 1106

Lizano, S. 2008, in ASPCS, Vol. 387, *Massive Star Formation: Observations Confront Theory*, ed. H. Beuther, H. Linz, & T. Henning, p. 232

Loinard, L., Castets, A., Ceccarelli, C., Caux, E., & Tielens, A. G. G. M. 2001, ApJL, 552, L163

Longair, M. S. 1981, *High energy astrophysics. An informal introduction for students of physics and astronomy* (Cambridge: Cambridge Univ. Press)

Lucas, P. W., Blundell, K. M., & Roche, P. F. 2000, MNRAS, 318, 526

Mac Low, M.-M. 1999, ApJ, 524, 169

Mac Low, M.-M., Balsara, D. S., Kim, J., & de Avillez, M. A. 2005, ApJ, 626, 864

Mac Low, M.-M. & Klessen, R. S. 2004, *Reviews of Modern Physics*, 76, 125

Mac Low, M.-M., Klessen, R. S., Burkert, A., & Smith, M. D. 1998, Physical Review Letters, 80, 2754

Mac Low, M.-M. & Ossenkopf, V. 2000, A&A, 353, 339

Machida, M. N., Inutsuka, S., & Matsumoto, T. 2008, ApJ, 676, 1088

Maret, S. & Bergin, E. A. 2007, ApJ, 664, 956

Maret, S., Bergin, E. A., & Lada, C. J. 2006, Nature, 442, 425

Martin, S. C. 1996, ApJ, 473, 1051

Martín-Pintado, J., Bachiller, R., & Fuente, A. 1992, A&A, 254, 315

Masunaga, H. & Inutsuka, S.-i. 2000, ApJ, 531, 350

Masunaga, H., Miyama, S. M., & Inutsuka, S.-i. 1998, ApJ, 495, 346

Matzner, C. D. 2007, ApJ, 659, 1394

Matzner, C. D. & McKee, C. F. 2000, ApJ, 545, 364

Maury, A. J., André, P., Hennebelle, P., et al. 2010, A&A, 512, A40

McCall, B. J., Geballe, T. R., Hinkle, K. H., & Oka, T. 1999, ApJ, 522, 338

McKee, C. F. 1989, ApJ, 345, 782

McKee, C. F. & Ostriker, E. C. 2007, ARA&A, 45, 565

McKee, C. F. & Tan, J. C. 2003, ApJ, 585, 850

McKee, C. F., Zweibel, E. G., Goodman, A. A., & Heiles, C. 1993, in *Protostars and Planets III*, ed. E. H. Levy & J. I. Lunine (Tuscon, AZ: Univ. Arizona Press), p. 327

Mellon, R. R. & Li, Z.-Y. 2008, ApJ, 681, 1356

Men'shchikov, A., André, P., Didelon, P., et al. 2010, A&A, 518, L103

Men'shchikov, A. B. & Henning, T. 1997, A&A, 318, 879

Mestel, L. & Spitzer, Jr., L. 1956, MNRAS, 116, 503

Millar, T. J., Bennett, A., & Herbst, E. 1989, ApJ, 340, 906

Montmerle, T. 1991, in NATO ASIC Proc. 342: *The Physics of Star Formation and Early Stellar Evolution*, ed. C. J. Lada & N. D. Kylafis, p. 675

Mookerjea, B., Casper, E., Mundy, L. G., & Looney, L. W. 2007, ApJ, 659, 447

Morata, O., Girart, J. M., & Estalella, R. 2005, A&A, 435, 113

Morrow, A. L., Luhman, K. L., Espaillat, C., et al. 2008, ApJL, 676, L143

Motte, F. & André, P. 2001, A&A, 365, 440

Motte, F., André, P., & Neri, R. 1998, A&A, 336, 150

Motte, F., André, P., Ward-Thompson, D., & Bontemps, S. 2001, A&A, 372, L41

Motte, F., Bontemps, S., Schilke, P., et al. 2007, A&A, 476, 1243

Motte, F., Schilke, P., & Lis, D. C. 2003, ApJ, 582, 277

Mouschovias, T. C. 1991, ApJ, 373, 169

Mouschovias, T. C. & Spitzer, Jr., L. 1976, ApJ, 210, 326

Mouschovias, T. C. & Tassis, K. 2009, MNRAS, 400, L15

Mouschovias, T. C., Tassis, K., & Kunz, M. W. 2006, ApJ, 646, 1043

Myers, P. C. 1983, ApJ, 270, 105

Myers, P. C. 2009, ApJ, 706, 1341

Myers, P. C., Adams, F. C., Chen, H., & Schaff, E. 1998, ApJ, 492, 703

Myers, P. C. & Benson, P. J. 1983, ApJ, 266, 309

Myers, P. C., Dame, T. M., Thaddeus, P., et al. 1986, ApJ, 301, 398

Myers, P. C., Evans, II, N. J., & Ohashi, N. 2000, in *Protostars and Planets IV*, ed. V. Mannings, A. P. Boss, & S. S. Russell (Tuscon, AZ: Univ. Arizona Press), p. 217

Myers, P. C., Fuller, G. A., Goodman, A. A., & Benson, P. J. 1991a, ApJ, 376, 561

Myers, P. C. & Ladd, E. F. 1993, ApJL, 413, L47

Myers, P. C., Ladd, E. F., & Fuller, G. A. 1991b, ApJL, 372, L95

Nagaoka, A., Watanabe, N., & Kouchi, A. 2005, ApJL, 624, L29

Nakamura, F. & Li, Z.-Y. 2005, ApJ, 631, 411

Nakamura, F. & Li, Z.-Y. 2008, ApJ, 687, 354

Nakano, T. 1984, Fundamentals of Cosmic Physics, 9, 139

Nakano, T. 1998, ApJ, 494, 587

Neufeld, D. A. & Dalgarno, A. 1989, ApJ, 340, 869

Neufeld, D. A. & Hollenbach, D. J. 1996, ApJL, 471, L45

Nutter, D. & Ward-Thompson, D. 2007, MNRAS, 374, 1413

Nutter, D., Ward-Thompson, D., & André, P. 2006, MNRAS, 368, 1833

Nutter, D. J., Ward-Thompson, D., & André, P. 2005, MNRAS, 357, 975

Öberg, K. I., van Broekhuizen, F., Fraser, H. J., et al. 2005, ApJL, 621, L33

Offner, S. S. R., Klein, R. I., McKee, C. F., & Krumholz, M. R. 2009, ApJ, 703, 131

Offner, S. S. R., Krumholz, M. R., Klein, R. I., & McKee, C. F. 2008, AJ, 136, 404

Ohashi, N., Lee, S. W., Wilner, D. J., & Hayashi, M. 1999, ApJL, 518, L41

Oka, T., Geballe, T. R., Goto, M., Usuda, T., & McCall, B. J. 2005, ApJ, 632, 882

Oliveira, C. M., Hébrard, G., Howk, J. C., et al. 2003, ApJ, 587, 235

Onishi, T., Mizuno, A., Kawamura, A., Tachihara, K., & Fukui, Y. 2002, ApJ, 575, 950

Oppenheimer, M. & Dalgarno, A. 1974, ApJ, 192, 29

Osorio, M., Anglada, G., Lizano, S., & D'Alessio, P. 2009, ApJ, 694, 29

Ossenkopf, V. & Henning, T. 1994, A&A, 291, 943

Ossenkopf, V. & Mac Low, M.-M. 2002, A&A, 390, 307

Padoan, P. & Nordlund, Å. 2002, ApJ, 576, 870

Padoan, P., Nordlund, Å., & Jones, B. J. T. 1997, MNRAS, 288, 145

Padoan, P., Nordlund, Å., Kritsuk, A. G., Norman, M. L., & Li, P. S. 2007, ApJ, 661, 972

Padoan, P., Willacy, K., Langer, W., & Juvela, M. 2004, ApJ, 614, 203

Padovani, M., Galli, D., & Glassgold, A. E. 2009, A&A, 501, 619

Pagani, L., Bacmann, A., Cabrit, S., & Vastel, C. 2007, A&A, 467, 179

Pagani, L., Bacmann, A., Motte, F., et al. 2004, A&A, 417, 605

Pagani, L., Lagache, G., Bacmann, A., et al. 2003, A&A, 406, L59

Pagani, L., Pardo, J.-R., Apponi, A. J., Bacmann, A., & Cabrit, S. 2005, A&A, 429, 181

Pagani, L., Ristorcelli, I., Boudet, N., et al. 2010, A&A, 512, A3

Pagani, L., Vastel, C., Hugo, E., et al. 2009, A&A, 494, 623

Palla, F. 2005, in IAU Symposium, Vol. 227, *Massive Star Birth: A Crossroads of Astrophysics*, ed. R. Cesaroni, M. Felli, E. Churchwell, & M. Walmsley, p. 196

Panagia, N. & Felli, M. 1975, A&A, 39, 1

Parise, B., Castets, A., Herbst, E., et al. 2004, A&A, 416, 159

Parise, B., Ceccarelli, C., Tielens, A. G. G. M., et al. 2002, A&A, 393, L49

Parsons, H., Thompson, M. A., & Chrysostomou, A. 2009, MNRAS, 399, 1506

Patel, N. A., Curiel, S., Sridharan, T. K., et al. 2005, Nature, 437, 109

Pavlyuchenkov, Y., Henning, T., & Wiebe, D. 2007, ApJL, 669, L101

Pérault, M., Omont, A., Simon, G., et al. 1996, A&A, 315, L165

Persi, P. & Tapia, M. 2008, in *Handbook of Star Forming Regions, Volume II: The Southern Sky*, ed. B. Reipurth (San Francisco: ASP), p. 456

Persi, P., Tapia, M., Roth, M., & Gómez, M. 2009, A&A, 493, 571

Peters, T., Mac Low, M., Banerjee, R., Klessen, R. S., & Dullemond, C. P. 2010, ApJ, 719, 831

Phillips, R. B., Lonsdale, C. J., Feigelson, E. D., & Deeney, B. D. 1996, AJ, 111, 918

Phillips, T. G. & Vastel, C. 2003, in SFChem 2002: *Chemistry as a Diagnostic of Star Formation*, ed. C. L. Curry & M. Fich, p. 3

Pillai, T., Wyrowski, F., Menten, K. M., & Krügel, E. 2006, A&A, 447, 929

Pineda, J. E., Goodman, A. A., Arce, H. G., et al. 2010, ApJL, 712, L116

Prantzos, N. & Aubert, O. 1995, A&A, 302, 69

Price, D. J. & Bate, M. R. 2009, MNRAS, 398, 33

Prodanović, T., Steigman, G., & Fields, B. D. 2010, MNRAS, 406, 1108

Pudritz, R. E., Ouyed, R., Fendt, C., & Brandenburg, A. 2007, in *Protostars and Planets V*, ed. B. Reipurth, D. Jewitt, & K. Keil (Tuscon, AZ: Univ. Arizona Press), p. 277

Puga, E., Feldt, M., Alvarez, C., et al. 2006, ApJ, 641, 373

Qiu, K., Zhang, Q., Wu, J., & Chen, H. 2009, ApJ, 696, 66

Raga, A. C., Curiel, S., Rodríguez, L. F., & Cantó, J. 2000, A&A, 364, 763

Ragan, S. E., Bergin, E. A., & Gutermuth, R. A. 2009, ApJ, 698, 324

Ramaty, R. 1969, ApJ, 158, 753

Rathborne, J. M., Jackson, J. M., Chambers, E. T., et al. 2005, ApJL, 630, L181

Rathborne, J. M., Jackson, J. M., Chambers, E. T., et al. 2010, ApJ, 715, 310

Rathborne, J. M., Jackson, J. M., & Simon, R. 2006, ApJ, 641, 389

Rathborne, J. M., Jackson, J. M., Simon, R., & Zhang, Q. 2009a, Ap&SS, 324, 155

Rathborne, J. M., Jackson, J. M., Zhang, Q., & Simon, R. 2008, ApJ, 689, 1141

Rathborne, J. M., Lada, C. J., Muench, A. A., et al. 2009b, ApJ, 699, 742

Rathborne, J. M., Simon, R., & Jackson, J. M. 2007, ApJ, 662, 1082

Rawlings, J. M. C., Hartquist, T. W., Menten, K. M., & Williams, D. A. 1992, MNRAS, 255, 471

Ray, T., Dougados, C., Bacciotti, F., Eislöffel, J., & Chrysostomou, A. 2007, in *Protostars and Planets V*, ed. B. Reipurth, D. Jewitt, & K. Keil (Tuscon, AZ: Univ. Arizona Press), p. 231

Redman, M. P., Rawlings, J. M. C., Nutter, D. J., Ward-Thompson, D., & Williams, D. A. 2002, MNRAS, 337, L17

Redman, R. O., Feldman, P. A., Wyrowski, F., et al. 2003, ApJ, 586, 1127

Reipurth, B. & Bally, J. 2001, ARA&A, 39, 403

Reynolds, S. P. 1986, ApJ, 304, 713

Richer, J. S., Shepherd, D. S., Cabrit, S., Bachiller, R., & Churchwell, E. 2000, in *Protostars and Planets IV*, ed. V. Mannings, A. P. Boss, & S. S. Russell (Tuscon, AZ: Univ. Arizona Press), p. 867

Roberts, H., Herbst, E., & Millar, T. J. 2002, MNRAS, 336, 283

Roberts, H., Herbst, E., & Millar, T. J. 2003, ApJL, 591, L41

Roberts, H. & Millar, T. J. 2000, A&A, 361, 388

Roberts, H. & Millar, T. J. 2007, A&A, 471, 849

Robitaille, T. P., Whitney, B. A., Indebetouw, R., Wood, K., & Denzmore, P. 2006, ApJS, 167, 256

Rodríguez, L. F. 1994, RMxAA, 29, 69

Rodríguez, L. F. 1997, in IAU Symposium, Vol. 182, *Herbig-Haro Flows and the Birth of Stars*, ed. B. Reipurth & C. Bertout, p. 83

Rodríguez, L. F., Anglada, G., & Curiel, S. 1999, ApJS, 125, 427

Rodríguez, L. F., Garay, G., Brooks, K. J., & Mardones, D. 2005, ApJ, 626, 953

Rodríguez, L. F., Ho, P. T. P., Torrelles, J. M., Curiel, S., & Canto, J. 1990, ApJ, 352, 645

Rodríguez, L. F., Myers, P. C., Cruz-Gonzalez, I., & Terebey, S. 1989, ApJ, 347, 461

Rohlfs, K. & Wilson, T. L. 2004, *Tools of radio astronomy* (Berlin: Springer)

Ruden, S. P. 1999, in NATO ASIC Proc. 540: *The Origin of Stars and Planetary Systems*, ed. C. J. Lada & N. D. Kylafis, p. 643

Sadavoy, S. I., Di Francesco, J., Bontemps, S., et al. 2010, ApJ, 710, 1247

Salpeter, E. E. 1955, ApJ, 121, 161

Sandell, G. & Wright, M. 2010, ApJ, 715, 919

Sanhueza, P., Garay, G., Bronfman, L., et al. 2010, ApJ, 715, 18

Saraceno, P., Andre, P., Ceccarelli, C., Griffin, M., & Molinari, S. 1996, A&A, 309, 827

Scheffler, H. & Elsässer, H. 1987, *Physics of the galaxy and interstellar matter* (Berlin and New York, Springer-Verlag)

Schilke, P., Benford, D. J., Hunter, T. R., Lis, D. C., & Phillips, T. G. 2001, ApJS, 132, 281

Schilke, P., Walmsley, C. M., Pineau des Forêts, G., & Flower, D. R. 1997, A&A, 321, 293

Schnee, S., Caselli, P., Goodman, A., et al. 2007, ApJ, 671, 1839

Schnee, S. & Goodman, A. 2005, ApJ, 624, 254

Schnee, S., Rosolowsky, E., Foster, J., Enoch, M., & Sargent, A. 2009, ApJ, 691, 1754

Schneider, N., Bontemps, S., Simon, R., et al. 2010, ArXiv e-prints

Sewilo, M., Churchwell, E., Kurtz, S., Goss, W. M., & Hofner, P. 2004, ApJ, 605, 285

Shang, H., Li, Z.-Y., & Hirano, N. 2007, in *Protostars and Planets V*, ed. B. Reipurth, D. Jewitt, & K. Keil (Tuscon, AZ: Univ. Arizona Press), p. 261

Shepherd, D. 2005, in IAU Symposium, Vol. 227, *Massive Star Birth: A Crossroads of Astrophysics*, ed. R. Cesaroni, M. Felli, E. Churchwell, & M. Walmsley, p. 237

Shepherd, D. S. & Churchwell, E. 1996, ApJ, 472, 225

Shepherd, D. S., Claussen, M. J., & Kurtz, S. E. 2001, Science, 292, 1513

Shetty, R., Kauffmann, J., Schnee, S., Goodman, A. A., & Ercolano, B. 2009, ApJ, 696, 2234

Shirley, Y. L., Claussen, M. J., Bourke, T. L., Young, C. H., & Blake, G. A. 2007, ApJ, 667, 329

Shirley, Y. L., Evans, II, N. J., & Rawlings, J. M. C. 2002, ApJ, 575, 337

Shirley, Y. L., Evans, II, N. J., Rawlings, J. M. C., & Gregersen, E. M. 2000, ApJS, 131, 249

Shu, F., Najita, J., Ostriker, E., et al. 1994, ApJ, 429, 781

Shu, F. H., Adams, F. C., & Lizano, S. 1987, ARA&A, 25, 23

Shu, F. H., Li, Z.-Y., & Allen, A. 2004, ApJ, 601, 930

Simon, R., Jackson, J. M., Rathborne, J. M., & Chambers, E. T. 2006a, ApJ, 639, 227

Simon, R., Rathborne, J. M., Shah, R. Y., Jackson, J. M., & Chambers, E. T. 2006b, ApJ, 653, 1325

Simpson, R. J., Nutter, D., & Ward-Thompson, D. 2008, MNRAS, 391, 205

Skinner, S. L. 1993, ApJ, 408, 660

Snell, R. L., Loren, R. B., & Plambeck, R. L. 1980, ApJL, 239, L17

Sohn, J., Lee, C. W., Park, Y.-S., et al. 2007, ApJ, 664, 928

Sollins, P. K., Hunter, T. R., Battat, J., et al. 2004, ApJL, 616, L35

Solomon, P. M., Rivolo, A. R., Barrett, J., & Yahil, A. 1987, ApJ, 319, 730

Sonnhalter, C., Preibisch, T., & Yorke, H. W. 1995, A&A, 299, 545

Sridharan, T. K., Beuther, H., Saito, M., Wyrowski, F., & Schilke, P. 2005a, ApJL, 634, L57

Sridharan, T. K., Williams, S. J., & Fuller, G. A. 2005b, ApJL, 631, L73

Stahler, S. W. & Palla, F. 2004, *The Formation of Stars*, ed. S. W. Stahler & F. Palla

Stamatellos, D., Whitworth, A. P., André, P., & Ward-Thompson, D. 2004, A&A, 420, 1009

Stamatellos, D., Whitworth, A. P., Boyd, D. F. A., & Goodwin, S. P. 2005, A&A, 439, 159

Stamatellos, D., Whitworth, A. P., & Ward-Thompson, D. 2007, MNRAS, 379, 1390

Stanke, T., Smith, M. D., Gredel, R., & Khanzadyan, T. 2006, A&A, 447, 609

Stark, R., Sandell, G., Beck, S. C., et al. 2004, ApJ, 608, 341

Stine, P. C., Feigelson, E. D., Andre, P., & Montmerle, T. 1988, AJ, 96, 1394

Stone, J. M., Ostriker, E. C., & Gammie, C. F. 1998, ApJL, 508, L99

Suzuki, H., Yamamoto, S., Ohishi, M., et al. 1992, ApJ, 392, 551

Swift, J. J. & Williams, J. P. 2008, ApJ, 679, 552

Tafalla, M., Myers, P. C., Caselli, P., & Walmsley, C. M. 2004, A&A, 416, 191

Tafalla, M., Myers, P. C., Caselli, P., Walmsley, C. M., & Comito, C. 2002, ApJ, 569, 815

Tafalla, M. & Santiago, J. 2004, A&A, 414, L53

Tafalla, M., Santiago-García, J., Myers, P. C., et al. 2006, A&A, 455, 577

Tan, J. C. 2008, in Astronomical Society of the Pacific Conference Series, Vol. 387, *Massive Star Formation: Observations Confront Theory*, ed. H. Beuther, H. Linz, & T. Henning, p. 346

Tassis, K. & Mouschovias, T. C. 2004, ApJ, 616, 283

Testi, L. & Sargent, A. I. 1998, ApJL, 508, L91

Tielens, A. G. G. M. 1983, A&A, 119, 177

Troland, T. H. & Crutcher, R. M. 2008, ApJ, 680, 457

Turner, B. E. 1991, ApJS, 76, 617

Turner, B. E. & Heiles, C. 2006, ApJS, 162, 388

Umebayashi, T. & Nakano, T. 1981, PASJ, 33, 617

van der Tak, F. F. S., Belloche, A., Schilke, P., et al. 2006, A&A, 454, L99

van der Tak, F. F. S. & Menten, K. M. 2005, A&A, 437, 947

van der Tak, F. F. S. & van Dishoeck, E. F. 2000, A&A, 358, L79

van Dishoeck, E. F. & Blake, G. A. 1998, ARA&A, 36, 317

van Dishoeck, E. F., Blake, G. A., Draine, B. T., & Lunine, J. I. 1993, in *Protostars and Planets III*, ed. E. H. Levy & J. I. Lunine (Tuscon, AZ: Univ. Arizona Press), p. 163

Vastel, C., Caselli, P., Ceccarelli, C., et al. 2006, ApJ, 645, 1198

Vastel, C., Phillips, T. G., & Yoshida, H. 2004, ApJL, 606, L127

Vasyunina, T., Linz, H., Henning, T., et al. 2009, A&A, 499, 149

Vázquez-Semadeni, E., Gómez, G. C., Jappsen, A., Ballesteros-Paredes, J., & Klessen, R. S. 2009, ApJ, 707, 1023

Vázquez-Semadeni, E., Kim, J., Shadmehri, M., & Ballesteros-Paredes, J. 2005, ApJ, 618, 344

Vorobyov, E. I. 2010, ApJ, 713, 1059

Vuong, M. H., Montmerle, T., Grosso, N., et al. 2003, A&A, 408, 581

Wada, K. & Norman, C. A. 2001, ApJ, 547, 172

Walmsley, C. M., Flower, D. R., & Pineau des Forêts, G. 2004, A&A, 418, 1035

Wang, Y., Zhang, Q., Rathborne, J. M., Jackson, J., & Wu, Y. 2006, ApJL, 651, L125

Ward-Thompson, D. 2002, Science, 295, 76

Ward-Thompson, D., André, P., Crutcher, R., et al. 2007, in *Protostars and Planets V*, ed. B. Reipurth, D. Jewitt, & K. Keil (Tuscon, AZ: Univ. Arizona Press), p. 33

Ward-Thompson, D., André, P., & Kirk, J. M. 2002, MNRAS, 329, 257

Ward-Thompson, D., Motte, F., & Andre, P. 1999, MNRAS, 305, 143

Ward-Thompson, D., Scott, P. F., Hills, R. E., & André, P. 1994, MNRAS, 268, 276

Weingartner, J. C. & Draine, B. T. 2001, ApJS, 134, 263

Werner, M. W., Roellig, T. L., Low, F. J., et al. 2004, ApJS, 154, 1

Whelan, E. T., Ray, T. P., Podio, L., Bacciotti, F., & Randich, S. 2009, ApJ, 706, 1054

White, R. J. & Hillenbrand, L. A. 2004, ApJ, 616, 998

White, S. M., Pallavicini, R., & Kundu, M. R. 1992, A&A, 259, 149

Whitney, B. A., Wood, K., Bjorkman, J. E., & Wolff, M. J. 2003, ApJ, 591, 1049

Willacy, K., Langer, W. D., & Velusamy, T. 1998, ApJL, 507, L171

Williams, J. P., Bergin, E. A., Caselli, P., Myers, P. C., & Plume, R. 1998, ApJ, 503, 689

Winkler, K.-H. A. & Newman, M. J. 1980, ApJ, 236, 201

Wolfire, M. G. & Cassinelli, J. P. 1987, ApJ, 319, 850

Wolk, S. J. & Walter, F. M. 1996, AJ, 111, 2066

Wootten, A., Loren, R. B., & Snell, R. L. 1982, ApJ, 255, 160

Yorke, H. W. 2004, in IAU Symposium, Vol. 221, *Star Formation at High Angular Resolution*, ed. M. G. Burton, R. Jayawardhana, & T. L. Bourke, p. 141

Yorke, H. W. & Bodenheimer, P. 2008, in ASPCS, Vol. 387, *Massive Star Formation: Observations Confront Theory*, ed. H. Beuther, H. Linz, & T. Henning, p. 189

Yorke, H. W. & Sonnhalter, C. 2002, ApJ, 569, 846

Young, C. H. & Evans, II, N. J. 2005, ApJ, 627, 293

Young, C. H., Shirley, Y. L., Evans, II, N. J., & Rawlings, J. M. C. 2003, ApJS, 145, 111

Young, K. E., Lee, J.-E., Evans, II, N. J., Goldsmith, P. F., & Doty, S. D. 2004, ApJ, 614, 252

Zapata, L. A., Ho, P. T. P., Schilke, P., et al. 2009, ApJ, 698, 1422

Zapata, L. A., Schmid-Burgk, J., & Menten, K. M. 2010, ArXiv e-prints

Zhang, Q., Hunter, T. R., Beuther, H., et al. 2007, ApJ, 658, 1152

Zhang, Q., Hunter, T. R., Sridharan, T. K., & Ho, P. T. P. 2002, ApJ, 566, 982

Zhang, Q., Wang, Y., Pillai, T., & Rathborne, J. 2009, ApJ, 696, 268

Zhu, Z., Hartmann, L., & Gammie, C. 2009, ApJ, 694, 1045

Zinnecker, H. & Yorke, H. W. 2007, ARA&A, 45, 481

Ziurys, L. M., Friberg, P., & Irvine, W. M. 1989, ApJ, 343, 201

Zubko, V., Dwek, E., & Arendt, R. G. 2004, ApJS, 152, 211

Zucconi, A., Walmsley, C. M., & Galli, D. 2001, A&A, 376, 650

Zweibel, E. G. 2002, ApJ, 567, 962

Zweibel, E. G. & Josafatsson, K. 1983, ApJ, 270, 511

Journal abbreviations

A&A	Astronomy & Astrophysics
A&AS	Astronomy & Astrophysics Supplement Series
AJ	The Astronomical Journal
ApJ	The Astrophysical Journal
ApJL	The Astrophysical Journal Letters
ApJS	The Astrophysical Journal Supplement Series
Ap&SS	Astrophysics and Space Science
ARA&A	Annual Review of Astronomy & Astrophysics
ASPCS	Astronomical Society of the Pacific Conference Series
MNRAS	Monthly Notices of the Royal Astronomical Society
NATO ASIC Proc.	NATO Air and Space Interoperability Council Proceedings
P&SS	Planetary and Space Science
PASJ	Publications of the Astronomical Society of Japan
PASP	Publications of the Astronomical Society of the Pacific
QJRAS	Quarterly Journal of the Royal Astronomical Society
RMxAA	Revista Mexicana de Astronomía y Astrofísica
RMxAC	Revista Mexicana de Astronomía y Astrofísica (Serie de Conferencias)
ZAp	Zeitschrift für Astrophysik